



Universidade do Minho
Escola de Engenharia

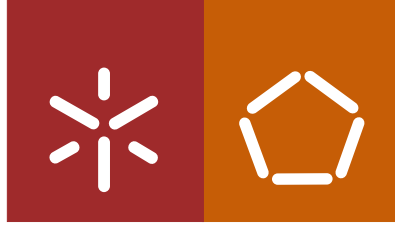
Alexandre Vieira de Sousa

**A guide for Functional
Magnetic Resonance Imaging**

Alexandre Vieira de Sousa **A guide for Functional Magnetic Resonance Imaging**

UMinho | 2016

abril de 2016



Universidade do Minho
Escola de Engenharia

Alexandre Vieira de Sousa

A guide for Functional Magnetic Resonance Imaging

Dissertação de Mestrado
Mestrado Integrado em Engenharia Biomédica
Ramo de Informática Médica

Trabalho efetuado sob a orientação do
Professor Victor Manuel Rodrigues Alves
e coorientação do
Doutor José Miguel Montenegro Soares

DECLARAÇÃO

Nome: Alexandre Vieira de Sousa

Endereço electrónico: xxxandre@gmail.com

Número do Bilhete de Identidade: 12345530

Título dissertação: A Guide for Functional Magnetic Resonance Imaging

Orientadores: Victor Manuel Rodrigues Alves, José Miguel Montenegro Soares

Ano de conclusão: 2016

Designação do Mestrado: Mestrado Integrado em Engenharia Biomédica

DE ACORDO COM A LEGISLAÇÃO EM VIGOR, NÃO É PERMITIDA A REPRODUÇÃO DE
QUALQUER PARTE DESTA DISSERTAÇÃO

Universidade do Minho, ___/___/_____

Assinatura: _____

Title: A guide for Functional Magnetic Resonance Imaging

Abstract

The brain is the most amazingly powerful and complex organ in the human body. Constituted by approximately 86 billion of highly interconnected neurons, it allows us to have unique cognitive capabilities, such as language production and comprehension, memory, judgement and problem solving, or even experience feelings. The full understanding of the organization and functioning of the human brain is receiving increasing attention but remains an exciting challenge for all neuroscientists.

To assist in this quest, fMRI stands as a safe and powerful non-invasive neuroimaging tool providing high visualization quality of the location of activity in the brain resulting from, for example, sensory stimulation, cognitive or motor function, or even resting state fluctuations, being then widely used for mapping the human brain. It allows the study of how the healthy brain works, how it is affected by different diseases, how it recovers from damage and how drugs can modulate activity or post-lesion recovery. Starting purely as a research tool, fMRI was quickly adopted for clinical purposes and has now a growing role in clinical neuroimaging.

Constantly gaining increased popularity among clinicians and researchers, fMRI is presently a promising tool for studying the brain function in living humans. However, it has a complex workflow that implicates knowledge of paradigm design, imaging artifacts, complex MRI protocol definition, a multitude of preprocessing and analysis methods in several software packages, statistical analyzes, and in results interpretation. In addition, fMRI data can be analyzed with a large quantity of commonly used tools, with minor consensuses on how, when, or whether to apply each one.

This dissertation aims to compile a practical guide of crucial information and essential references to consider in setting up fMRI studies, optimizing data quality, and interpreting results. All the major stages are covered with the aim to ultimately help the fMRI beginner researcher, clinician to consider and overcome the most significant difficulties along the process and expand the use of this imaging technique. To validate this guide two examples of fMRI studies were analyzed, with real data, obtaining results according to similar studies literature.

Título: Guia para Imagem por Ressonância Magnética Funcional

Resumo

O cérebro é o órgão mais poderoso e complexo do corpo humano. Constituído por aproximadamente 86 mil milhões de neurões altamente interligados, confere-nos capacidades cognitivas únicas, tais como a criação e compreensão de linguagem, formação de memória, resolução de problemas, ou experienciar sentimentos. O conhecimento profundo da organização e funcionamento do cérebro humano continua a ser um desafio para os neurocientistas, apesar da crescente atenção que tem recebido.

Para auxiliar na pesquisa deste conhecimento, a Imagem por Ressonância Magnética funcional (IRMf) posiciona-se como uma poderosa ferramenta que para além de ser segura, é não-invasiva e proporciona visualizações de alta qualidade das localizações de actividade cerebral resultante de, por exemplo, estimulação sensorial, função cognitiva, ou até mesmo de flutuações em repouso, sendo por isso amplamente utilizada para o mapeamento do cérebro humano. Permite desta forma o estudo do funcionamento do cérebro saudável, de como é afectado por diferentes doenças, como recupera de lesões, e como fármacos influenciam a actividade cerebral e recuperação de lesões. Apesar de começar por ser uma ferramenta usada para investigação, a IRMf foi rapidamente adoptada para aplicações clínicas, tendo agora uma crescente importância em neuroimagem clínica.

Ganhando crescente popularidade entre médicos e investigadores, IRMf é neste momento uma ferramenta muito promissora no estudo *in-vivo* do funcionamento do cérebro em humanos. Contudo implica um conhecimento e domínio do seu fluxo de trabalho, nomeadamente desenho do paradigma, artefactos de imagem, definição de protocolos complexos de IRM, uma multitude de métodos de pré-processamento e análise estatística, e finalmente na interpretação dos resultados. Tudo isto usando uma ampla colecção de diferentes *softwares*, sem que haja consenso em quais são os mais adequados.

Esta dissertação tem como objectivo compilar um guia prático contendo a informação crucial e referencias essenciais à definição, optimização e interpretação de estudos de IRMf. Todas as principais etapas estão cobertas de forma a auxiliar os principiantes em IRMf a considerar e ultrapassar as principais dificuldades normalmente encontradas e assim expandir a utilização desta técnica de imagem médica. Para validar este guia, dois exemplos de estudos de IRMf foram analisados com dados reais e foram obtidos resultados de acordo com os de estudos semelhantes já publicados.

Contents

ABSTRACT	III
RESUMO	V
CONTENTS	VII
LIST OF FIGURES	IX
LIST OF TABLES	XI
LIST OF EQUATIONS	XI
LIST OF ACRONYMS	XII
1 - INTRODUCTION	1
1.1 - BRIEF HISTORY OF FMRI	2
1.2 - CONTEXT	4
1.3 - OBJECTIVES	6
2 - APPLICATION FIELDS	7
2.1 - PRESURGICAL PLANNING AND NEURONAVIGATION	7
2.2 - EEG-FMRI	8
2.3 - RADIOTHERAPY	8
2.4 - CONSCIOUSNESS DISORDERS	8
2.5 - RESTING-STATE FMRI	8
2.6 - REAL-TIME FMRI AND NEUROFEEDBACK	9
2.7 - PHARMACO-FMRI.....	10
2.8 - COMMERCIAL APPLICATIONS.....	10
3 - FMRI SIGNALS	11
3.1 - BOLD	12
3.2 - ASL	14
3.3 - VASO	14
3.4 - SEEP	15
3.5 – DETECTING NEURONAL OR GLIAL ACTIVITY?	16
4 - EXPERIMENTAL DESIGN	17
4.1 - BLOCK PARADIGM.....	18
4.2 - EVENT-RELATED PARADIGMS	19
4.3 - MIXED BLOCK/EVENT-RELATED PARADIGM	21
4.4 - BOLD CEILING FMRI.....	21
4.5 - RESTING STATE PARADIGM	22
5 - DATA ACQUISITION AND ARTIFACTS	25
5.1 - HARDWARE	25
5.2 - BIOEFFECTS AND SAFETY	32
5.3 - FMRI DATA ACQUISITION	36
5.4 - ARTIFACTS	39
6 - QUALITY CONTROL AND PREPROCESSING	45
6.1 - FILE FORMAT CONVERSION	46
6.2 - SLICE-TIMING CORRECTION.....	47
6.3 - MOTION CORRECTION.....	48
6.4 - FUNCTIONAL-STRUCTURAL COREGISTRATION	49

6.5 - SPATIAL NORMALIZATION	50
6.6 - TEMPORAL FILTERING	51
6.7 - SMOOTHING (SPATIAL FILTERING).....	52
7 - STATISTICAL ANALYSIS OF BOLD FMRI DATA.....	53
7.1 - GLM - GENERAL LINEAR MODEL.....	54
7.2 - DATA-DRIVEN, MULTIVARIATE ANALYSIS METHODS	60
7.3 - GROUP ANALYSIS.....	60
8 - PROCESSING AND VISUALIZATION	63
8.1- BRAIN CONNECTIVITY.....	63
8.2 - FMRI SOFTWARE	68
8.3 - SOFTWARE ANALYSIS	72
8.4 - VISUALIZATION	74
9 - MULTIMODAL NEUROIMAGING.....	79
9.1 - STRENGTHS AND LIMITATIONS OF FMRI.....	79
9.2 - COMPARISON WITH OTHER FUNCTIONAL IMAGING MODALITIES	81
9.3 - MULTIMODAL DATA INTEGRATION	82
10 - RESULTS INTERPRETATION.....	85
11 - THE FUTURE OF FMRI	89
12 - PRACTICAL EXAMPLE OF FMRI STUDIES	93
12.1- TASK FMRI.....	93
12.2 - RESTING STATE STUDY	119
13 - CONCLUSION AND FUTURE WORK	139
14 - REFERENCES.....	141

List of Figures

FIGURE 1: EVOLUTION OF NEUROIMAGING PUBLICATIONS. DATA FROM ISI WEB OF KNOWLEDGE [12]. 3

FIGURE 2: WORKFLOW OF A TYPICAL FMRI STUDY..... 5

FIGURE 3: SCHEMATIC ILLUSTRATION OF THE ORIGINS OF THE BOLD EFFECT IN FMRI [46]..... 12

FIGURE 4: CANONICAL HEMODYNAMIC RESPONSE FUNCTION (HRF). THIS IS THE TYPICAL BOLD RESPONSE TO A SINGLE, IMPULSE STIMULATION [111]. 13

FIGURE 5: SIGNAL ENHANCEMENT BY EXTRAVASCULAR WATER PROTONS, SEEP [122]. 15

FIGURE 6: REPRESENTATION OF A VOXEL (VOLUME ELEMENT). REPRESENTED IN RED THE VOXELS WHERE FUNCTIONAL ACTIVATION WAS DETECTED [145]. 18

FIGURE 7: TYPICAL FMRI STUDY PARADIGMS 20

FIGURE 8: A- DEFAULT MODE NETWORK. B- SOMATOMOTOR NETWORK. C- VISUAL NETWORK. D- LANGUAGE NETWORK. E- DORSAL ATTENTION NETWORK. F- VENTRAL ATTENTION NETWORK. G- FRONTOPIRIETAL CONTROL NETWORK [65]... 23

FIGURE 9: A SUPERCONDUCTING MAGNET 1.5 T SIEMENS MAGNETOM AVANTO MRI SCANNER (SIEMENS, ERLANGEN, GERMANY) AT HOSPITAL DE BRAGA. 27

FIGURE 10; HOST COMPUTER OF THE MRI SYSTEM AT HOSPITAL DE BRAGA. 30

FIGURE 11: DEMONSTRATION OF VISUAL, AUDIO STIMULI PRESENTATION ACCESSORIES AND BUTTON RESPONSE COLLECTION AT HOSPITAL DE BRAGA. 30

FIGURE 12: STIMULI PRESENTATION, RESPONSE COLLECTION, AND SYNCHRONIZATION SYSTEM AT HOSPITAL DE BRAGA..... 32

FIGURE 13: DIFFERENT IMAGE CONTRASTS OF AN AXIAL BRAIN SLICE AT 3T: (A) PROTON-DENSITY-WEIGHTED IMAGE (B) T1-WEIGHTED IMAGE (C) T2-WEIGHTED IMAGE (D) T2* -WEIGHTED IMAGE [258]. 36

FIGURE 14: SCHEMATIC REPRESENTATION OF THE EPI PULSE SEQUENCE (ON THE LEFT) AND CORRESPONDING SAMPLING OF THE K-SPACE (ON THE RIGHT) FOR IMAGING OF ONE SLICE. ONLY ONE RF PULSE IS USED TO SAMPLE THE WHOLE SLICE [258]..... 38

FIGURE 15: RINGING ARTIFACT, MANIFESTS AS SUBTLE HYPOINTENSE LINES OVERLYING CORTEX. INDICATED WITH ARROWS IN THIS IMAGE [165]. 42

FIGURE 16: ALIASING ARTIFACT ON BRAIN MRI WITH FOV=24x18 CM (A). SAME PATIENT WITH FOV=24x24 CM (B) [259]..... 42

FIGURE 17: EFFECT OF TEMPORAL FILTERING ON SIMULATED FMRI DATA FOR A SINGLE VOXEL [129]. 52

FIGURE 18: BASIC PRINCIPLES OF THE GLM IN FMRI. THE GLM ATTEMPTS TO FIND THE SET OF EXPERIMENTAL PARAMETERS \mathbf{B} FOR A DESIGN MATRIX \mathbf{G} THAT BEST ACCOUNTS FOR THE ORIGINAL DATA \mathbf{r} , BY MINIMIZING THE UNEXPLAINED ERROR \mathbf{e} [43]..... 56

FIGURE 19: ILLUSTRATION OF THE ANALYSIS STEPS CARRIED OUT IN A TYPICAL FMRI GROUP STUDY [34]. 59

FIGURE 20: SCHEMATIC OF AN “IDEAL” CONNECTOMIC MAP. NODE ROLE HETEROGENEITY IS REPRESENTED BY DIFFERENT COLORS. THE EDGES ARE DIRECTED (ARROWS), WEIGHTED (EDGE THICKNESS) AND ENCODE DIFFERENT FORMS OF INTER-REGIONAL INTERACTION (SOLID VS BROKEN LINES). THE MAPS ALSO VARY OVER TIME [260]. 64

FIGURE 21: ACTIVATION MAP VISUALIZATION IN DIFFERENT PLANES [261]. 75

FIGURE 22: SURFACE BASED VISUALIZATION. IMAGES ADAPTED FROM “VISUALIZATION AND QUANTIFICATION OF FMRI RESULTS” [262]. 76

FIGURE 23: 3D NODE LINK AND CIRCLE REPRESENTATION OF A RSN. NODES CORRESPONDING MOST CLOSELY TO THE NETWORK IN QUESTION ARE ISOLATED AND REPRESENTED IN PURPLE WHILE THE OTHERS ARE SHOWN IN BLUE. STRONGER CONNECTIONS ARE SHOWN IN RED WHILE WEAKER CONNECTIONS ARE SHOWN IN YELLOW [225]. 77

FIGURE 24: CONNECTIVITY MATRIX AND CORRESPONDING CIRCLE VIEW. STRONGER CONNECTIONS ARE SHOWN IN ORANGE WHILE WEAKER CONNECTIONS ARE SHOWN IN BLUE [225].	77
FIGURE 25: EEG-FMRI RECORDING HARDWARE SETUP [263].	83
FIGURE 26: THE COLOUR-CODED LINES REPRESENT DISTINCT FUNCTIONAL NETWORKS OF PATIENTS IN VEGETATIVE STATE. DATA COLLECTED FROM THREE DIFFERENT PATIENTS WITH DISTINCT DEGREES OF CONSCIOUSNESS ARE DISPLAYED [264].	91
FIGURE 27: PARTICIPANTS EDUCATION LEVEL.	93
FIGURE 28: MATLAB COMMAND WINDOW	95
FIGURE 29: SPM12 MENU WINDOW	95
FIGURE 30: SPM12 – BATCH EDITOR.	96
FIGURE 31: MOTION CORRECTION PARAMETERS PLOTS.	97
FIGURE 32: NORMALISED MUTUAL INFORMATION HISTOGRAMS.	98
FIGURE 33: SPM - CHECK REGISTRATION. ON THE LEFT THE SUBJECT'S IMAGE AND ON THE LEFT AN MNI TEMPLATE.	100
FIGURE 34: BEFORE SMOOTHING (TOP) VS AFTER SMOOTHING (BOTTOM).	101
FIGURE 35: SEGMENTATION OF STRUCTURAL T1 IMAGE. FROM TOP TO BOTTOM: GM; WM; CSF; BONE; SOFT-TISSUE.	102
FIGURE 36: IMAGE RESULTING FROM COMBINATION OF GM AND WM OF ONE SUBJECT.	103
FIGURE 37: 3D SURFACE MODEL EXTRACTED FROM GM AND WM IMAGES.	104
FIGURE 38: REVIEW OF STUDY DESIGN.	106
FIGURE 39: REVIEW OF PARAMETERS.	107
FIGURE 40: BRAIN REGIONS OF SUBJECT SW0081C IN WHICH LOCAL VOLUME WAS SIGNIFICANTLY RELATED WITH WORKING MEMORY. CLUSTERS (>80VOXELS), SIGNIFICANT AT $P<0.05$ (FWE CORRECTED), ARE PROJECTED ON CORONAL, AXIAL AND SAGITTAL SECTIONS. THE COLOR BAR REPRESENTS THE T VALUES.	108
FIGURE 41: 3D SURFACE MODEL OF A SINGLE SUBJECT OVERLAID WITH ITS INDIVIDUAL STATISTICAL MAP WITH TWO CONTRASTS. RED: $NB1>NB0$. GREEN: $NB2>NB0$. THE BOTTOM IMAGE IS AN INFLATED VERSION OF THE SURFACE MODEL.	109
FIGURE 42: SPM – REVIEW DESIGN.	110
FIGURE 43: BRAIN REGIONS FROM ALL SUBJECTS IN THE GROUP IN WHICH LOCAL VOLUME WAS SIGNIFICANTLY RELATED WITH WORKING MEMORY ($NB1>NB0$). CLUSTERS (>89VOXELS), SIGNIFICANT AT $P<0.001$ (UNCORRECTED), ARE PROJECTED ON CORONAL, AXIAL AND SAGITTAL SECTIONS OF A TEMPLATE. THE COLOR BAR REPRESENTS THE T VALUES.	112
FIGURE 44: BRAIN REGIONS FROM ALL SUBJECTS IN THE GROUP IN WHICH LOCAL VOLUME WAS SIGNIFICANTLY RELATED WITH WORKING MEMORY ($NB2>NB0$). CLUSTERS (>75VOXELS), SIGNIFICANT AT $P<0.001$ (UNCORRECTED), ARE PROJECTED ON CORONAL, AXIAL AND SAGITTAL SECTIONS OF A TEMPLATE. THE COLOR BAR REPRESENTS THE T VALUES.	113
FIGURE 45: STUDY DESIGN OF TWO-SAMPLE T-TEST. GROUP 1: FEMALE SUBJECTS. GROUP 2: MALE SUBJECTS	117
FIGURE 46: BRAIN REGIONS IN WHICH LOCAL VOLUME FROM FEMALE GROUP WAS MORE SIGNIFICANTLY RELATED WITH WORKING MEMORY THAN MALE GROUP. VOXEL SIGNIFICANT AT $P<0.001$ (UNCORRECTED), ARE PROJECTED ON CORONAL, AXIAL AND SAGITTAL SECTIONS OF A TEMPLATE. THE COLOR BAR REPRESENTS THE T VALUES.	118
FIGURE 47: PARTICIPANTS EDUCATION LEVEL.	119
FIGURE 48: SCREENSHOT OF A BASH SESSION WITH FSL COMMAND “BET” INSTRUCTIONS.	121
FIGURE 49: ON THE TOP THE ORIGINAL STRUCTURAL IMAGE, IN THE MIDDLE THE ORIENTED VERSION, AND ON THE BOTTOM THE CROPPED (PART OF THE NECK WAS REMOVED) AND ORIENTED IMAGE.	122
FIGURE 50: SKULL STRIPPED STRUCTURAL IMAGE.	123

FIGURE 51: OVERLAY OF BRAIN MASK ON THE ORIGINAL STRUCTURAL IMAGE.	124
FIGURE 52: TIME SERIES OF ONE VOXEL.	127
FIGURE 53: MEAN OF FUNCTIONAL IMAGES.	128
FIGURE 54: MOTION CORRECTION PARAMETER PLOTS. THE MIDDLE VOLUME IS USED AS REFERENCE.	130
FIGURE 55: FSLVIEW GUI – MOVIE MODE	130
FIGURE 56: SKULL STRIPPED FUNCTIONAL IMAGE.	132
FIGURE 57: FUNCTIONAL IMAGE NORMALIZED TO MNI SPACE.	133
FIGURE 58: SPATIALLY SMOOTHED FUNCTIONAL IMAGE	134
FIGURE 59: FUNCTIONAL IMAGE WITH NORMALIZED INTENSITIES.	135
FIGURE 60: TEMPORALLY FILTERED FUNCTIONAL IMAGE.	136
FIGURE 61: INDEPENDENT COMPONENT NUMBER 1 TIMECOURSE AND POWERSPECTRUM OF TIMECOURSE.	137
FIGURE 62: COMPONENT NO. 1 – THRESHOLDED IC MAP. ALTERNATIVE HYPOTHESIS TEST AT $P > 0.5$	138

List of Tables

TABLE 1: FMRI SOFTWARE ANALYSIS*	73
TABLE 2: TEMPLATE OF AN FMRI RESULTS TABLE.....	74
TABLE 3: PARTICIPANTS DEMOGRAPHIC DATA	93
TABLE 4: GREY MATTER REGIONS SHOWING A POSITIVE CORRELATION WITH WORKING MEMORY (NB1>NB0). EACH CLUSTER’S COORDINATES IN MNI SPACE (x, y, z), MAXIMUM Z-VALUE AND SIZE ARE GIVEN. FROM CLUSTERS (>89VOXELS), SIGNIFICANT AT $P < 0.001$ (UNCORRECTED) DIFFERENT BRAIN REGIONS WERE AUTOMATICALLY LABELED USING AAL2 TOOLBOX FOR SPM WITH THE ROI_MNI_V5 ANATOMICAL PARCELLATION DATABASE.	114
TABLE 5: GREY MATTER REGIONS SHOWING A POSITIVE CORRELATION WITH WORKING MEMORY (NB2>NB0). EACH CLUSTER’S COORDINATES IN MNI SPACE (x, y, z), MAXIMUM Z-VALUE AND SIZE ARE GIVEN. FROM CLUSTERS (>75VOXELS), SIGNIFICANT AT $P < 0.001$ (UNCORRECTED) DIFFERENT BRAIN REGIONS WERE AUTOMATICALLY LABELED USING AAL2 TOOLBOX FOR SPM WITH THE ROI_MNI_V5 ANATOMICAL PARCELLATION DATABASE.	115
TABLE 6: PARTICIPANTS DEMOGRAPHIC DATA	119

List of Equations

EQUATION 1: LARMOR EQUATION IN MRI [142].	26
EQUATION 2: SIGNAL-TO-NOISE RATIO IN MRI	37
EQUATION 3: GENERAL LINEAR MODEL EQUATION	55
EQUATION 4: T-STATISTIC	56

List of Acronyms

2D	Two-Dimensional	GE	Gradient Echo
3D	Three-Dimensional	GRE	Gradient Refocused Echo
ATP	Adenosine Tri-Phosphate	HRF	Hemodynamic Response Function
ASL	Arterial Spin Labeling	HbO₂	Oxygenated Hemoglobin
ANOVA	Analysis of Variance	Hb	Deoxygenated Hemoglobin
ANCOVA	Analysis of Covariance	ICA	Independent Components Analysis
AFNI	Analysis of Functional NeuroImages	LCD	Liquid-Crystal Display
BCI	Brain-Computer Interface	MEG	Magnetoencephalography
BCT	Brain Connectivity Toolbox	MRI	Magnetic Resonance Imaging
BOLD	Blood Oxygenation Level Dependent	MVPA	Multi Voxel Pattern Analysis
CO₂	Carbon Dioxide	MNI	Montreal Neurological Institute
CBF	Cerebral Blood Flow	NMRI	Nuclear Magnetic Resonance Imaging
CBV	Cerebral Blood Volume	PCA	Principal Components Analysis
CMRO₂	Cerebral Metabolic Rate of Oxygen	PET	Positron Emission Tomography
CT	Computed Tomography	PLS	Partial Least Squares
CSF	Cerebrospinal Fluid	PNS	Peripheral Nerve Stimulation
CNR	Contrast-to-Noise Ratio	PSF	Point Spread Function
CVU	Connectome Visualization Utility	RF	Radiofrequency
DTI	Diffusion Tensor Imaging	rtfMRI	Real-time fMRI
dMRI	Diffusion MRI	RS-fMRI	Resting State fMRI
DC	Direct Current	RSN	Resting State Network
DCM	Dynamic Causal Model	ROIs	Region of Interest
EPI	Echo-Planar Imaging	SAR	Specific Absorption Rate
EEG	Electroencephalography	SNR	Signal-to-Noise Ratio
EV	Explanatory variables	SEM	Structural Equation Modelling
FA	Flip Angle	SEEP	Signal Enhancement by Extravascular Water Protons
FDR	False Discovery Rate	SPM	Statistical Parametric Mapping
FCA	Fuzzy Clustering Analysis	T	Tesla
FOV	Field of view	TR	Repetition Time
FWEs	Family-Wise Errors	TE	Echo Time
fMRI	functional Magnetic Resonance Imaging	TI	Inversion Time
FWHM	Full Width at Half Maximum	VASO	Vascular-Space-Occupancy
fNIRS	functional Near Infrared Spectroscopy	V	Voxel Volume
FSL	FMRIB Software Library	QA	Quality Assurance
GLM	General Linear Model		

1 - Introduction

We are living in an exciting era, marked by an unprecedented rate of technological changes and constant advances in multiple domains that include engineering, life sciences and healthcare. In this process, Biomedical Engineering positions itself as a crucial class to make the link between these different areas and boost the creation of outstanding inventions that ultimately help people to live a better, longer and healthier life.

Many of the advances have been fueled by the continuously increasing computational power and potentiated by information technologies. From its application to the medical domain, the specific branch of Medical Informatics emerges from the Biomedical Engineering field. It is now a difficult exercise to imagine healthcare being provided without, for example, the use of digital imaging applications or where the patients' medical record is not stored electronically. On the other hand, it is a relatively easy exercise to imagine a future where for example image guided robot-assisted remote telesurgery, or brain-computer interfaces will become common practice.

There are many specialties within Medical Informatics that have revolutionized healthcare; one good example is Medical Imaging. Being defined as a relatively new multidisciplinary field that intersects with the biological sciences, health services, information sciences and computing, medical physics, and engineering, it touches every aspect of the imaging chain and forms a bridge between imaging and other medical disciplines [1]. Within the most used medical imaging modalities one will find X-rays, ultrasound, nuclear medicine and Magnetic Resonance Imaging (MRI). The latter is of particular interest as it is non-invasive, not using ionizing radiation, and portray anatomical details with superior resolution (on the order of 1 mm or better), in three dimensions, allowing excellent differentiation of soft tissues.

Since its inception, medical imaging has provided a huge contribute to the understanding of the structure and functioning of the different components of the human body. However, our expedition seems to be just starting when it comes to the most mysterious and complex organ in our body, the human brain. From all the human

body structures, brain outstands as being essential to life, commanding and controlling all the body. Due to the difficulty in accessing its complex network of interactions it is one of the most difficult organs to study and understand, both in structure and in function. The area responsible for studying the structures of the brain and its respective functions through the use of imaging techniques is called Neuroimaging and has several modalities such as Positron Emission Tomography (PET), Computed Tomography (CT), Electroencephalography (EEG), Magnetoencephalography (MEG), and MRI.

Neuroimaging can be divided into its two interconnected categories, structural and functional neuroimaging. Within functional neuroimaging, the most used technique is functional Magnetic Resonance Imaging (fMRI), which is a powerful non-invasive tool, that uses MRI technology to detect neuronal activity, being used, for example, by psychologists, psychiatrists, and neurologists, to study how the human brain functions and is organized.

1.1 - Brief history of fMRI

MRI is based on the principles of nuclear magnetic resonance (NMR); a spectroscopic technique used to acquire microscopic chemical and physical information about molecules [2]. The beginning of this new science field is recognized to Bloch and Purcell who independently discovered NMR in 1946 [3] [4] [5]. They figured out that it was possible to detect a signal (voltage in a coil) when one places a sample in a magnetic field and irradiate it with radiofrequency (RF) energy of a certain frequency, the resonant or Larmor frequency. The signal is produced by the interaction of the sample nuclei with the magnetic field.

A few decades later, in 1973, Lauterbur [6] and simultaneously Mansfield [7] used the previously mentioned discoveries and added to it magnetic field gradients. This development allowed them to acquire spatial information in NMR experiments, and with that to produce the first 2D and 3D images by NMR, known as MRI. It might be more accurate to refer to this field as Nuclear Magnetic Resonance Imaging (NMRI) rather than MRI, but because of the negative connotations associated with the word

nuclear during the cold war years, this word has been suppressed, having the public and the profession embraced the MRI acronym. Although, the nuclear component simply refers the role of the 'spin' of the nucleus in the process [8].

In the late 1970's the introduction of Fourier transform imaging techniques by Ernst [9], and the development of echo-planar imaging (EPI) technique by Mansfield [10] have tremendously accelerated the development of MRI, setting the foundations to decrease the imaging time from hours to just a few seconds.

In 1990 Ogawa [11] discovers the contrast dependent on blood oxygenation (stated as BOLD – blood oxygenation level dependent) and since then fMRI use has grown exponentially, as it can be observed by the number of fMRI publications in figure 1 [12].

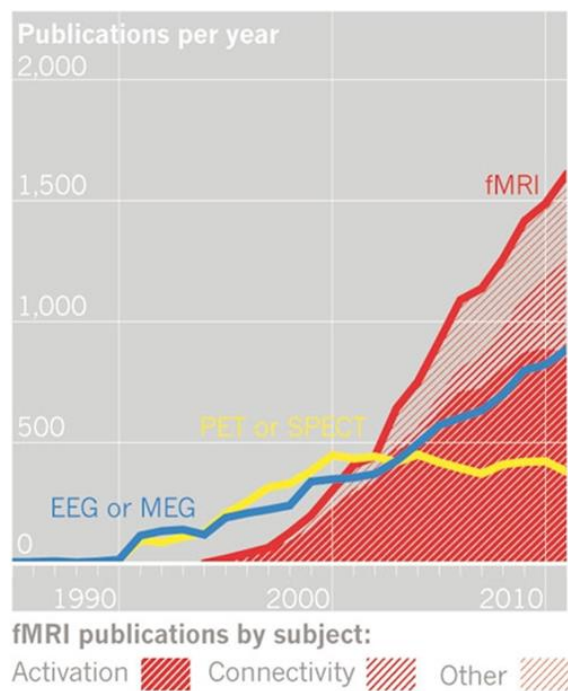


Figure 1: Evolution of neuroimaging publications. Data from ISI Web of Knowledge [12].

1.2 - Context

The exponential growth of fMRI studies arises from its capacity to give high-quality visualization, typically displayed as a statistical map, of the location of activity in the brain, resulting from sensory stimulation, cognitive function or even resting state fluctuations. Compared to other functional neuroimaging methods, fMRI offers much higher spatial resolution and it is entirely non-invasive, which has allowed to improve the mapping of the functional parcellation in the human brain [13]. fMRI is now well established in many centers, and to support its ever-increasing availability is the fact that it uses similar imaging techniques and the same equipment as conventional MRI, which is extensively used for radiological diagnosis.

The main concept behind fMRI is that, as the neurons in the brain function, they consume glucose and oxygen, supplied by the blood flow. The higher the neuronal activity in one location of the brain is, the more blood and, therefore, the more oxygen, flows there. The blood oxygen levels also vary proportionately to how quickly the active neurons are consuming oxygen; the higher the activity, the faster oxygen is consumed [14]. The majority of the fMRI techniques are based on the detection of the localized MRI signal variations linked to increased blood flow at sites of neural activity, such as may be produced, for example, by a stimulus or task. It takes advantage of the oxygenation-dependent magnetic properties of hemoglobin and its interaction with the surrounding, the so-called blood oxygenation level dependent (BOLD) contrast. Specifically, deoxygenated hemoglobin tends to reduce the local MR signal within and around the blood vessels [15].

There is a long tradition in fMRI neuroscience to investigate the differential neuronal responses to stimuli and activity during task performance. Typical studies involved comparing periods of brain activation during a task against periods of a matched baseline task or a "rest" condition (supposed that neural circuits were apparently quiescent without an external stimulus) [16-20]. However, evoked activation is in fact, only the tip of the iceberg in brain functioning. More recently, a new perspective in functional imaging has brought the recognition that spontaneous/intrinsic brain activity is crucial to the normal brain functioning. Technical advances in neuroimaging methods have contributed to this paradigm shift, instigating

new insights to interpret the brain as a network of functionally connected (co-activated) interacting regions, focused on understanding patterns of activation rather than localized blobs [21-27]. Refer to figure 1 for fMRI “activation vs. connectivity” publications plot.

Constantly gaining increased popularity among clinicians and researchers, fMRI is presently a promising tool for studying the brain function in living humans, both in healthy conditions and in disease. However, it has a complex workflow (summarized in figure 2) that implicates knowledge of paradigm design, imaging artifacts, complex MRI protocol definition, a multitude of preprocessing and analysis methods in several software packages, statistical analyzes, and in results interpretation. In addition, fMRI data can be analyzed with a large quantity of commonly used tools, with minor consensuses on how, when, or whether to apply each one. This situation may introduce considerable variability in the analysis outcome. A recent publication [28] identified 6912 slightly different paths through the analysis pipeline, resulting in 34560 different sets of results for the same dataset. Several papers and books describing the main technical issues and pitfalls related to both intrinsic and evoked fMRI analyses have been published [29-36].

However, given the exceedingly complex data processing, constant methodological advances and the increase in fMRI applicability across clinical and research domains it becomes tough for newcomers to fMRI to know even where to start on such a complex information scattered space.

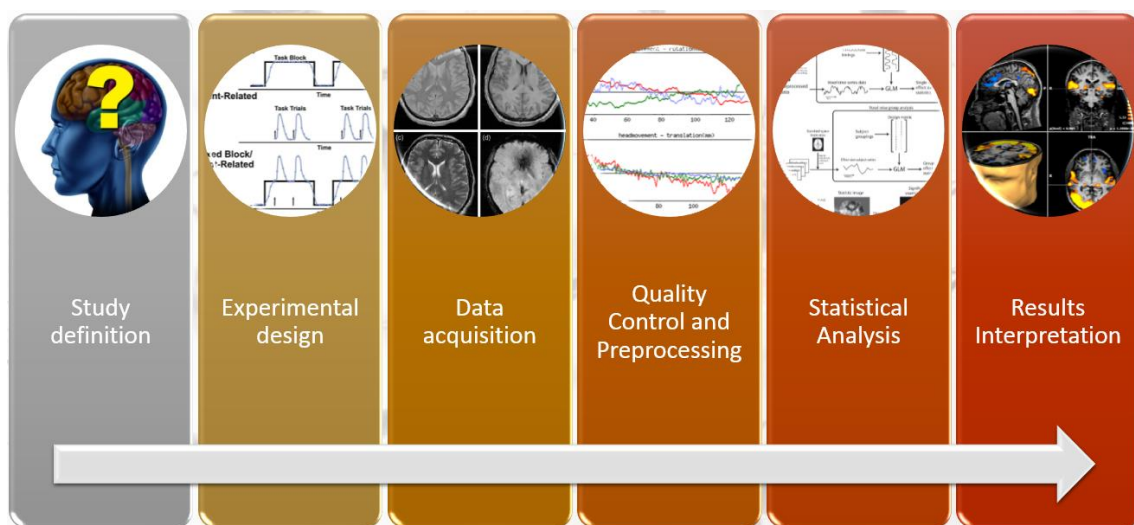


Figure 2: Workflow of a typical fMRI study

1.3 - Objectives

Taken into consideration the complexity previously described, this dissertation aims to compile a practical guide of crucial information and essential references to consider in setting up fMRI studies, optimizing data quality, and interpreting results. All the major stages are covered with the aim to ultimately help the fMRI beginner researcher and clinician to consider and overcome the most significant difficulties along the process, expanding the use of this imaging technique. To validate the proposed guide, 2 practical cases will be analyzed, one with task stimulation and one during resting-state fMRI, reporting all the workflow details from the fMRI idea to the final results interpretation.

2 - Application fields

In the last 25 years, fMRI has grown, matured and gained widespread acceptance and utilization. With a vast impact in the neuroscience domain, it has overtaken other modalities as the predominant mean for detecting changes in brain activity [37-40]. As previously mentioned, fMRI can give high visualization quality of the location of activity in the brain resulting from, for example, sensory stimulation, cognitive function or motor function, being then widely used for mapping the human brain. It allows the study of how the healthy brain works, how it is affected by different diseases, how it recovers from damage and how drugs can modulate activity or post-lesion recovery [31, 34, 41-43].

2.1 - Presurgical planning and neuronavigation

Starting purely as a research tool, fMRI was quickly adopted for clinical purposes and has now a limited but growing role in clinical neuroimaging. The best developed clinical application involves the use of fMRI for presurgical evaluation of functional areas prior to brain surgery [44]. Preoperative mapping has revolutionized the neurosurgical care of brain tumor patients and is now a valid and widely available clinical application of fMRI [45]. By mapping, for example, brain auditory, visual, motor and language areas, and identifying healthy brain tissue near a site of operable brain abnormality, it serves as a tool to determine resectability, to estimate surgical risk and the necessity for intraoperative monitoring [46-48]. Maximizing resections more safely have improved diagnosis, optimized treatment algorithms, and significantly decreased potentially devastating postoperative deficits associated with injury to functional brain networks [49, 50]. Although fMRI is a useful preoperative tool, it is not perfect. Tumors and vascular malformations can affect the normal vascular coupling of neuronal activity, the basis of BOLD fMRI, and thereby produce false-negative fMRI results. Due to this limitation fMRI is typically used as a complement to other methods, typically integrated into neuronavigation systems. To cross-validate fMRI results, each fMRI activation cluster is usually verified by intraoperative electrocortical stimulation during awake surgery [51, 52].

2.2 - EEG-fMRI

The multimodal EEG-fMRI approach, by combining evoked potentials with fMRI, presents an accurate way to detect eloquent cortical areas, assisting in the planning of neurosurgery or rehabilitation, and overcoming the previously mentioned limitation of fMRI, especially concerning its temporal resolution. Currently, the most promising application of this technique lies in epileptic surgery, through the detection of cortical areas involved in epileptic activity [53-55].

2.3 - Radiotherapy

The identification of functionally critical areas by fMRI, complemented by Diffusion Tensor Imaging (DTI), allows target delineation and critical organ avoidance when constructing treatment plans for brain radiotherapy. It constitutes a major step forward as conventional radiotherapy of brain tumor is ineffective, due to imprecisions in target delineation, inadequate radiation dose, and difficulties in identifying radio-resistant high-grade tumor for dose escalation [56-58].

2.4 - Consciousness disorders

An emerging field of clinical application for fMRI (specifically resting-state) is the evaluation of cerebral function in patients with consciousness disorders such as coma, vegetative states or minimally conscious state [59-61]. Neuroimaging, including fMRI, has started a new era of coma and consciousness science. It is transforming the clinical care, diagnosis, and prognosis of patients suffering such disorders, with profound implications in the ethical and medical–legal decision-making process. It is also starting to address more basic scientific questions regarding the nature of consciousness and the neural representation of thoughts and intentions [62, 63].

2.5 - Resting-State fMRI

The study of consciousness and differential diagnosis of its disorders is supported, in between others, by an emerging method of fMRI which is resting state

fMRI (RS-fMRI). It is distinctive for measuring spontaneous low-frequency fluctuations in the BOLD signal, occurring in the absence of a task or stimulus, and investigates synchronous activations between regions that are spatially distinct, in order to identify resting state networks (RSNs).

Though clinical applications of RS-fMRI are still limited, many prospective clinical applications are being explored, including presurgical planning for brain tumor and epilepsy patients, and the identification of biomarkers for the diagnosis of Alzheimer disease and various other neurologic and psychiatric illnesses (e.g. Multiple Sclerosis, Parkinson) [27, 64-67]. In addition, RS-fMRI is used in combination with other MRI techniques to study *in vivo* human brain development, perinatal brain injury and developing brain of premature births. Being noninvasive and not demanding patient collaboration makes RS-fMRI particularly advantageous for use with patients who are not capable of following the currently available methods of fMRI paradigm studies [68, 69]. A novel approach has just been published, and it is believed to finally widespread the clinical application by reliably providing a unique, personalized map of the different functional networks of an individual's brain [70].

2.6 - Real-time fMRI and neurofeedback

Another technique that received increased attention in recent years is real-time fMRI (rtfMRI) and specifically its application to neurofeedback, i.e. biofeedback of neuronal responses. In rtfMRI technique, the fMRI data is simultaneously processed and presented, as it is being acquired, in nearly real-time, and in an incremental way (new incoming data is included in the statistical model as it is acquired) [71]. This can be used as immediate data quality assurance; control changes of subject's attention and performance; rapid functional localizers guiding the main fMRI experiment or surgical interventions; and brain-computer interfaces (BCI) for neurofeedback, in which the subject sees images of its own brain activations, in real time while laying in the scanner. rtfMRI allows for BCI with a high spatial and temporal resolution and whole-brain coverage, which is capable of translating brain activity into digital code and be used for communication and control of devices. Its clinical application with the most potential is the use of rtfMRI-BCI to neurofeedback, allowing the subjects to acquire control over

their own brain activity. In patients with neuropsychiatric disorders, this control can potentially have therapeutic implications. Promising results have been achieved in disorders such as chronic pain, Parkinson disease, tinnitus, stroke, depression, and schizophrenia. The potential use of neurofeedback as a supplementary treatment is not limited to psychiatric diseases but might also be applied to lifestyle diseases such as obesity or addiction [71-80].

2.7 - Pharmaco-fMRI

As mentioned already, fMRI has the potential to provide biomarkers for several diseases and disorders, thus facilitating diagnosis and helping to predict which individuals are at higher risk to later develop the disorder. In addition, it provides a scientific basis for the development of novel pharmacological approaches [81-83]. fMRI offers an unparalleled opportunity to assess and compare how different drugs affect human brain activity and to provide systems-level predictions for how new drugs will affect the brain. Such key metric can increase confidence in early decision-making, thereby improving success rates, reducing risk, development times and costs of drug development, ultimately accelerating drug discovery [84-90]. The growing interest in pharmaco-fMRI is confirmed by the more than 455 different drugs being investigated worldwide in 438 fMRI clinical studies, out of a total of 1423 currently registered at the U.S. National Institutes of Health [91].

2.8 - Commercial applications

There have been several projects to capitalize on fMRI, all being quite controversial and raising social, ethical and legal issues [92]. Investigation in the neurolaw field is increasing, and some tentative have been made to bring fMRI to the court, though not being yet considered sufficiently reliable to be considered as evidence. Lie detection using fMRI has been performed, and even two companies have been set up in North America offering this service [93-97]. On a purely business field, several neuromarketing companies are using fMRI to gain insights into consumer thought and behavior [98, 99].

3 - fMRI Signals

The human brain represents only 2% of the total body mass, however, it consumes 20 to 25% of all the energy that the body produces in its basal state. For all the neural signaling processes it requires energy in the form of adenosine triphosphate (ATP). Despite this vital high cerebral energetic demand the brain has very limited means of energy storage, therefore, normal brain activity depends on the continuous supply of oxygen and glucose through cerebral blood flow (CBF). To enable neuronal function and respond to peaks of energy demand, the brain has developed mechanisms that increase the flow of blood to regions in which neurons are active, a process designated as hemodynamic response to the neural event. Hence, local brain activity has to be matched with a concomitant increase in local CBF, the neurovascular coupling, constituting this phenomenon the key of fMRI signal [100-103].

The exact mechanisms of neurovascular coupling are unknown, but one well-accepted theory is that, as mentioned before, when a task activates a region or network of brain regions there is a local increase in energy demand, resulting in increased cerebral metabolic rate of oxygen ($CMRO_2$) in the vicinities of active brain region(s) [104]. As glycolysis transiently consumes the local reserves of oxygen in tissues adjacent to capillaries, byproducts build up, and various chemical signals (CO_2 , NO , H^+) trigger a vasomotor reaction in arterial sphincters upstream of the capillary bed, with consequential dilation of these vessels. The increased blood flow acts to restore the local $[O_2]$ level required to overcome the momentary deficit. However, still inexplicably, more oxygen is delivered than what's needed to simply balance the increase in $CMRO_2$. This results in an initial build-up of deoxygenated hemoglobin [Hb] and a decrease in oxygenated hemoglobin [HbO_2] in the intra- and extravascular spaces. Followed, within a second or two, by a vasodilatory response that reverses the situation to result in a decrease in [Hb] and a significant increase in [HbO_2] compared to the resting condition [100, 105, 106]. This locally increased CBF and changes in hemoglobin oxygenation (BOLD contrast) can be detected by MRI and are the source of fMRI signals.

3.1 - BOLD

S. Ogawa has first demonstrated BOLD contrast in 1990 [11, 107, 108] and since then it was adopted by most of the fMRI studies. Such that it is commonly mistakenly assumed that 'fMRI' means 'BOLD', and vice-versa, when in fact these have two very different meanings.

The exact mechanisms of neurovascular coupling are unknown, but the physical origins of the BOLD signal are reasonably well understood. The BOLD contrast is closely linked to a physical phenomenon called magnetic susceptibility, and its difference in oxy- and deoxy- hemoglobin. Susceptibility quantifies the degree to which a substance becomes magnetized when it is placed in an external magnetic field, in this case, the MRI scanner. When matter interacts with the magnetic field, an internal magnetization or polarization (J) is created that either opposes (diamagnetism) or augments the external field (paramagnetism) [109].

Nearly all biological tissues are weakly diamagnetic. This includes fully oxygenated hemoglobin (HbO_2) which consequently is magnetically indistinguishable, in terms of susceptibility, from brain tissue. However, fully deoxygenated hemoglobin (Hb) has four unpaired electrons and is highly paramagnetic [110] being then a natural contrast agent for MRI [11, 108]. Its presence in the blood leads to susceptibility gradients, i.e. local non-uniformities in the magnetic field. These gradients exist mainly near the vessels because of their high Hb content, and their size and strength depend on the vessel size and Hb concentration among other things. Spins within these microscopic gradients experience additional dephasing, which leads to MRI T_2^* based signal loss, as represented in figure 2 [13].

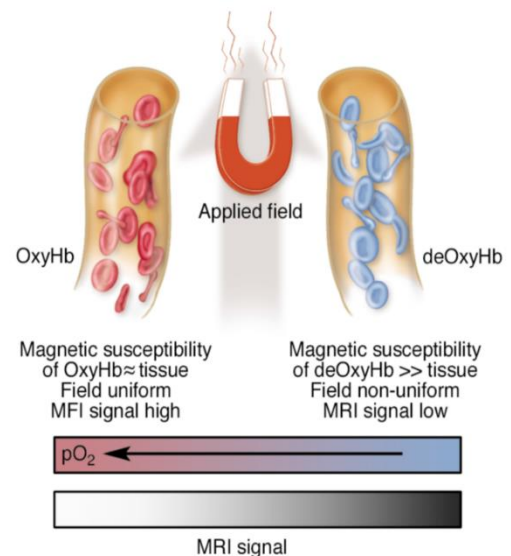


Figure 3: Schematic illustration of the origins of the BOLD effect in fMRI [46].

Thus, by making the MRI acquisition sensitive to $T2^*$ it is possible to detect tiny signal variations, caused by brain activity, which follow the hemodynamic response function (HRF) profile. The maximum signal variation is typically in the order of ~2 to 3% and is delayed of around ~5 to 6s from the stimulus. Subsequently, when the stimulus is turned off, the signal takes ~10 to 12s to return to baseline. However, instead of returning directly back to baseline, the BOLD signal decreases below its initial level for a short period, referred to as the post-undershoot [105]. This relatively long hemodynamic response was initially considered a limiting factor for the temporal resolution of fMRI studies. Though with experimental design techniques, it is possible to improve significantly the temporal resolution [111].

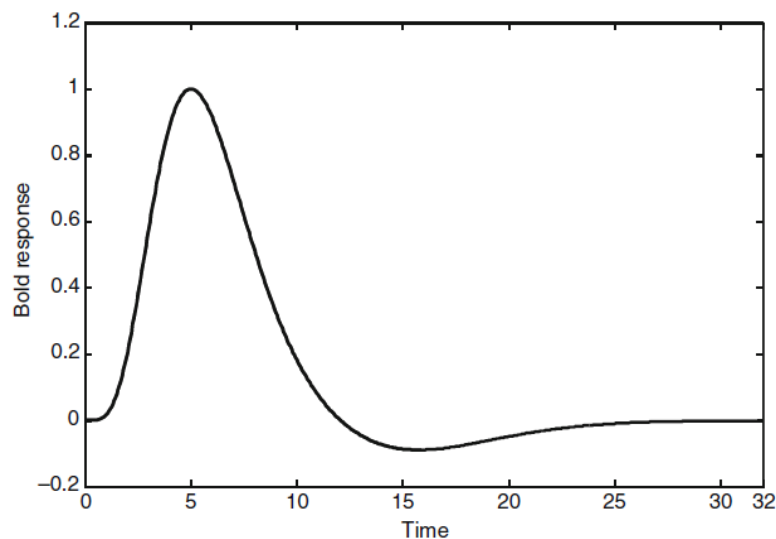


Figure 4: Canonical hemodynamic response function (HRF). This is the typical BOLD response to a single, impulse stimulation [111].

It is important to highlight that the activation signal measured with BOLD fMRI is based on indirectly measuring changes in the concentration of deoxyhemoglobin that arise from the increase in blood oxygenation in the vicinity of neural firing. This signal is dependent on both the underlying physiological events and the imaging physics. BOLD contrast, although sensitive, is not a quantifiable measure of neural activity [112].

3.2 - ASL

Another way to sense brain activity is by detecting changes in local CBF. These changes can be observed using an injected contrast agent and perfusion-weighted MRI, first demonstrated by Belliveau [113], or non-invasively by arterial spin labeling (ASL) [100, 114].

ASL is a magnetic resonance method for the measurement of cerebral blood flow. In this technique, intravascular water flowing to the brain is saturated in the neck region with a slice-selective saturation imaging sequence, generating an endogenous tracer in the form of proximally saturated spins. These magnetically labeled water molecules flow to the activated brain region and interact with tissue water, altering the tissue magnetization and consequently the MR signal [114]. In its simplest form, the perfusion contrast revealed by this technique comes from the subtraction of two sequentially acquired images: one with, and the other without, proximal labeling of arterial water spins [115].

The utility of ASL perfusion fMRI in drug development and validation is currently being explored. ASL methods are quantitative, stable over time and less variable across subjects. These properties make ASL an especially useful noninvasive method to measure CBF in longitudinal and treatment studies [116]. It is also well suited for examining neural responses to pharmacological agents and abstinence states as these are sustained effects lasting hours or longer [117].

However, compared with the BOLD contrast method, ASL suffers from reduced sensitivity, presents longer acquisition time, and increased sensitivity to motion. Therefore, its use is more centered in modeling the neurobiological mechanisms of activation and vasoreactivity, rather than in standard mapping of brain function [33, 100, 104, 106].

3.3 - VASO

Vascular-Space-Occupancy (VASO) fMRI is a non-invasive, dynamic, and repeatable method for mapping brain function based on changes in Cerebral Blood Volume (CBV). It explores the T_1 differences between blood and adjacent tissue and

uses an inversion recovery pulse sequence to attenuate blood signal while maintaining part of the tissue signal. When neural activation causes CBV to increase, the VASO signal shows a decrease, allowing the detection of activated regions in the brain. This technique complements the previously referred fMRI methods, BOLD and ASL, providing a better understanding of the metabolic and hemodynamic changes resultant from neural activation and also improving the quantification of extravascular BOLD signals. Its sensitivity is the primary disadvantage when compared with BOLD but with technical developments in image acquisition and processing, VASO fMRI has the potential to be a valuable tool in neuroscience and clinical applications [118, 119].

3.4 - SEEP

Signal enhancement by extravascular water protons (SEEP) is a contrast mechanism for fMRI that rose from the findings that at short echo times, spin-echo sequences showed signal changes with significant deviations from the BOLD model, suggesting a second, non-BOLD component of signal change [120].

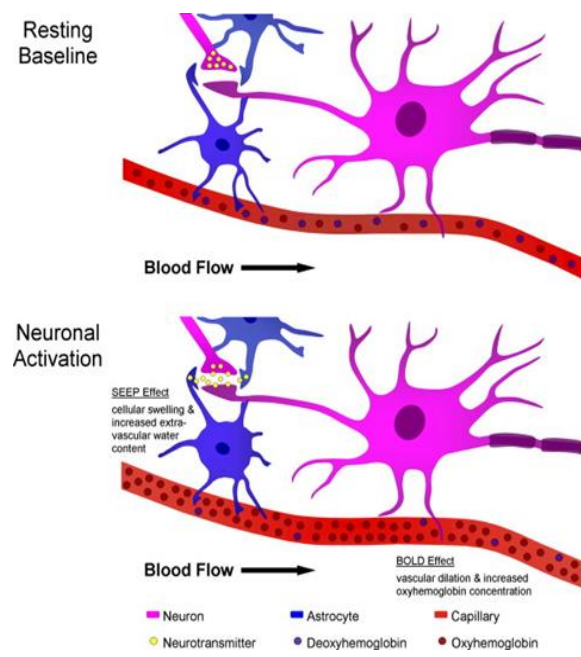


Figure 5: Signal enhancement by extravascular water protons, SEEP [122].

SEEP contrast is based on variations in tissue water content that result from the increased production of extracellular fluid, together with neuron and neuroglia cellular swelling at sites of neuronal activity [121]. As the primary sources of MRI signal in biological tissues are water and lipids, a rise in tissue water content leads to a local increase in MR signal intensity. These image contrast changes correspond to changes in neuronal activity, and as such changes are independent of magnetic susceptibility, SEEP

offers new and improved possibilities for carrying out fMRI in regions that may not be ideal for BOLD imaging. Such as those near air–tissue and bone–tissue interfaces as well as regions close to large blood vessels [122].

3.5 – Detecting Neuronal or Glial activity?

In the neuroscience community, there is a consensus that despite its immense complexity, the human nervous system, in its most elementary form, is composed of two general cell types – neurons and neuroglia. However, concepts of how neuronal activity is coupled with the vascular supply of glucose and oxygen are the subject of intense debate and are changing rapidly.

Traditionally, it was thought that active neurons generate a metabolic signal (CO_2 , NO, H^+) which triggers an increase in blood flow. This idea has recently been challenged, following the discovery that neurotransmitter-mediated signaling, particularly by glutamate, has a major role in regulating cerebral blood flow and that much of this control is mediated by astrocytes – a particular type of neuroglia [101]. Furthermore, it is suggested that astrocytes are responsible for the metabolic and hemodynamic changes detected with fMRI [123].

Several studies [101, 103, 123-126] have revealed that most functional neuroimaging techniques (including those based on BOLD, VASO, ASL, SEEP) are, in fact, more closely tied to the underlying functioning and metabolic activity of astrocytes than of neurons [127]. Additional findings by Yevgeniy B. Sirotnin, also contest the current understanding of the connection between brain hemodynamics and local neuronal activity. They suggest the existence of a mechanism in the brain that brings additional arterial blood to cortex in anticipation of expected tasks [128].

In light of these recently reported disparities between hemodynamic and neurophysiological changes some investigators are suggesting that a revised interpretation of functional neuroimaging signals is necessary and that it might involve going beyond the traditional assumption that these signals are based exclusively on neuronal processes [123].

4 - Experimental Design

fMRI is based on detecting the slight MR signal variations indirectly caused by neural activity. Therefore, it is crucial to induce a signal that is as strong as possible. A key concept that is common to every fMRI study is that the neuronal activity of interest must be systematically optimized so that any voxels that change signal intensity in relation to this activity can be detected. Typical fMRI studies compare sets of images, acquired during two or more different conditions, using some form of statistical analysis. Multiple recordings of the MRI signal allow a degree of signal averaging that increase the statistical reliability of the results. The focus of fMRI study design is, therefore, to determine which tasks or stimuli can be compared to reveal the optimal neuronal activity of interest, and the most efficient timing for applying it [34, 46, 129].

It is important to design the study to detect specifically the function(s) of interest, unambiguously from other neuronal functions or other sources of signal change, such as random noise and physiological motion (respiration and cardiac pulsatility). The choices of tasks or stimuli and how they will be compared must be guided by a clear hypothesis, which is a statement of the proposed result, formed in a way that it can be tested, and shown to be either true or false. By having a clearly defined question to answer, the expected result can often be stated as the hypothesis, being often this the first step to take when defining a new fMRI study [129].

Commonly, an fMRI task activation experiment utilizes visual, auditory or other stimuli to alternately induce two or more different mental states in the subject while continuously collecting MRI volumes. With a two-condition design, one state is called the experimental condition, while the other is denoted the control/baseline condition, and the goal is to test the hypothesis that the signals differ between the two states [100]. There is no single fMRI study design that is optimal for all situations. Therefore, researchers have developed different approaches to design the fMRI studies. The main ones will be discussed in this chapter. By understanding the key elements that affect the sensitivity and effectiveness of fMRI results, and by having a precise question to investigate, many of the design choices become clear. It is important to remark that there are several software packages that, in addition to present the stimuli to the subjects, help the researcher to define and simulate the intended study design [129].

4.1 - Block paradigm

The classic design of an fMRI experiment is a block design of stimulus presentation, with individual trials or events tightly clustered into “on” periods of activation alternated with equally long “off” control/baseline periods [130]. In a typical study, task blocks duration range from ~16s to a minute and, multiple task blocks will be presented in a single fMRI run (continuous period of data acquisition), to allow the contrast of fMRI signals [131]. With this design, the neural activity produces a relatively strong BOLD response that reaches a peak after about 6s and images can be obtained at multiple time points during the response so that it can be detected with high sensitivity [129].

The voxels within the brain that are affected by the stimulus provide a set of data points in which the signal intensity alternate in synchrony with the stimulation, as a result of the BOLD effect. By detecting which voxels show this alternating pattern, different functional areas of the brain can be identified [46].

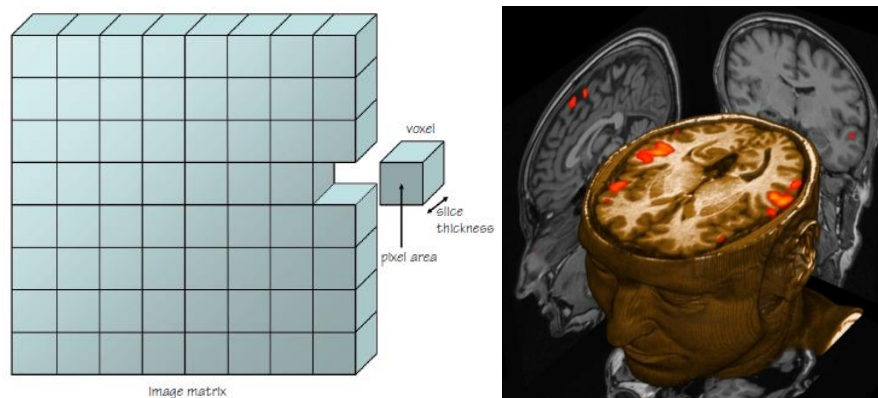


Figure 6: Representation of a Voxel (volume element). Represented in red the voxels where functional activation was detected [145].

The block design is easy to implement and can be used to identify and localize several basic functions as: (i) primary sensory areas, e.g., by presenting auditory stimuli versus silence; (ii) motor areas, by finger tapping versus no movement; (iii) higher-order visual areas, by displaying faces versus objects and identify regions that respond

preferentially to faces; and (iv) higher-order language areas by presenting speaking versus other complex sounds [46].

Furthermore, while this method provides optimum statistical power, it also presents a variety of potential confounds, including changes in attention, alertness, expectancy, task habituation and practice effects within and between blocks [132].

4.2 - Event-related paradigms

An alternative to block design is to present the stimulus in an unpredictable and randomized sequence, the event-related paradigm. This technique is used since decades by EEG studies, and while it offers many advantages, it comes with certain costs. Each stimulus will evoke BOLD activity that is only a fraction of the maximum possible. Therefore, by reducing the mean number of stimuli presented per second, there is a reduction both in the absolute magnitude of BOLD signal and the resulting signal contrast between conditions [132]. Many repetitions are necessary to compensate for the lower signal-to-noise ratio. Consequently, it frequently takes longer to acquire sufficient data in event-related designs than for blocked studies, which can lead to fatigue of the subjects and, particularly in clinical patients, less tolerance and compliance with the fMRI paradigm [32].

The temporal dispersion of BOLD fMRI activity makes it challenging to perform rapid event-related paradigms using fMRI. If the interval between stimuli is sufficiently long (i.e., greater than about 10 s), the hemodynamic response decays to baseline after each stimulus. However, when events are considerably close together, special analysis procedures are used to separate their hemodynamic responses [43], in which the fMRI response is modeled as the linear summation of the hemodynamic response of discrete events [133].

By modeling brain function as a series of transient changes, rather than as an ongoing state, event-related fMRI allowed researchers to create much more complex paradigms and more dynamic analysis methods [134]. This flexibility is possible due to the assumption that the fMRI response to external stimuli is approximately the response of a linear time-variant system [133]. However, some contradict this

assumption, as it will not account for the (in particular higher level) neuronal processing occurring in most cases. There is also evidence of an upper limit for the maximum BOLD response, which implies that various cognitive processes cannot simply add up linearly or nonlinearly to ever-increasing BOLD responses [32, 135].

Although presenting some limitations, event-related designs are now a standard part of the fMRI experimental repertoire.

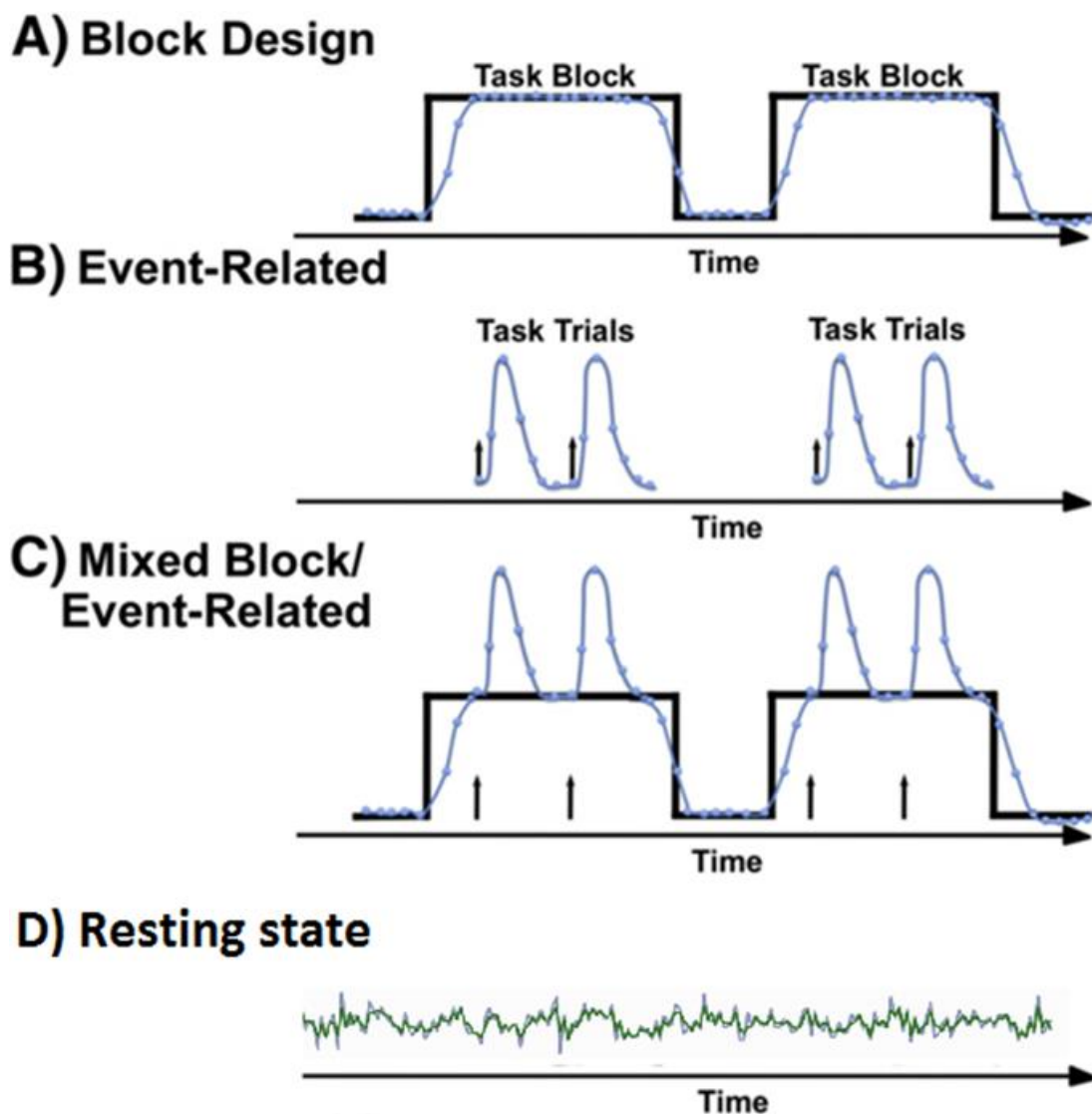


Figure 7: Typical fMRI study paradigms

4.3 - Mixed block/event-related paradigm

Although block and event-related designs brought many insights into brain functions, researchers identified that these fMRI design types ignored components of the BOLD signal that could provide additional information. The development of the mixed block/event-related fMRI design allowed for a broader characterization of nonlinear and time-sensitive neuronal responses [19].

In the mixed design, control blocks are interleaved with task blocks, during which trials are presented at varying intervals. Mixed designs allow researchers a mean to examine brain activity associated with continuous processes, potentially related to task-level control signals. Neural activity linked to task state can be distinguished from activity related to individual trials. This dissociation of effects with different temporal profiles should allow researchers to determine better which functions are served by particular activation patterns [136].

4.4 - BOLD Ceiling fMRI

The need of repetitive ON-OFF periods demonstrates a limitation of standard fMRI when mapping continuous activations, such as, for example, in subjects suffering chronic tinnitus (subject continuously hears noise or ringing even when no external sound is present). One solution to circumvent this limitation is to apply carbon dioxide (CO₂) as a potent vasodilator. CO₂ induces a BOLD response in the entire brain. The neurovascular coupling in conjunction with the limited cerebral vasodilation implies a limitation or ceiling of the BOLD response. Since the cerebral vasodilatation is limited, active areas with a preexisting BOLD response related to the task or stimulation can be detected because these areas have a diminished CO₂-induced BOLD response. This concept of BOLD ceiling fMRI was successfully demonstrated for continuous auditory activations in healthy volunteers. BOLD ceiling fMRI offers a complement to standard fMRI for those conditions where ON-OFF paradigms are impossible [32, 135].

4.5 - Resting state paradigm

Resting state fMRI (RS-fMRI) has become widely accepted as a viable technique for studying functional connectivity of the human brain [137]. Several electrophysiology studies aided in the acceptance of the resting-state paradigm as a valid neuroscience method for functional connectivity. RS-fMRI focuses on spontaneous low-frequency fluctuations (~ 0.1 Hz) in the BOLD signal and in some of these studies, it was shown that an extended coherent network of neurons activates simultaneously in the absence of any external stimulus [138]. This observation of the spontaneous firing of a group of neurons was direct evidence that, at rest, the brain is capable of activating coherent networks of neurons, the so-called resting state networks (RSNs) [137]. However the concrete meaning of these inherent processes, seemingly fundamental to the human neural functional architecture, remains elusive [66].

Numerous group resting-state studies have since then consistently reported the formation of functionally linked RSNs during task-free paradigms. These studies, although all using distinct groups of subjects, methods, and types of MR acquisition protocols, show significant concordance between their results, indicating the robust formation of functionally linked RSNs in the brain during rest. The amount and precise spatial pattern of distinct RSNs vary in the literature. Figure 7 displays the surface plots of the most consistent reported RSNs [139].

A relatively reduced number of data points, compared to task fMRI, are sufficient to identify RSNs, with the additional advantage that multiple functional networks can be derived from the same dataset. Therefore less scanning time is necessary, with typical resting experiments lasting approximately 5-10 min, in during which the subjects are instructed to relax and "think about nothing in particular" while keeping their eyes either closed or fixated on a crosshair for the duration of the scan. There is little consensus on the optimal length of a resting state session and if multiples sessions are needed. Having eyes open or close in awake subjects or having asleep subjects is also point of discussion among researchers [66, 140].

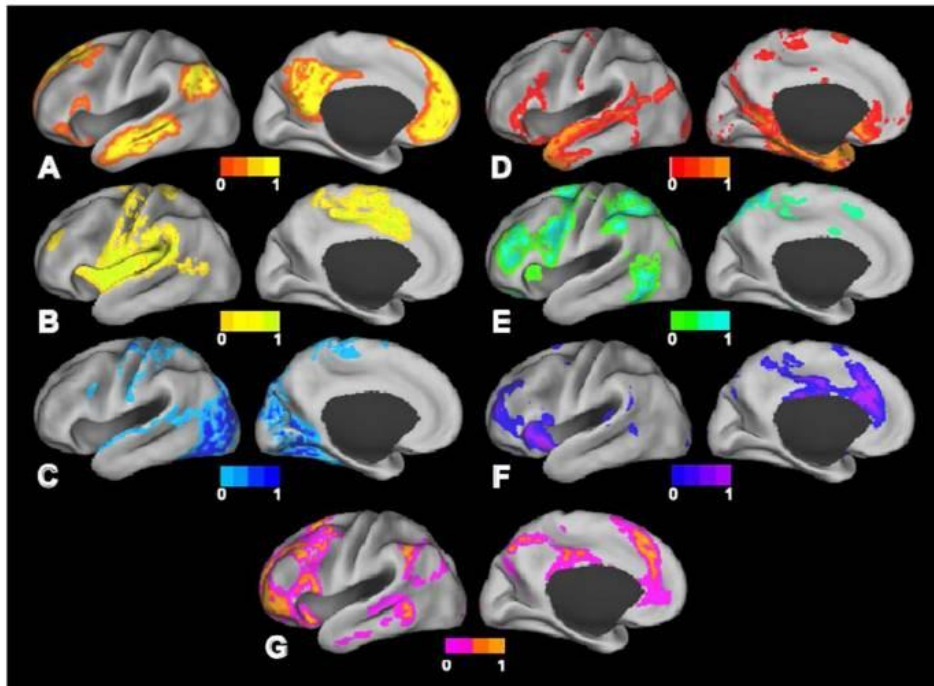


Figure 8: A- Default mode network. B- Somatomotor network. C- Visual network. D- Language network. E- Dorsal attention network. F- ventral attention network. G- Frontoparietal control network [65].

Resting state is characterized by its simple experimental design and short time to acquire a dataset from which multiple RSNs can be identified. The minimal demands on clinician and patient allow its implementation for patients with neurological deficits that are not capable of following the other currently available methods of fMRI experimental design paradigms.

5 - Data Acquisition and Artifacts

In this chapter the data acquisition and common image artifacts are discussed. Starting by describing the hardware used, basic physical principles of MRI acquisition, and considering the bioeffects of this acquisition and the necessary safety precautions. To finalize the specifics of fMRI data acquisition and common image artifacts are described. The success of the fMRI study and its outcomes is deeply connected to the quality of the data acquired.

5.1 - Hardware

For the data acquisition, fMRI uses the same equipment used for clinical MRI with often some specific extra accessories needed for stimulus presentation and response collection.

5.1.1- Environment

The MRI scanner should be placed in a controlled temperature and humidity environment; typical requisites are variability of less than 3°C per hour and 5% per hour, respectively. Normal operating ranges are in the 15–25°C temperature range and 30–75% humidity range [34].

Although modern scanners have very efficient shielding, that can drop the magnetic field strength to 0.5 mT at a four meters radius from the magnet, the scanner should be placed in a shielded room able to contain the magnetic field inside it. Doing so, prevents it from interfering with other medical or electronic equipment, for example, pacemakers, CRT monitors, that might be or pass near the scanning room.

MRI scanners construct images from RF electromagnetic signals. Thus, radio stations, mobile phones, and other wireless communications will interfere with the MRI experiment and severely degrade image quality unless they are properly isolated. MRI rooms are usually encased in a copper shield box that blocks external RF radiation and contains the MRI's RF radiation as well. The quality of the shield is crucial to the performance of the scanner [34].

5.1.2 - Magnet

Some atoms, such as ^1H or ^{13}C have a nuclear spin, and associated with the nuclear spin is a magnetic moment. In its natural state their orientation is random, neutralizing each other. However, in the presence of a static magnetic field, B_0 , slightly more magnetic moments align parallel to B_0 , and thus produce, what can be represented in a classical way, as longitudinal magnetization, M_z . Another effect is that the magnetic moments will precess (spin with a motion in which their axis sweeps out a cone, like a toy spinning top), with a Larmor (resonance) frequency [141].

$$\omega_0 = \gamma B_0 \quad \text{Equation 1: Larmor equation in MRI [142].}$$

ω_0 is the Precessional or Larmor frequency. (MHz)

γ is the Gyro Magnetic Ratio, a constant specific to each nucleus. (MHz/T)

B_0 is the Magnetic field strength. (T)

To create this potent static magnetic field, B_0 , three main magnet types can be used: permanent, resistive and superconducting. Each has advantages and disadvantages regarding cost, ease of siting, patient and physician friendliness, and image quality. The one that is mostly used and offers the best characteristics, though being the most expensive, is the superconducting magnet [143].

Superconducting magnets use the special properties of certain materials, which at temperatures approaching absolute zero (-273.16°C , 0 K) have zero electrical resistance [143]. To create the static magnetic field a current is introduced to large solenoid coils made of superconducting metal (niobium alloys, typically) that are kept cooled at approximately 4K by liquid Helium to achieve and maintain superconductivity. Once the specified current has been built up, the circuit is closed such that the current "recirculates" through the coil constantly and there is no need to supply more power to it. It is crucial to maintain the low temperature to prevent the coil from resisting the current flow [34].

The static magnetic field is oriented horizontally, defined as the z-axis, and its strength B_0 is measured in tesla (T). A 1.5 T system provides a magnetic field of $\approx 30,000$ times that of the earth, with no permanent effects on human physiology and negligible temporary alterations [141, 144]. Typically the scanner used for fMRI will have a magnetic field strength of 1.5T or greater (3T or 7T) as BOLD contrast increases with field strength, though not linearly.

Besides the strength, one must consider the spatial homogeneity and temporal stability of the magnetic field. All magnets suffer from some degree of inhomogeneity as a consequence of design limitations and compromises. Fixed shimming is used to improve the magnet homogeneity and to correct for field distortions induced by nearby ferromagnetic structures and may be performed either passively, actively, or as a combination of both. The homogeneity achievable using these fixed shims is usually adequate for imaging over relatively large volumes. One challenge is that the shape of the magnetic field changes when an object (i.e., the patient) is introduced into the field. The homogeneity may be further adjusted on a per-patient basis using dynamic shimming [143].

In addition to being homogeneous, it is quite important that the magnetic field is as constant as possible over time. The field tends to drift over time due to some factors, among them the temperature of the room and the equipment. Thus, the room temperature specifications mentioned previously. These drifts are typically subtle and slow enough that they do not affect clinical/structural imaging. fMRI, however, is based on signal subtle changes over time and therefore, field drifts act as a significant confound, especially in slow paradigms. Statistical and signal processing tools do exist to reduce these drifts effects, but it is much more desirable to minimize it during acquisition [34].



Figure 9: A superconducting magnet 1.5 T Siemens Magnetom Avanto MRI scanner (Siemens, Erlangen, Germany) at Hospital de Braga.

Superconducting magnets are usually cylindrical in shape with the patient being placed inside the bore. The bore has a size of approximately 0.4–0.6 m to accommodate the patient comfortably. Although both ends are open, patients may experience claustrophobia from being inside this ‘tunnel’ [143].

5.1.3 - Radiofrequency system

The RF system comprises a transmitter, coil and receiver units. The transmitter generates an oscillating magnetic field (pulse), through the RF coil, during a determined time. If the frequency, or range of frequencies, match the Larmor frequency (63.855 MHz at 1.5T for Hydrogen nucleus) resonance occurs which causes the longitudinal magnetization vector M_z to flip into the transverse plane M_{xy} . That will then generate a current (following Faraday’s law of induction), the MRI signal, in the same coil, which also works as a receiver [142-145].

5.1.4 - Gradient system

Magnetic field gradients are applied for slice selection and spatial encoding. A set of three separate gradient coils (G_x , G_y , G_z), usually magnetically decoupled from the main magnet through the use of a shield, is needed to alter the magnetic field strength along the x-, y-, and z-axes [144]. These three independent sets of fields are superimposed on the main static field being switched on separately or in combination, e.g. to define an oblique slice. The isocenter is the geometric center of the main magnetic field, where the field strength is not affected by any of the three gradients [146]. Currents driven through a gradient coil provide a linear change in magnetic field strength along one direction, causing the magnetic moments to have different precessional frequencies depending on location. An RF pulse with a predefined frequency range, bandwidth, can then be applied, with the result being that only those magnetic moments in resonance with these frequencies will be excited. This is the fundamental principle of slice selective excitation. The slice thickness is determined by the slope of the gradient and the RF bandwidth [141, 145].

Then two additional gradients, in the direction of the two other axes, and RF pulses are applied for spatial encoding (phase and frequency encoding). The spatial linearity of the gradients must be maintained over the volume of the sample to be

imaged, or the images will appear warped (although these distortions can be corrected during reconstruction if the true shape of the gradient is known). The spatial linearity of the gradient fields is primarily a function of the shape of the gradient coils, and a great deal of effort goes into their design and construction [34].

The gradient coils must also be able to produce magnetic field gradients very quickly and accurately. The rate at which a gradient is achieved is referred to as the slew rate. Sudden changes in the magnetic field can induce currents in the peripheral nervous system causing muscle contractions and unpleasant or even painful sensations in the patient. This phenomenon is referred to as peripheral nerve stimulation (PNS). Technology has progressed to the point where the patient is the limiting factor. Therefore, a stimulation monitor assesses the setup and prevents the recommended slew rates limits from being reached [34, 141, 145].

The gradient coils create magnetic fields that are small compared with the main field but nevertheless need a current of several hundred amperes. The changing magnetic fields generated when the gradients are switched lead to the typical banging sound heard during an MR scan. Similar to a loudspeaker, which is nothing but a coil inside a magnetic field, the gradient coils "try to move" when the current is switched on and off, which causes a noisy clanging [146].

5.1.5 - Computer system

The multi-tasking nature of MR means that it is impractical to control the many processes requiring accurate timing directly from the main or host computer, so, many subsystems will have their own microprocessors whose commands can be downloaded from the host. A typical MRI system will have a host computer (see figure 10) on which the operator will set up the scan regarding the pulse sequence, its timing, and various geometry factors. These parameters will then be converted into commands that are transferred to another microprocessor system that controls the hardware, known as the pulse programmer. It ensures that the RF, gradients, and data acquisition are all properly synchronized. Once the data have been acquired, a separate computer system known as the array processor carries out the image reconstruction. The host computer then manages the image display and processing, as for example, windowing, hardcopy production, archiving and networking [143].

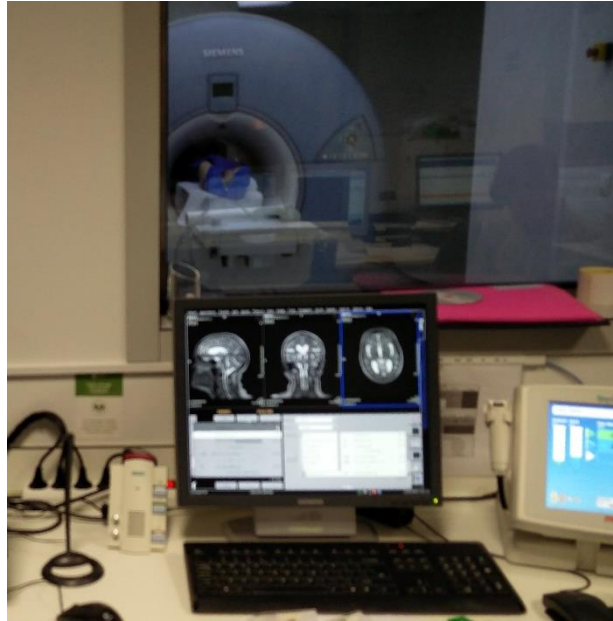


Figure 10; Host computer of the MRI system at Hospital de Braga.

5.1.6 - Stimulus Presentation and Behavioral Data Collection Devices

With the growing popularity of fMRI studies, there are now a small but increasing number of manufacturers offering hardware and software adequate for such experiments. Those are mainly divided in stimulus presentation, response collection, and experiment synchronization.



Figure 11: Demonstration of visual, audio stimuli presentation accessories and button response collection at Hospital de Braga.

A special characteristic of such hardware is that, as it needs to enter or be near the magnet, it must not be susceptible to magnetic forces (defined as MRI-ready equipment), as it would otherwise constitute a safety risk. Additionally, the presence of metals in head mounted devices (e.g. headphones, video glasses) can generate field distortions that cannot be compensated by shimming, even if they are not ferromagnetic. This results in severe image degradation, and it is thus important that the devices be thoroughly tested on phantoms for image degradation [34].

For audio stimulation and communication, the speakers and microphone are typically based on piezoelectric technology, still they require RF shielding of the cables and the electronics to prevent artifacts.

For visual stimulation many different techniques are used, being the simplest approach an LCD projector equipped with narrow focus lenses that project the images onto a back projection screen placed inside the bore of the magnet. The subject then can see the display through a set of mirrors that are mounted on the head coil assembly. The main advantages of this approach are simplicity and lower cost. The disadvantages are related to positioning issues and a reduced visual field for the subject.

Other response recording devices are primarily “button response units” that are built into hand rests and strapped to the subject’s hands. They typically carry direct current (DC) through twisted pair cables and RF noise is not an issue as the electronics to drive the system are kept outside the scanner room. There are some other response units, such as MR compatible joysticks and keyboards that are manufactured by small companies [34, 145].

To have valid fMRI results, all the previously mentioned hardware and software for stimuli presentation and response collection need to be perfectly synchronized with the image acquisition by the scanner. For each image acquisition, the MRI scanner produces a trigger signal that is used to synchronize the stimulus presentation with the image acquisition and in some cases response collection.

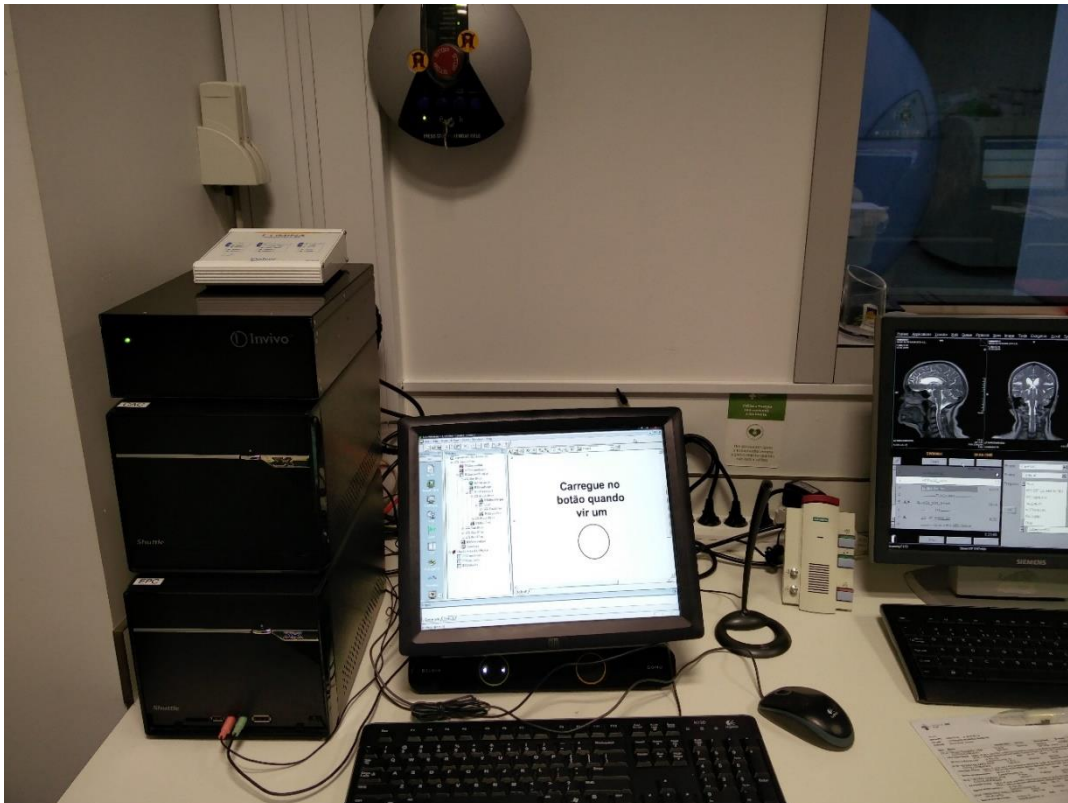


Figure 12: Stimuli presentation, response collection, and synchronization system at Hospital de Braga

5.2 - Bioeffects and Safety

MRI technology is considered to be safe and effective, as long as proper safety measures are taken into account [141]. Since its origin in the 1980s, millions of clinical MRI scans have been performed with a much-reduced number of incidents, which confirms the safety of the technology [43].

However, the few exceptions can cause severe damage and even be fatal. In 25 years there were ten documented fatalities related to MRI scans, seven of these involving persons with cardiac pacemakers, one involving displacement of an aneurysm clip, one involving a projectile and the other from an unknown cause [143].

Referring to any biological effects on the human body resulting from the contact with the MR scanner, these effects can be categorized into three categories: static field (B_0) effects; time varying field (gradient); and RF effects [147].

5.2.1 - Static field (B_0) effects

Current guidelines recommend a maximum limit of 8 T for clinical imaging rising to 12 T for research purposes and spectroscopy. Most clinical units operate at 1.5 T or 3 T [145]. There are no known long-term irreversible effects from exposure to fields below 12 T, still there are some mild sensory effects that have been reported, including vertigo, fatigue, nausea and taste sensations. These sensations happen infrequently, and it needs to be remembered that the exposure of human subjects in MRI is for short periods only and that these effects cease with the exposure [43, 143, 145].

The biggest risk of static magnetic field is the potential of turning any ferromagnetic material, even quite heavy ones, into high-speed projectiles. Those will fly from any place where the magnetic field is present (fringe field can extend to several meters away from the scanner) straight to the isocenter of the magnetic field, seriously compromising the safety of anyone sited between the object and the magnet system. Even small objects such as paperclips and hairpins pose a serious risk to the patient and anyone else present in the scan room. One must keep in mind that the magnetic field is always present, even when it is not scanning, or there is a power cut [43, 143, 145]. In the case of superconducting magnets the only way to stop it is by quenching.

Quenching is an expensive procedure (it may happen accidentally or can be manually instigated in the case of an emergency) consisting in a sudden loss of refrigeration of the magnet coils, so they cease to be superconducting and become resistive. Those will dissipate the electrical energy in the form of heat and boil the liquid helium. The rapid rate of helium boiling can build up a great deal of pressure in the magnet and also flood the room with helium gas and suffocate whoever is there. While helium is not toxic, it displaces the oxygen in the room. Thus, it is crucial that the magnet is equipped with emergency vents (manufacturers of MRI scanners typically include emergency quench ventilation systems). Additionally, magnet rooms are outfitted with sensors that sound an alarm when the oxygen level falls below safe levels [34, 145].

Due to the hazards particularly associated with projectiles, all persons entering the controlled area must satisfy a safety screening procedure. In addition, it is advised that all nursing, housekeeping, fire department, emergency, and MR personnel are

educated about the potential risks and hazards of the static magnetic field. Signs should be attached at all entrances to the magnetic field (including the fringe field), to deter entry into the scan room with ferromagnetic objects [145]. A screening of everyone entering the scan room, patient and other personnel, must be done regarding the presence of implants as well as magnetically, and/or electrically activated devices, as those can pose serious hazards to anyone with such an implant or device entering the scan room. For example, certain types of intracranial aneurysm clips represent a contraindication to MR due to the force that can be exerted, leading to displacement and potentially death. Top contraindications (among a long list) include metal within the globe (eye), a ferromagnetic aneurysm clip, or a cardiac pacemaker [141].

Fortunately, most biomedical implants used today can be safely scanned at field strengths of up to 4.0 T. The metals employed nowadays are typically not ferromagnetic and are therefore unlikely to get dislodged when exposed to the magnetic field of a medical MR scanner, though these may still induce image artifacts [146].

5.2.2 - Time varying field (gradient) effects

Gradients create a time-varying magnetic field. This changing field only occurs during the scanning sequence; it is not present on other occasions. Therefore, exposure is restricted to patients and to relatives who may be present in the scan room during the examination. The health consequences are not related to the strength of the gradient field, but to changes in the magnetic field that cause induced currents, the so-called eddy currents. Nerves, blood vessels, and muscles, which act as conductors in the body, may be affected resulting in mild cutaneous sensations and involuntary muscle contractions [145].

Concerns have been voiced that these fields may interfere with cardiac conduction and thus cause arrhythmia. Such an effect has not been observed with the gradient strengths used in routine clinical MR imaging at present. However, optical hallucinations like flashes of light have been attributed to these gradient fields [146].

Ultra-fast imaging techniques, such as EPI, play a crucial role in fMRI and are characterized by utilizing gradient sets that can generate very high slew rates, and ultra-small rise and fall times [144], aggravating the effects mentioned before.

5.2.3 - RF effects

The predominant biological effect of RF irradiation absorption is the potential heating of tissue, with possible physiological effects including changes in cardiac output and decreased mental function. Of particular concern are heat-sensitive organs such as the eyes, although there is no evidence of any harmful effect of MR [145]. As an excitation pulse is applied, some nuclei absorb the RF energy and enter the high-energy state. As they relax, nuclei give off this absorbed energy to the surrounding lattice. As excitation frequency is increased, absorbed energy is also increased. Therefore, heating of tissue is largely frequency dependent [143].

The Specific Absorption Rate (SAR) determines how much electromagnetic energy is absorbed by the body, and is typically expressed in units of watts per kilogram, or W/kg. SAR depends on the pulse sequence and the size, geometry, and conductivity of the absorbing object [43]. SAR is monitored by both software and hardware on current MR scanners, preventing the guidelines from being exceeded. A major safety issue due to applied RF, mandating careful patient screening, is that metal, outside or inside the patient, may experience rapid and extreme heating under certain circumstances. Reported incidents include (up to) third-degree burns and coma. Extreme care should be taken with any electrically conductive material that must remain within the bore of the MR scanner during imaging, e.g. ECG electrodes, fMRI accessories. Dangers exist due to contact of any conductive material with the patient, leads or wires close to the wall of the magnet bore, and skin-to-skin contact points (a closed loop, with current flow possible within the body). Detailed specific recommendations exist and should be followed closely. As an example *The Reference Manual for Magnetic Resonance Safety, Implants, and Devices*, published annually [141].

5.3 - fMRI data acquisition

In MRI, the Hydrogen nuclei receive energy from the RF pulse at the Larmor frequency and resonates (H is used because of its abundance in the human body, e.g. water and fat). Once the RF pulse is turned off, the excited nuclei relax at different rates releasing this energy to its surroundings (spin-lattice relaxation, T_1) while at the same time, but independently, losing precessional phase coherence (spin-spin relaxation, T_2). A direct consequence is that depending on the density of Hydrogen nuclei and what's surrounding them, different contrasts can be observed, as the measured signal intensity of each tissue will decrease over time at various rates [46].

In addition to the natural loss of precessional phase coherence (T_2) due to interactions of the intrinsic magnetic fields of adjacent nuclei (spin-spin relaxation), nuclei also lose their phase coherence due to inhomogeneities of the external magnetic field, referred as T_2^* , being this effect the base of BOLD fMRI. As previously described, it explores the additional local field inhomogeneities due to the different magnetic susceptibility of oxy- and deoxyhemoglobin. Using a gradient echo (GE) MRI pulse sequence the acquisition is made sensitive to T_2^* [145]. Another advantage of the use of GE to fMRI is that it has reduced scanning time.

By the manipulation of extrinsic contrast parameters through pulse sequences (a series of RF pulses, gradient applications, and signal reading timings) one can produce images that are weighted on a particular characteristic of the tissues (T_1 , T_2 , T_2^* , or proton density weighted) [148].

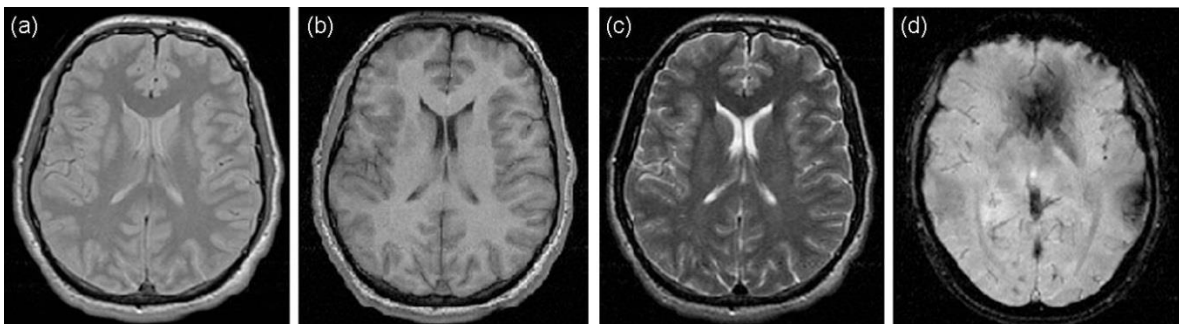


Figure 13: Different image contrasts of an axial brain slice at 3T: (a) Proton-density-weighted image (b) T1-weighted image (c) T2-weighted image (d) T2* -weighted image [258].

The primary parameters that will influence contrast are TE (echo time) and TR (repetition time). TE is the time between the RF excitation pulse and the echo (measurement of the signal). TR is the time between two consecutive applications of an RF excitation pulse. The other parameters that can be used to vary the image contrast are the flip angle (FA) and the inversion time (TI). The voxel volume and, therefore, spatial resolution are defined by the matrix size (MX), the field of view (FOV) and slice thickness (ST). The voxel volume (V), number of times a scan is repeated (NEX), number of phase encoding steps (N_y), and receiver bandwidth (BW) [146] have a direct impact in the signal-to-noise ratio (SNR) [129] that is defined as:

$$SNR \propto V \cdot \sqrt{\frac{N_y NEX}{BW}}$$

Equation 2: Signal-to-noise ratio in MRI

Noise in fMRI data may be roughly characterized into three groups: thermal noise, system noise, and subject/task-related noise. The first two are related to properties of the scanner and intrinsic to the imaging process, while the latter is inevitable by the living nature of the subject. A high SNR is desirable in MRI and fMRI. Though noise can't be eliminated completely, the researchers can optimize SNR through the configuration of the pulse sequence parameters [149]. However, as one can easily deduce, there must be a compromise between SNR, spatial resolution and scanning time as it is not possible to have the best of all [146]. Another fMRI data quality parameter is the contrast-to-noise ratio (CNR), also designed as functional SNR, which will compare the neural-activation-related signal change (contrast) with the non-activation-related variability (noise) over time [150].

In fMRI it is important to collect each image in a snapshot mode to limit the effect of head motion, physiological processes of respiration [151], and cardiovascular functions [152] adding noise signals that are unrelated to the neural processing being studied [100]. This can be achieved with Echo Planar Imaging (EPI), a gradient-echo-based ultra-fast imaging method in which data from all of the k-space for an entire 2D plane is collected following a single RF-excitation pulse [148].

At a glance, k-space is a spatial frequency domain, i.e. where information about the frequency of a signal and where it comes from (in the patient) is collected and stored. Fourier transform will then use its mathematical power to convert the “raw data” to signal intensity at each voxel of the image matrix [148]. The image matrix size is set by the product of the number of echoes acquired and the number of data points sampled in each echo [112].

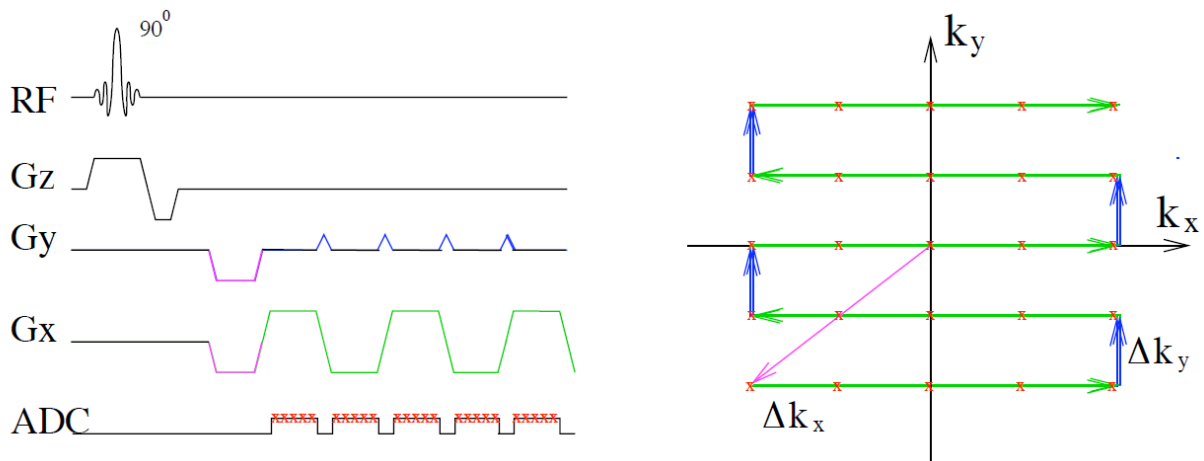


Figure 14: Schematic representation of the EPI pulse sequence (on the left) and corresponding sampling of the k-space (on the right) for imaging of one slice. Only one RF pulse is used to sample the whole slice [258].

Most fMRI acquisitions are performed using an EPI method, which can collect data for a two-dimensional image in approximately 60ms at typical resolutions ($3 \times 3 \times 3 \text{ mm}^3$ voxel size). Although these images have poorer resolution and overall quality than the images used for radiological diagnosis, it allows multi-slice recording of the entire brain in a few seconds [46]. Typically, whole brain scans with ~ 32 2D slices are acquired with a repetition time (TR) of 2s/volume, for the duration of the defined paradigm. Each voxel in the resulting scan produces a time series that is subsequently analyzed in accordance with the experimental design [100].

Very high-resolution structural MRI scans with good gray-white matter contrast are usually acquired as part of an fMRI study so that the EPI data can be overlaid onto images showing cortical structure. These high-resolution images are usually normalized (see Chapter 6 – Preprocessing) into a standard brain space [153] so that Talairach or MNI coordinates can be reported for functional activations [112]. One issue that arises is that EPI data suffer from geometric distortions caused by static field

inhomogeneities, and do not properly align spatially with conventionally acquired MRI scans that show structural information. So, to accurately locate the images to the underlying structure, it is necessary to perform some form of geometric distortion correction. Another solution is the increasing use of ultra-high field scanners (≥ 7 T) where high-resolution EPI data can be acquired and acts itself as the structural scan.

In addition to geometric distortion there are two other artifacts, dropout and Nyquist ghosting, that are characteristic and present, in more or less degree, in every EPI acquisition. Even so, EPI remains the workhorse acquisition pulse sequence for fMRI because it still offers the most time efficient approach to image acquisition, for an application where many samples of the brain are desirable [131].

5.4 - Artifacts

Artifact refers to any undesired signal contribution/distortion which is caused by the technique used and does not reflect the original specimen. In fMRI, the artifacts are originated mainly from the hardware, from the subject, or from operator error, and it is important to limit its impact on the quality of the data.

5.4.1 - Geometric and intensity distortions

The most common cause of distortions in the image is field inhomogeneities. Static field inhomogeneities typically cause geometric distortions, although they can also lead to signal losses under severe conditions. RF excitation field inhomogeneities (i.e., uneven excitation or reception across space) usually cause intensity variations within the image, a similar effect as head motion [43].

The manufacturers of the scanners concentrate their efforts on creating the most homogeneous static field possible, using active and dynamic shimming. Still, even in the best conditions, there is always a certain degree of inhomogeneity present, especially at very high magnetic field strengths, which may remain significant enough to induce noticeable geometric distortions. Furthermore, when the subject is introduced in the scanner, it creates itself field inhomogeneities due to the varying magnetic susceptibilities of the different tissues within the field of view. These effects are especially prominent at the interface between tissue and air, resulting in, for

example, distortion of the frontal lobe in regions close to the nasal sinuses (for example in the orbitofrontal cortex) [34].

There are some approaches for correcting geometric distortions in the images. A field map of the main magnetic field can be created by acquiring two images of the signal phase with slightly different TE. The difference between these images is proportional to the strength of the field at any particular location. If the field is perfectly uniform, then the phase difference generated by the different echo times will be the same in all the voxels, and the resulting image will be a uniform gray. Field maps can be determined for a phantom or human brain and be integrated into the imaging processing to correct for any geometric distortions [43]. Care must be taken as head motion and geometric distortion will interact in a non-linear way, with the result that a field map acquired at the start of the fMRI run may not be strictly valid for all time points. One approach to deal with this problem is to embed field map acquisitions into the EPI time course thereby ensuring that the field maps are registered and are updated as the head is moved [131, 154].

Other approaches include estimating the local point spread function (PSF) of the image at each pixel by adding 'hyper' phase encode loops in the readout and blip direction of a standard EPI sequence. Geometric distortion and intensity corrections can then be calculated at each point in space from the PSF data [155, 156]. The last correction approach that is worthy of mention is the acquisition of EPI data with reverse phase encoding polarities, resulting in opposite spatial distortion patterns, being then the resulting images aligned using a fast nonlinear registration procedure [157].

5.4.2 - Dropout

EPI is the pulse sequence used in fMRI because it is sensitive to microscopic magnetic field alterations caused by BOLD susceptibility effects in areas of neuronal activity. However, it is also sensitive to macroscopic field inhomogeneities generated by the differences in magnetic susceptibility of air and tissue, which may result in localized image distortions and signal losses. Substantial signal dropout occurs especially in the frontal and temporal lobes. Several approaches can be taken to reduce the effect of this artifact, mainly by adjusting the TE, the slice tilt, the slice thickness, the direction of the phase-encoding and the z-shim moment [158].

5.4.3 - Ghosting

Ghosting is also sometimes referred as Nyquist or N/2 ghost artifact. A characteristic of EPI is that odd and even lines of k-space are acquired with opposing polarity. Inaccurate timing of the sampling, temporal asymmetries in the analog filter or inhomogeneities in the static field causes a modulation of alternate lines in k-space. This leads to a ghost image shifted by N/2 pixels in the phase encode direction. The effect can be seen globally, every slice exhibits the same ghosting, or locally, some regions affected in just one or few slices.

Approaches to correct for ghosting artifacts include multi-echo reference scan phase correction [159], two-dimensional phase correction [160], using k-space-based parallel imaging and auto calibrated methods, such as generalized autocalibrating partially parallel acquisitions (GRAPPA) [161], Dual-polarity GRAPPA [162], Parallel EPI Artifact Correction (PEAC) [163].

5.4.4 - Chemical shift

Chemical shift is a spatial misregistration phenomenon occurring in the frequency-encoding direction. Protons in fat and water precess at slightly different resonance frequencies. Therefore, during frequency-encoding, the signal from a single voxel containing fat and water will have assigned two discrete spatial positions based on these two resonance frequencies. The result is an accentuated bright or dark margin corresponding to fat–water interfaces.

Since resonance frequency increases linearly with field strength, the difference between the fat and water also increases, making high field strength magnets more susceptible to the chemical shift artifact. RF bandwidth, gradient strength and TE considerations can mitigate chemical shift artifacts [164].

5.4.5 - Ringing

The ringing artifact, sometimes also referred as Gibbs or truncation, is characterized by appearing as multiple, alternating bright and dark lines – “ringing”. The lack of an adequate number of high-frequency terms, results in an imperfect approximation of sharp edges by Fourier series. This is the inevitable consequence of using a digital approximation, with a discrete space (k-space), to map something that is

continuous in space. It is an artifact that isn't unique to EPI but is a feature of all MRIs, as they are obtained via Fourier transformation.

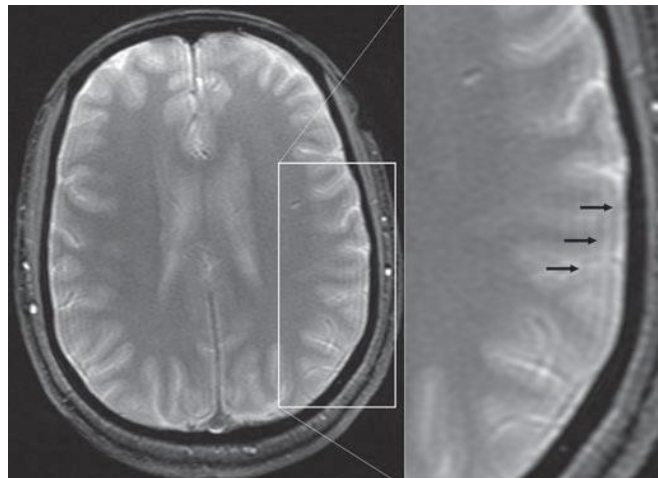


Figure 15: Ringing artifact, manifests as subtle hypointense lines overlying cortex. Indicated with arrows in this image [165].

The strongest effects of ringing appear where there are fine details or boundaries between high and low-intensity signals, and it becomes more noticeable when too few phase-encoding steps are performed. Increasing the number of phase-encoding steps (e.g., from 128 to 256) will ameliorate this artifact [165].

5.4.6 - Aliasing

Aliasing artifact occurs when excited nuclei from outside the field of view (FOV) overlay with those of identical phases inside it. Mathematically indistinguishable by the Fourier transform, these structures are assigned to the same spatial position in the image, causing them to wrap around to the other side. One can eliminate this artifact by increasing the FOV [165].

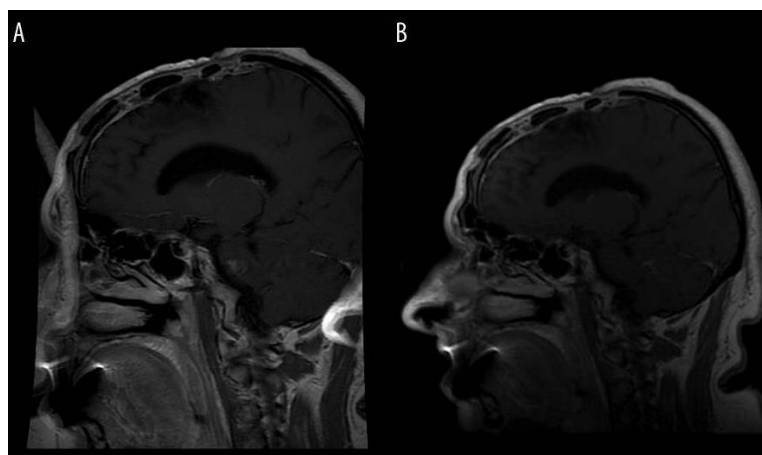


Figure 16: Aliasing artifact on brain MRI with FOV=24×18 cm (A). Same patient with FOV=24×24 cm (B) [259].

5.4.7 – Motion artifact

The most abundant and noticeable artifacts in MRI arise from patient motion, including voluntary and involuntary movement, and flow (blood, CSF). Eye and head movements, talking, coughing, swallowing, yawning, sneezing, cardiac and respiratory cycles, and body movements will impact the quality of the data. The best way to prevent it is to make the subject the most comfortable possible and explain the importance of staying immobile.

In Chapter 6.3 Motion Correction, several techniques are referred to correct for motion effects as part of the preprocessing steps, i.e. after data is acquired. Another interesting approach is to compensate for motion in real-time during data acquisition. Several prospective real-time motion corrections methods show some promising results, substantially reducing false positive activations and increasing statistical power [166]. These methods can be imaged-based or use optical video tracking devices and magnetic field probes which can measure position using the scanners gradient fields, to account for rigid body movement of the brain. A common issue with all external tracking devices is finding a subject-friendly way to attach the fiducial to the skull. Prospective real-time motion corrections compensate for motion during the acquisition of an fMRI time series on a slice-by-slice basis, by continuously updating the imaging volume position to follow the motion of the head [167-170].

RS-fMRI data are also easily contaminated by low-frequency physiological effects including cardiac and respiratory events. These sources of noise can mimic or mask true functional connectivity. Consequently, the minimization of these effects has been both a point of concern and controversy for resting state investigations since their inception [171, 172].

6 - Quality Control and Preprocessing

Preprocessing refers to the series of computational procedures that are taken, before analyzing fMRI data, to remove sources of signal variation within the data that are not of interest and to prepare the data for statistical analysis [129].

The order in which preprocessing steps are done is important as the output of one procedure will be the input of the next one. How (or if) these steps are applied depend on the analysis software that is used. Although these programs are essentially automated, users should always check the output of automated steps and do quality control, as errors will propagate throughout the rest of the preprocessing steps and analysis. To note that most of these steps are usually applied, regardless of the experimental design [43].

Later, statistical analysis is often seen as the most important part of fMRI analysis; however, without the pre-processing steps, the statistical analysis is, at best, greatly reduced in power, and at worst, rendered invalid [173]. Nonetheless, one must keep in mind that each pre-processing step may ultimately change the final activation clusters in the sense of potential confounds, i.e. leading to wrong conclusions, inferences [32].

An important and often underutilized aspect of preprocessing is quality assurance (QA) testing. Scanner stability is obviously key to a successful fMRI research, and stability throughout a run is essential because of the low signal (BOLD) that is being measured. Stability across runs within a study and between scanners at different sites can also be quite important depending on the study being conducted. It is then recommended to have a routine QA protocol defined, to control as much as possible all the hardware and software used during fMRI studies [174].

In addition to a recommended routine QA protocol, a significant action that the investigator can do as part of the preprocessing is to visually examine the data. An effective way of viewing experimental data is as a time series movie, in which an entire experimental run is shown, one volume after another, in a rapid sequence. This will allow the detection of major interferences in the images [43].

Furthermore, one should also apply statistical tests that evaluate the quality of collected fMRI data. These can include calculations of the mean image intensity, the raw SNR (over space), or the image intensity divided by the standard deviation over time (as a rough approximation of functional SNR). Some analysis packages and many imaging centers have developed quality assurance testing, some of which can be run automatically and in real time during fMRI sessions [43].

6.1 - File Format Conversion

Often the first step of preprocessing is to convert the data file format, as most MRI scanners produce image data in a format that conforms to the DICOM Standard, which is the standard used in all hospitals worldwide, and most analysis packages cannot work directly with the original data in this format. Additionally, in the research world, along with numerous fMRI data analysis software packages, several different file formats more suitable for fMRI data arose. Many of these were variants of the ANALYZE™ 7.5 format, which consists of a “.img” file containing the image data itself, plus a “.hdr” file containing various pieces of descriptive information [34].

The NIfTI-1 data format was recently developed to facilitate interoperability among fMRI data analysis packages. The authors of the major data analysis packages have all committed to support this format for both input and output [175].

One of the biggest issues of the different file formats is the different ways in which the voxels of an image are ordered, which often caused uncertainty about the laterality of the brain when the same data was used on different data analysis packages. The NIfTI-1 format will prevent this issue as it allows storage on disk to be in either a left- or a right-handed coordinate system. However, the format includes an implicit spatial transformation into a right-handed coordinate system. This convert maps from data coordinates (e.g., column i , row j , slice k) into some real-world (x,y,z) positions in space [34].

The conversion between file formats can be performed with several tools such as PANDA, CMTK, Data Format Tools, BXH/XCEDE Tools, MRICron, SPM, FSL.

6.2 - Slice-timing correction

As each slice is acquired at slightly different times, it is necessary to adjust the data in such a way that it acts as if all voxels within one volume had been acquired at exactly the same time (all subsequent processing is simplified if this is done) [41]. This is achieved by phase shifting the time series of values at each voxel. Phase shifting means sliding the 1D time plot forward or backward. This is usually achieved by Fourier transforming each voxel's time series into a frequency representation, applying a phase shift to this data, and then applying the reverse Fourier transformation to recover the corrected time series [173].

Currently, most fMRI studies use interleaved slice acquisition, in which all of the odd-numbered slices are collected first followed by all of the even-numbered slices, to avoid cross-slice excitation. In this case, the most common approach for slice-timing correction is by interpolation. This technique uses information from nearby time points to estimate the amplitude of the MR signal, for every slice, at a single point within the TR [43]. Though if long TR values are used the interpolation may not be very accurate. It is, therefore, necessary to decide whether or not slice timing correction using interpolation is necessary, or suitable, for a particular fMRI study [129]. It is important to emphasize that interpolation techniques are intrinsically imperfect. Once this step is performed, any attempt to recover the original data is limited by the variability in the experimental data, in particular, variability that is not associated with the task. This can ultimately lead to data loss [43].

Another approach is instead to shift the predicted signal intensity response patterns to model the expected BOLD response at the times that each slice was acquired. Though, this approach may not be practical for most fMRI studies, which may include a large number of slices. Another alternative, when using a GLM analysis, is to define more than one timing pattern to fit the data to accommodate slight shifts in the recorded BOLD response [129].

6.3 - Motion Correction

Probably the most damaging and frustrating issue investigators face with fMRI studies is head motion. It introduces uncertainty and has been demonstrated to produce systematic spurious results [176]. Considering a typical $3 \times 3 \times 3 \text{ mm}^3$ voxel size, an almost imperceptible head movement of 5mm will generate a shift of nearly two voxels. In addition to the position shift of brain matter in space, this movement will have a whole range of effects in the measured signal: causing the same voxel in the volume to contain signal from two very different types of tissue; loss of signal in the imaging edges; change in BOLD signal as a consequence of the trail of RF pulses missing to excite or exciting twice or more the same slice [43].

The impact depends mainly on how well the subject can stay motionless during each run, which can be difficult to achieve considering the length of some studies. Prevention is recommended by limiting head movement and placing the subject as comfortable as possible, but a small amount of movement is almost inevitable. To compensate for these effects, it is common practice to realign data between successive images by applying slight translations, rotations, and in some cases even changes in curvature to the images [129], so that the spatial location of a voxel within each volume is aligned with that in every other volume. However, it cannot correct the signal alterations that occur as a result of movement [177].

Additional steps can be taken to counteract the movement-related interference in BOLD signal. Several different approaches have been adopted, which can be divided into two classes of methods: motion regression and motion censoring. In motion regression, various regressors based on realignment estimates are included as nuisance regressors in the general linear model (GLM) estimation (see Chapter 7 – Statistical analysis) [178-180]. In motion censoring, volumes acquired during gross movement [181] or that contain stimulus-correlated motion are ignored in the statistical analysis [182]. A new and promising technique named “scrubbing” achieves motion censoring by identifying motion-induced spikes in the data and removing it using temporal masks being the adjacent time points concatenated [177].

Motion correction has become a standard part of fMRI preprocessing and is now used in nearly all published fMRI studies. When different motion correction

approaches have been systematically compared, both on simulated and real fMRI data, the results have been equivocal. To a first approximation, all major packages do a creditable job correcting for motion, in that they all provide significant and measurable increases in the amplitude and specificity of BOLD activation. However, no one's approach seems substantially superior to the rest, and the impact of head motion could not be completely removed by any of these published techniques. This suggests that the current approaches to motion correction provide robust and efficient methods for improving fMRI data quality, although future advances remain possible [43, 183].

6.4 - Functional-Structural Coregistration

The fMRI analysis involves taking a series of low-resolution functional images, which appear as a relatively undifferentiated blurry globule with only the ventricles and the barest outlines of gray matter distinguishable, and then analyzing these to produce a map of brain regions which are thought to have been significantly activated [173]. Therefore it is advantageous to overlay the functional image on a high resolution and exquisitely detailed structural image of the same brain, to better identify the areas that are active. The computational processes that map two types of images onto each other is known as coregistration [43]. Before this preprocess step it is beneficial to have performed geometric distortion correction and reduced large scale intensity inhomogeneities, as described in section 5.4.1 of this dissertation [173].

At its simplest, image coregistration involves estimating a mapping between two images. One image is presumed to remain static (the reference image) while the other (the source image) is spatially transformed to match it. In order to transform the source to match the reference, it is necessary to determine a link from the location of each voxel in the reference to a corresponding location in the source. Initially, this was mainly supported by manually defining *landmarks* in both images, being now also supported by an automated image registration algorithm based on a similarity measure between images.

The mapping can be described as a function of a set of estimated transformation parameters. The shape of human brain changes slightly with head

movement, so rigid-body transformations (six degrees of freedom - rotation and translation only) can be used to model different head positions and orientations of the same subject. Though degrees of freedom in the transformation might need to be increased to twelve (includes translation, rotation, scaling and skewing) or more (non-linear warping) to compensate for geometric image distortion, changes in actual brain shape (as the brain is not a completely rigid body) and head motion during the scanning process [34, 173].

6.5 - Spatial Normalization

The human brain has a remarkably variable morphology, so to be able to compare the individual results from all the subjects in an fMRI study, those images have to be transformed so that the anatomy for all people matches [129]. This preprocessing step is referred to as spatial normalization, which is in its essence a form of coregistration, though with more complex transformation parameters due to the considerable variability in the shape and size of the human brain. This step will allow signal averaging across subjects and their activation sites to be reported according to their Euclidean coordinates within a standard coordinate system [34, 184]. The first commonly adopted coordinate system, or stereotaxic space, within the brain imaging community is described by Talairach and Tournoux. They created the Talairach coordinate system, based on eight landmark points, and a reference brain atlas, from meticulous post-mortem observations on two series of sections from a single 60-year old female brain [185].

The use of a single brain presents many problems, notably that the brain used was unrepresentative of the population as a whole. A better approach has come from recent attempts at creating probabilistic spaces using combined data from hundreds of individual scans. A now commonly used stereotaxic space was created by the researchers at the Montreal Neurological Institute (MNI) [186], and was based on the anatomies of more than one hundred individuals and has been scaled to match *landmarks* within the well-established Talairach atlas [43].

A common criticism of stereotaxic analysis is that the templates employed in widely-used software packages (SPM, FSL, AFNI) may not be appropriate for a particular population, e.g. pediatric, elderly or disease-specific. This led to the creation of an increasing variety of population-specific or even study-specific templates. The optimal choice of atlas template and mapping function take into consideration age, gender, hemispheric asymmetry, anatomical correspondence, spatial normalization methodology and disease-specificity [185]. This expanding variety of templates creates a limitation as for two different studies to be comparable they need to have been normalized in the same fashion [43].

The image normalization process can be applied to images at each time point of the fMRI time series before applying one of the analysis methods, or can be implemented only to the results of the analysis. The advantage of normalizing only the analysis results is that any imperfections in the normalization will not affect the analysis itself [129].

6.6 - Temporal filtering

The main point of temporal filtering is to remove unwanted components of a time series, such as high-frequency fluctuations or slow trends that cannot be attributed to the BOLD response (or other neural activity-related contrast) [129], without, of course, damaging the signal of interest. For example, if a stimulation is applied for 30 s, followed by 30 s rest, and this pattern is repeated many times, the signal of interest will be close to a square wave of period 60 s. Temporal filtering will normally attempt to remove components in the time series which are more slowly varying than this 60 s periodic signal (high-pass filtering or drift removal) and also remove components which are more quickly varying (low-pass filtering, or noise reduction). Such confounds could be physiological effects like heartbeat or breathing, or scanner-related drifts. The choice of the high- and low-frequency limits depends then on the study design that is used [129, 173].

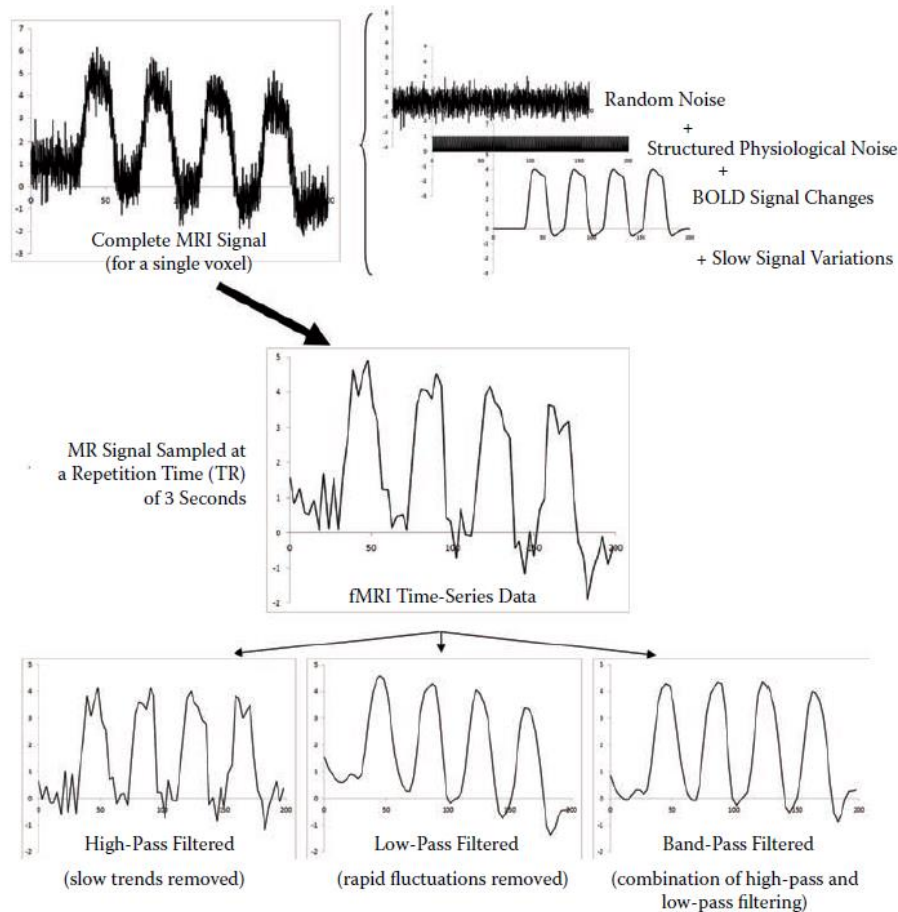


Figure 17: Effect of temporal filtering on simulated fMRI data for a single voxel [129].

6.7 - Smoothing (Spatial filtering)

Smoothing, or spatial filtering, is a procedure that can increase functional SNR, reduce apparent noise, and increase the validity of comparisons between subjects. Smoothing is used to increase the amount of overlap between subjects, which increases the significance of the results. Therefore, more smoothing would typically be used for group analysis than for the single-subject ones [34]. An optimal spatial filter should be wide enough to accurately blend functionally homologous anatomic regions, yet narrow enough not to blur the functionally distinct regions [187]. One of the simplest approaches to spatially smoothing the fMRI data is by convolution each volume using a Gaussian smoothing kernel with a full width at half maximum (FWHM) that is normally twice the voxel dimensions [129, 173].

The current rule within fMRI investigators is to smooth the spatially normalized images, as opposed to smoothing the native images and then warping them. It is usually the final step of the pre-processing pipeline [34].

7 - Statistical Analysis of BOLD fMRI data

Once the experimental design is defined and the fMRI images are acquired and preprocessed, it is then time to analyze the data to infer which areas of the brain are active, relative to the study's hypothesis. As seen in the previous chapters, the fMRI signal is based on the BOLD contrast resulting from the haemodynamic response to the local neural activity. The intrinsic difficulty with this analysis is that the effect is very subtle, which with a cerebral blood flow change of 30% causes a BOLD signal change of only approximately 1% at 1.5 T [15, 43].

Because the BOLD contrast is small, simply averaging images over the experimental and control conditions and then subtracting is inadequate to identify reliably those voxels in which the signal intensity increases when the stimulus is ON. This is because the noise, that sometimes can be larger than the signal of interest, will compete to render false positives and false negatives. The noise results from thermal sources in the subject and electronics, bulk motion of the head, cardiac and respiratory-induced noise, and variations in baseline neural metabolism [15, 100]. Therefore one can only approximately estimate the signal changes. Additionally, as often the fMRI studies are carried out with the intention of answering some question about a population of individuals and only a sample is studied, the population differences in neural activation can also only ever be approximated and statistics are needed to see if those are significant given the quality of those approximations [34].

The result of the statistical analysis of fMRI data will be an activation map. To obtain it, the simplest approach is to generate a map of the t statistic for signal changes on a voxel by voxel basis, referred to as "univariate" analysis. A related approach is to correlate the time course of signal change in each voxel with a model time course based on the expected neural response (suitably convolved with a model of the expected haemodynamic response function corresponding to the experimental design), which can also be used to generate a t statistic map, referred to as "model-based method" [173].

The other broad category of analysis will be “multivariate”, also referred as multi-voxel pattern analysis (MVPA), processing all data from multiple voxels together, which is mostly used in “model-free methods” also known as “data-driven methods” [41]. On these, significant signal variations that are consistent across sets of voxels are detected to reveal both anatomical locations and temporal patterns that may be of interest. Data-driven methods commonly used for fMRI include independent components analysis (ICA), principal components analysis (PCA), and fuzzy clustering analysis (FCA) [129]. These methods are mainly applied for RS-fMRI analysis.

Univariate activation analyses have the advantage of being easily implemented, offering an efficient testing of representational change in the time domain and good anatomical localization. As disadvantages, it misses multidimensional representations coded across voxels and also misses representational relationships coded by neurons encompassed in a single voxel. On the other hand multivariate analysis, allow for combinatorial effects across voxels and is potentially a more direct measure of multidimensional stimulus representations, often offering greater sensitivity than other techniques. The disadvantages of multivariate compared to univariate will be that it is less localizable, less efficient in estimating in the time domain and more sensitive to a variety of signals that co-vary with stimulus features and conditions [30].

At present, there are no universally accepted strategies for rigorous analysis of fMRI data [46]. The choice of approach to use depends on the questions that are being asked about the data and whether or not a specific response model can be reliably predicted. The most common form of analysis used for fMRI (especially paradigm driven) is the general linear model (GLM), which is a model-based, univariate approach [129, 188].

7.1 - GLM - General Linear Model

The GLM is the most widely used analysis method for fMRI because it is flexible and can reliably detect signal intensity variations of interest, even in the presence of confounding effects [129]. The general linear model is the framework for many

commonly used statistical analysis techniques, including multiple regression analysis, analysis of variance (ANOVA), analysis of covariance (ANCOVA), t-test and F-tests.

In its essence, it sets up a model (i.e. an estimation of the expected response) and fits it to the acquired data. If the model is derived from the timing of the paradigm that was applied to the subject in the MRI scanner, then a good fit between the model and the acquired data means that the stimulation probably caused the fMRI data [173]. Using the HRF and convolving it with the stimulus time course provides a way to obtain a reasonable prediction of the response to any general stimulus type.

GLM assumes that each of the stimuli has its own predicted response, and that the predicted responses add together linearly, in some combination unique to each voxel, to explain the data measured in that voxel [34]. The overall predicted response is given by a linear combination of the predicted responses:

$$y(t) = \beta_1 x_1(t) + \beta_2 x_2(t) + \dots + \beta_n x_n(t) + e(t) \quad \text{Equation 3: General Linear Model equation}$$

Where $y(t)$ is the data in one voxel, and is a 1D vector (time course) of intensity values with one value for each time point. $x_n(t)$ are the model responses for the experimental stimuli, being also 1D time courses with one value for each time point. The linear combination of the predicted responses, needed to explain the data in a particular voxel, is described by the parameters β_n . The error, i.e. noise, which is present in the fMRI data is modeled by $e(t)$ [34][43]. Model fitting involves adjusting the parameters β_n to best fit the data.

There are different names used to describe the different components of the GLM. The model responses $x_n(t)$ within a GLM are often referred to as explanatory variables (EVs), as they explain different processes in the data. They can also be referred to as regressors, and the β as regression parameters, as this fitting is in fact a multiple regression. The regression parameters, β , are also known as parameter estimate (PE), and sometimes are also referred to as *effect sizes*, as they describe the size of the response to the corresponding underlying experimental stimuli [34].

In fMRI experiments, the simple equation given above is replaced by a set of matrices. Note that the spatial structure of the fMRI data is not used in the GLM, since the values of the parameter estimate and error term are calculated independently for

each voxel. Instead, all voxels in the imaging volume are arranged along one dimension, for ease of calculation. Of these matrices, the data matrix is obtained experimentally, the design matrix is constructed by the experimenter based on the hypothesized effects of the experimental manipulations, and the parameter estimate weights and residual error are calculated during the analysis [43].

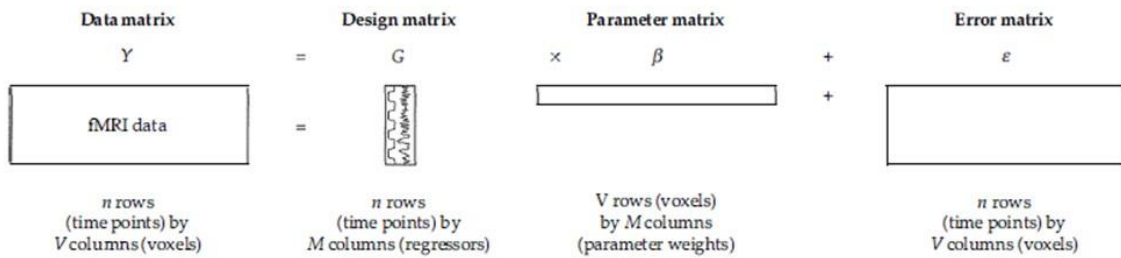


Figure 18: Basic principles of the GLM in fMRI. The GLM attempts to find the set of experimental parameters β for a design matrix G that best accounts for the original data Y , by minimizing the unexplained error ϵ [43].

The GLM is fit to the data at each voxel separately. This is achieved by adjusting the estimates of the regression parameters to find the best fit of the model to the data. When a particular GLM is fit to a particular voxel's data, the regression parameters estimate β give an indication of how much of each EV is needed to explain what is seen in the data. If the parameter estimate of β for any particular EV is non-zero, then it might seem reasonable to assume that the voxel in question is responding to the stimulus that the EV represents. However this is obtained from a limited amount of noisy fMRI data, and one cannot be certain that a particular β is non-zero [34].

With any statistical analysis, a critical question is whether the estimated amplitudes are statistically significant. To convert a parameter estimate (i.e. the estimated β value) into a useful statistic, its value is compared with the uncertainty in its estimation, resulting in what is known as a T-statistic value, t .

$$t = \frac{\hat{\beta}}{std(\hat{\beta})} \quad \text{Equation 4: } t\text{-statistic}$$

If the parameter estimate is low relative to its estimated uncertainty, the T-statistic, t , will be low, implying that β is unlikely to be significantly non-zero (and vice versa). Thus t is a good measure of whether the estimate of β is significantly different

from zero, i.e. whether there is believable activation. Converting a t value into a p (probability) or Z statistic requires standard statistical transformations; however, t , p and Z all contain the same information; they describe how significantly the data are related to a particular part of the model [3].

When analyzing fMRI data, researchers want to evaluate hypotheses about brain function. Because fMRI provides no information about absolute levels of activation, only about changes in activation over time, most research hypotheses involve comparison of activation between two conditions. For example, when identifying brain regions that support the perception of biological motion, the experiment might involve testing whether activation increases when subjects view a biological stimulus (e.g., a person walking) compared with a similar non-biological stimulus (e.g., a machine with moving levers and gears). The statistical evaluation of whether the experimental manipulation evokes a significant change in activation is called a contrast [43]. In the GLM, the contrast will compare two different PEs to test directly whether one EV is more “relevant” to the data than another EV.

The next step is thresholding, where two hypotheses are set up: an experimental hypothesis with some prediction about the data and a null hypothesis based on the random chance. A threshold alpha value is also set up, and the probability that the data could have occurred under the null hypothesis is compared with the threshold alpha value, and if this threshold is not exceeded, then the result is declared significant. Two types of errors are possible in hypothesis testing. Type I errors occur when a non-significant result is declared significant (a false positive), while Type II errors occur when a significant result is missed (a false negative). Functional MRI analyzes typically attempt to exclude Type I errors, but as a consequence, it may lead to many Type II errors [43].

A problem with thresholding is that as many tests are being carried out, because there are so many voxels in the brain, many errors can occur. If 20 000 voxels are tested for at a significance of $p < 0.01$ then it is expected that 200 will activate by chance, even if no stimulation is applied. This “multiple-comparison problem” means that it is not valid to accept all activations reported by this method; a correction is necessary to reduce the number of false positives [41]. The Bonferroni correction

accounts for multiple comparisons by dividing the desired p-value by the number of voxels to define a new, corrected p-value, and is one method of limiting the rate of family-wise errors (FWEs), but it is very conservative and increases Type II errors. Another method of correcting for multiple comparisons is to control the false discovery rate (FDR) by adjusting the p-value. As its name implies, the false discovery rate describes the proportion of positive results (i.e., discoveries) that are in fact false positives [43]. The drawbacks are that it is very conservative when there is little activation, but it is less conservative when there are many activations. An alternative approach to the correction of multiple comparisons is by cluster-size thresholding, based on Monte Carlo simulations [189, 190]. If only a single isolated voxel passed a significance threshold, then that voxel's activation may result from mere chance. It is less likely, however, that a group of contiguous voxels will all be active by chance. The only disadvantage is that the method is quite computer intensive.

To test the efficiency of the methods mentioned above to account for false positive errors, a team of researchers has performed a study [191] and has found alarming conclusions. They have demonstrated that the three most popular software packages, using the standard parametric statistical method for brain activation detection in fMRI data, have FWE rates that in some cases reach up to 60%. Their experiment consisted of using resting state data of four groups of twenty and forty participants and analyzing it as if it was part of a task based experiment. They considered hundreds of variant analyzes and numerous different parameters with the vast majority of the tested parametric analyzes producing too many false positive clusters. This calls into question the validity of countless published fMRI studies based on parametric cluster-wise inference. Their suggestion is to use the only tested method that obtained FWE within the acceptable 5%, nonparametric permutation tests [192].

In the last step of the analysis pipeline significantly active voxels are displayed on statistical maps, usually with the degree of significance indicated using a color scale [43].

The advantages of the model-driven approach with a GLM are that specific signal change patterns in time can be detected, even in the presence of confounding effects that produce very different signal fluctuations in time, and the results are

quantitative. The disadvantages of this approach are that the expected pattern(s) of signal change arising from the neural activity of interest must be predicted, and a statistical threshold must be chosen to determine when a β parameter is significantly different from zero.

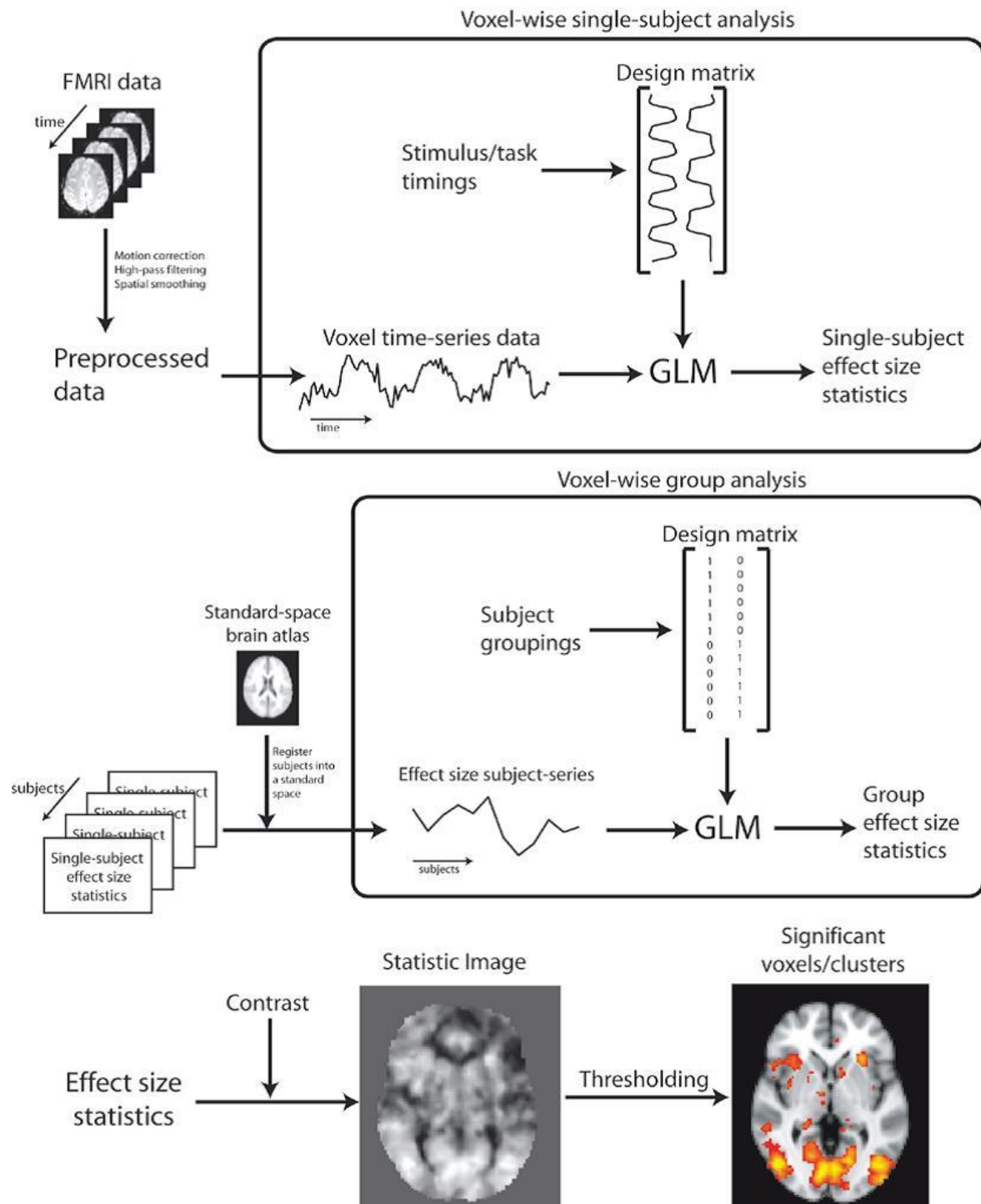


Figure 19: Illustration of the analysis steps carried out in a typical fMRI group study [34].

7.2 - Data-Driven, Multivariate Analysis Methods

One advantage of data-driven methods is that unknown or unexpected patterns of signal change in time in response to a sequence of tasks or stimuli can be determined. Another advantage is that these methods, being multivariate, can be applied to search for either the dominant temporal or spatial patterns of signal change, meaning that both when and where signal changes occur consistently can be detected in the fMRI data. These characteristics are suitable for RS-fMRI analysis. A disadvantage of data-driven methods, however, is that the dominant pattern(s) of signal change within a set of time series fMRI data may not be due to neuronal activity, but may be due to body movement or physiological motion such as related to the heartbeat and breathing. It is, therefore, necessary to assess the patterns that are detected to determine which may be attributed to neuronal activity and which may be ascribed to motion or other effects. As previously mentioned, data-driven methods commonly used for fMRI include ICA, PCA, and FCA [43].

7.3 - Group analysis

Some methods have been developed for group analysis, and the choice of method depends on the reason for the group analysis or the question that is being asked.

Two methods that have some common features are the *fixed-effects* and *random-effects*. A first-level analysis is done first, at each voxel, on the fMRI data from each individual using a model-driven method as described previously. The resulting maps of statistical values from the individuals are then spatially normalized and combined with the group analysis, or second-level analysis [129]. In a fixed-effects analysis, the experimental effect is assumed to be constant (i.e., fixed) across the subject population, so the experimental manipulation has the same effect on all subjects. The data from all subjects are combined and then undergo testing for significance. In a random-effects analysis, the experimental effect is considered to vary between subjects. A statistical map is created for each subject, and then the output of those statistical tests is subjected to a further level of analysis. Fixed-effects analysis

allow inferences about the group of subjects who were used in a particular study; while random-effects analyses allow inferences about the population from which the subjects were drawn [43].

A data-driven approach for group analysis is provided by the partial least squares (PLS) method. It is distinct in this way from the methods described above because the PLS method is not applied to the results of a previous, first-level analysis, but rather to the image data itself to detect consistent features of the responses across people or studies [129].

8 - Processing and Visualization

The previous chapter covered an overview of the most common statistical analysis of fMRI data. Many different research centers are focusing on the development, validation and interpretation of new analysis methods, presenting a plethora of different approaches to process and visualize this data, still in the search of the most suitable one. This chapter will provide an overview of the most important of these approaches, reflecting the shift in paradigm that occurred in the neuroimaging field in the past decade, from functional segregation to functional integration. To conclude, there is a reference to the different ways of visualizing the results of fMRI studies and software that can be used to process and display it.

8.1- Brain Connectivity

Since the formulation of phrenology by Gall in the 19th century, the identification of a specific brain region with a particular function has become a central theme in neuroscience [193]. In the last 25 years, fMRI has become a central tool used by neuroscientists in brain mapping, for which now more of them believe to be a complex network of functionally connected interacting regions (functional integration), shifting their focus to understanding patterns of network activation rather than of localized blobs (functional segregation and location of function).

The study of brain connectivity is fueling the understanding of how the human brain is organized and functions. Recent evidence shows that it could also be helpful for the early diagnosis and prognosis of neurological and psychiatric diseases. Therefore, several organizations across the globe are now focusing on this area of research. An example is the National Institutes of Health that launched in 2010 the Human Connectome Project [194], a large-scale project which combines data from 1200 healthy subjects from different centers. These data combine four modalities: RS-fMRI, diffusion imaging (dMRI), task fMRI, and structural MRI. This project is expected to produce the most detailed, large-scale *in vivo* whole-brain connectivity mapping achieved to date. A dataset of 820 subjects processed data was published in January 2016 and is freely and publicly available at the Human Connectome Project website, aiming to reach and be used by not only neuroscientists but also by scientists from

other fields. Similar projects, as the “1000 Functional Connectomes” Project [195] an open collaborative data-sharing platform for the neuroimaging community, or the European Union’s “Human Brain Project” [196] are aiming to boost the brain connectivity knowledge.

Brain connectivity can be abstracted to a network of nodes, representing neural elements (neurons, brain regions), linked by edges, representing some measure of functional, structural, or causal interaction between the nodes. This representation opens the doors of brain connectivity to the realms of graph theory. Recent studies, using this technique, suggest that the human structural and functional brain systems possess characteristics of complex networks such as small-world topology, highly connected hubs and modularity [197]. This topology allows a high efficiency with minimal wiring and energy cost. Its modular organization permits a high level of adaptation. The detected structure revealed highly connected hubs that are crucial for the whole network functioning. Many of these hubs were identified in regions belonging to the default-mode network and the attentional networks [198].

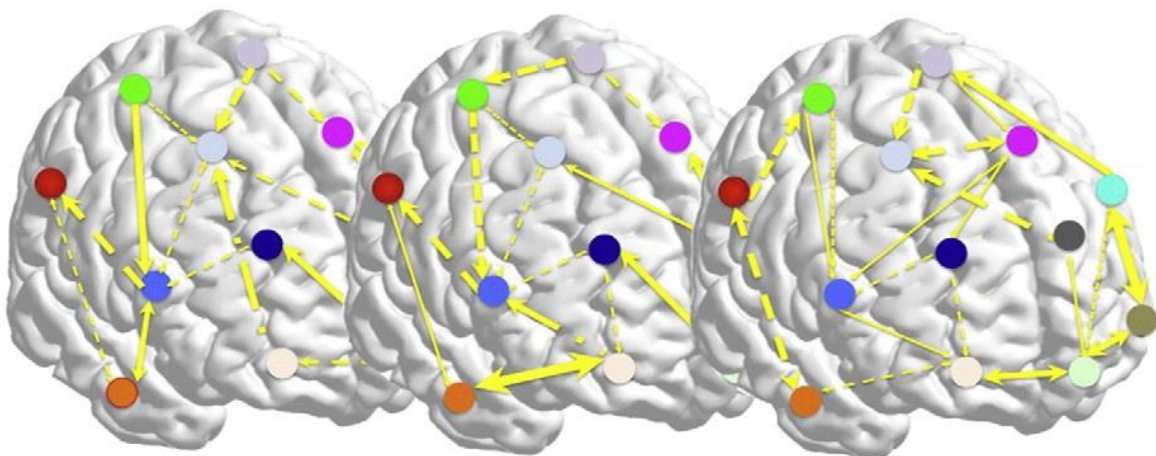


Figure 20: Schematic of an “ideal” connectomic map. Node role heterogeneity is represented by different colors. The edges are directed (arrows), weighted (edge thickness) and encode different forms of inter-regional interaction (solid vs broken lines). The maps also vary over time [260].

Structural and functional brain networks are commonly explored using graph theory through the following four steps: (i) Define the network nodes; (ii) Estimate a continuous measure of association between nodes; (iii) Generate a binary adjacency

matrix (or undirected graph) from thresholding each pairwise associations between nodes; (iv) Estimate the network parameters of interest and compare them to the equivalent parameters of a population of random networks [197].

There are many ways to define network nodes from fMRI, the choice will depend on the type of questions of interest in each study, and the scale at which one wants to look at the data. One can look at the data at the voxel level and consider each voxel as a node. At a larger scale, nodes can be defined as spatial regions of interest (ROIs), for example, as obtained from task-fMRI activation or brain atlases. Caution is advised for results derived from structural atlases and inappropriately defined ROIs. Alternatively, parcellation via a data-driven clustering of the fMRI data itself can be run to define clusters or ICA maps which can be considered network nodes [27, 199].

Once the nodes are defined, each has its associated timecourse (e.g., the average time series from all voxels within the node). The analysis methods used to obtain the edges, range from very simple measures that consider the fMRI time series associated with just two nodes at a time to complex approaches that consider all nodes at the same time and estimate one global network model. In general, the more similar the time series between any particular pair of nodes are, the more likely there is a functional connection between those nodes (functional connectivity). Of course, correlation between two nodes' time series does not imply either causality or provides the direction of the information flow [27].

Within brain connectivity, it is important to distinguish between functional connectivity and effective connectivity. Functional connectivity is an observable phenomenon that can be quantified with measures of statistical dependencies, such as correlations, coherence, or transfer entropy, and does not provide any information about causality or directionality. On the other hand, effective connectivity refers explicitly to the influence that one neural system exerts over another, either at a synaptic or population level. It is dynamic (activity-dependent), and depends on a model of interactions or coupling. It provides not only the locations of the connections between regions of the brain (functional connectivity) but, more importantly, the direction of the causal relationship between those regions, being sometimes, effective connectivity also referred to as directed functional connectivity [193].

Several methods attempt to estimate causality and directionality in a brain network, which fall into a few general classes. One class is temporal lag-based, being the most common example Granger causality, used in the context of autoregressive models of fMRI data. It assumes that if one time series is approximately a time-shifted version of the other, then the one with chronological precedence caused the other, giving an estimation of the connection directionality. There are several discussions about the use of Granger causality in fMRI analysis, with a recent study demonstrating that this method performs poorly in discovering brain networks. Some of the limitations that are recognized are the lack of a biologically based generative model, in addition to the likelihood of spurious estimated "causality" being in fact caused by systematic hemodynamic lag differences across brain regions [27, 200].

The second class, centers on the idea of conditional independence, typically including Bayesian networks and structural equation modeling (SEM). SEM takes advantage of changes in the covariance among neural elements to conduct a path analysis of a predefined anatomically connected regional brain network. The parameters in the SEM are connection strengths or path coefficients between different variables and reflect the effective connectivity in a neural network model. One of the drawbacks of SEM is that it requires prior specification of a structural causal model that consists of a limited number of brain regions, representing then, a data-driven but hypothesis-constrained approach [201-203].

The term "Bayesian" is used for the type of network analysis based on the Bayesian decomposition rule, specifically the chain rule of conditional probabilities, which simplifies the probability distribution. These approaches can often operate on larger sets of nodes and run searches over a wide range of candidate networks. Care must be taken when choosing a model or software package for estimating networks of fMRI data, being recommended approaches that have been validated specifically for fMRI data. Specifically, methods that rely on non-Gaussianity to direct causal relationships in the network are demonstrated to perform well. The key to Bayesian network modeling for fMRI is to use a Gaussian approach to identify the skeleton of the graph (undirected connections) and then use the non-Gaussian information to infer directionality, given the proper high pass filter has been used [204].

A third class derives from the Bayesian approach, and is based on conditional dependence, as proposed by Patel, it simply looks at an imbalance between the conditional probability, to arrive at a measure of connectivity/causality. For example, if the main activity flow is from A to B, then the probability of B given A ($P(B|A)$) is higher than the probability of A given B ($P(A|B)$) [205]. Two measures can be derived from the conditional dependences: K , a measure of connection strength, and τ , a measure of connection directionality. Being this last one considered to be reasonably better performing compared to other methods [27, 202].

Another popular method of brain connectivity analysis is the dynamic causal model (DCM), as an hypotheses-driven method, it is used to test a set of hypotheses, like for example a specific activity pattern of the brain network. In particular, DCM uses an explicit forward or generative model of how the observed fMRI data were caused. Since both the lag-based and the conditional independence-based methods can estimate direct connections at the neuronal level, DCM makes use of these methods to infer causality. Combining DCM with model selection methods, such as the Bayesian model, provides an efficient way to test which model gives the most likely explanation of the observed fMRI data [205][206, 207].

There is also a significant amount of fMRI connectivity research that is not working within the nodes+edges network framework. The most obvious area is the seed-based analysis of resting-state fMRI data, where one might take a single voxel's or ROI timecourse and regress all other voxels' timecourses against this, resulting in a spatial map of correlation scores. An advantage of this approach when compared with a graph analysis, is for example, if a connectivity difference between groups of subjects is one of shape rather than correlation strength [23, 199, 208, 209].

Another popular approach is ICA, a mathematic technique that maximizes statistical independence among its components. For RS-fMRI data, ICA can be used to identify spatially distinct RSNs. Compared with seed-based methods, ICA has the advantage of requiring few a priori assumptions but does require the user to select the important components manually and distinguish noise from physiologic signals. Despite the differences in these two approaches, the results of seed-based analysis and ICA were found to be significantly similar in a group of healthy subjects [65, 210, 211].

8.2 - fMRI Software

With the use of positron emission tomography (PET) for neuroimaging in the 1980's, and after with the discovery of BOLD contrast together with the first fMRI studies in 1990, the investigators had the need to develop adequate software packages. Statistical parametric mapping (SPM) was at the time the most adopted software package by the PET neuroimaging community, proving to be the most popular way of characterizing brain activation data, [212] and was rapidly adapted and adopted by the fMRI community. This period coincided with the exponential growth of both the Internet and the open-source software movement. This environment stimulated the creation and dissemination of many neuroimaging software projects, being some quite successful and broadly adopted [213]. The most popular fMRI software packages are:

8.2.1 - SPM

SPM (Statistical Parametric Mapping) is probably the most popular and most used fMRI software package. Despite being one of the pioneers, its popularity is aided by the ease of development of additional features, as it is coded as a Matlab toolbox. This provides increased flexibility as the large active user base contributes with a considerable number of additional toolboxes and extensions to the base program that can do almost every task needed in an fMRI study. An up-to-date list is maintained at the SPM website [214, 215].

8.2.2 - FSL

FSL (the FMRIB Software Library) is an extensive library of analysis tools for structural, functional, and diffusion MRI brain imaging data. Being mainly developed by the members of the Analysis Group, FMRIB, Oxford. It has great flexibility in virtue of its array of command-line utilities to analyze a wide range of MR modalities (task fMRI, resting fMRI, ASL, diffusion, structure), and can be easily scripted to run over computing clusters. It is particularly suitable for multimodal MRI neuroimaging investigations and will increasingly support a wide-range of connectivity-based analyzes [216].

8.2.3 - AFNI

AFNI (Analysis of Functional NeuroImages) is an open source software package used for the analysis and display of fMRI data. It was created in 1994 to meet the particular need of mapping activation maps to the Talairach–Tournoux space. It has, since then, being expanded steadily into a wide-ranging set of tools for fMRI data analysis. AFNI was the first platform to perform real-time 3D functional activation and registration calculations. Its main strengths are flexibility and transparency. Recently the user-friendliness of AFNI's fMRI and processing stream were improved with the introduction of graphical frontends and “super-scripts” that allow to setup the entire analysis [217].

8.2.4 - SUMA

SUMA is an open-source program that complements the AFNI suite of programs by adding cortical surface based functional imaging analysis. It displays 3D cortical surface models and maps volumetric data. With SUMA, AFNI can simultaneously and in real-time render fMRI data in four modes: Slice, Graph, Volume and Surface with direct links between them. SUMA provides tools for performing spatial operations such as controlled smoothing, clustering, and interactive ROI drawing on folded surfaces in 3D, in addition to the various level-1 and level-2 fMRI statistics including FDR and FWE correction for multiple comparisons [218].

8.2.5 - BrainVoyager

It started as a simple fMRI tool created by researchers studying visual and auditory perception [219]. It was, later on, developed to become a commercially available cross-platform neuroimaging tool for fMRI, DTI, EEG, MEG, and Transcranial Magnetic Stimulation (TMS) neuronavigation. Its strength is the familiar user interface and the constant updates to introduce new features [214].

8.2.6 - FreeSurfer

FreeSurfer is a collection of tools for the analysis of neuroimaging data. It provides a selection of algorithms for the functional, connectional and structural study of the human brain. It has progressed from a package primarily aimed at generating surface representations of the cerebral cortex into one that automatically creates

models of most macroscopically visible structures in the human brain given any reasonable T1- weighted input image [220].

8.2.7 - Caret

Caret is used for analyzing and visualizing many types of fMRI data, often in combination with experimental data from other modalities. The main feature of Caret is the ease of visualizing data, on surfaces, volumes, atlases, and individual subjects. It can overlay many types of experimental data allowing various combinations (e.g., fMRI activation maps, cortical parcellations, areal boundaries), and it has special features that facilitate the analysis and visualization of complex neuroimaging datasets [221].

8.2.8 - BROCCOLI

BROCCOLI is a recently developed software that takes advantage of parallel computation, CPU-GPU, to run fMRI data analysis efficiently. It allows the researcher to increase the computational power significantly, thus reducing processing time, with little investment. The main reasons are that Graphical Processing Units (GPUs) are low-cost, power efficient and capable of running several thousand processes in parallel, usually providing a performance boost of 1–2 orders of magnitude.

As a “young” software it still does not have the large number of functions offered by the most popular software previously mentioned, being currently limited to image registration and first and second level fMRI analysis [222].

8.2.9 - Connectome Workbench

The Connectome Workbench is an open source, freely available visualization and discovery tool used to map neuroimaging data, especially for data generated by the Human Connectome Project. It is linked to the ConnectomeDB, the project’s data management platform, allowing direct import to the Workbench of datasets with functional task and connectivity, diffusion, and behavioral data from single subjects or groups of subjects.

8.2.10 - BCT

The Brain Connectivity Toolbox (BCT) is a freely available and open source Matlab toolbox for complex-network analysis of structural and functional brain-

connectivity data sets. The open source nature of this toolbox allows researchers to customize individual functions for their needs, and to incorporate functions into larger analysis protocols [223].

8.2.11 - CONN

The CONN-functional connectivity toolbox is a Matlab-based software used for the processing, display, and analysis of functional connectivity in fMRI. Connectivity measures include, ROI-to-ROI connectivity matrices, graph metrics, ICA networks, Seed-to-Voxel connectivity maps and other Voxel-to-Voxel measures. CONN is enabled for resting state data as well as task-related designs, covering the entire pipeline from raw fMRI data to hypothesis testing [224].

8.2.12 - CVU

The Connectome Visualization Utility (CVU) is a new powerful free and open source visualization tool designed for the exploration and analysis of the human connectome. CVU complements existing software packages by offering expanded interactive analysis and advanced visualization features, including the automated visualization of networks in three different complementary styles and features the special visualization of scalar graph theoretical properties and modular structure. It leverages its functionality from powerful tools available for neuroscientific analysis in the scientific python environment [225].

8.2.13 - BrainCAT




























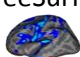





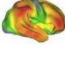











































BrainCAT (Brain Connectivity Analysis Tool) is a simple and straightforward tool for an automated and standard multimodal analysis of combined fMRI/DTI data. It combines multiple freely available tools to implement an optimized and automated data processing pipeline to combine ICA results with tractography outcomes. Requiring minimal user input and with a friendly user graphical interface it facilitates and accelerates brain connectivity studies [226].

8.3 - Software Analysis





There are plenty more software packages, toolkits, extensions that can be used by the investigators, the majority of which are free. This makes the decision of which tools to use in the setup of a novel fMRI study quite challenging. The literature comparison reviews [227-229] are scarce, only cover a few packages and get quickly outdated as it is hard to cope with the pace of updates and addition of new features. Table 1 offers a high level comparison of some of the most popular and relevant tools.

NITRC (Neuroimaging Informatics Tools and Resources Clearinghouse), which is a very useful web-based tool to find and compare neuroimaging analysis software, publicly available data sets, or even computing power, was created in 2009 by the National Institutes of Health. With NITRC and its components a researcher can get pilot or proof-of-concept data to validate a hypothesis with zero or little investment [230].

Table 1: fMRI Software Analysis*

Software	URL	OS	Interface	Availability	Prerequisite	Programming skills recommended
 SPM	http://www.fil.ion.ucl.ac.uk/spm	  	 		MATLAB [◇]	X
 FSL	http://fsl.fmrib.ox.ac.uk/fsl/fslwiki/FslOverview	 	 		x	X
 AFNI	https://afni.nimh.nih.gov/afni/	 			x	✓
 BrainVoyager	http://www.brainvoyager.com/	  		€€€	x	X
SUMA	https://afni.nimh.nih.gov/afni/suma	 			AFNI	✓
 FreeSurfer	http://surfer.nmr.mgh.harvard.edu/fswiki	 	 		x	✓
 Caret	http://brainvis.wustl.edu/wiki/index.php/Caret:Download	  	 		x	✓
 BROCCOLI	https://github.com/wanderine/BROCCOLI	  			x	✓
 BCT	https://sites.google.com/site/bctnet/	  	 		MATLAB	✓
 Connectome Workbench	http://www.humanconnectome.org/software/	  	 		x	✓
 CONN toolbox	http://www.nitrc.org/projects/conn/	  	 		SPM	✓
CVU	https://github.com/aestrivex/cvu	  	 		Python packages	✓
BrainCAT	http://www.icvs.uminho.pt/research-scientists/neurosciences/resources/braincat		 		FSL, MRICron, Diffusion Toolkit, TrackVis	✓

Legend:

 - Microsoft Windows;  - Mac OS;  - Linux;  - Open Source; €€€ - Commercial

 - Graphical User Interface;  - Command line;

◇ - there is also a standalone version of SPM but it has some limitations.

*To the best of my knowledge at the date of submission, based on information gathered from the software manuals, main webpages, and published papers.

8.4 - Visualization

There are many different ways to effectively present fMRI results, for which it mostly involves the presentation of figures with thresholded color-coded statistical maps, connectivity node-link diagrams and matrices, various types of plots, and tables listing locations of significant activation. Each representation highlights certain features of the results, thus, the best approach to visualize the data depends on the structure of the dataset and the hypotheses that are being tested [231].

For an optimized visualization, the fMRI results reported in tables should clearly specify, at least, the exact coordinates of brain activations in stereotactic space, the statistical source (e.g., Z, t, p) and threshold applied, number of voxels and activation statistics of each brain area (e.g., peak activation), along with anatomical labels and their respective source (e.g., atlas, automated labeling method).

Table 2: Template of an fMRI results table.

Condition	Regions	Peak MNI coordinates	Cluster size (voxels)	Maximum Z-score
<i>Task > Control</i>				

Though tables provide detailed information about the results, a figure allows for an easier and quicker visualization of its specific locations in the brain. These figures are commonly a graphical representation of the activated brain areas often using a thresholded color-coded statistical map that specifies the intensity of brain activations and reveals the number of activated voxels. This functional image is superimposed on a high-resolution image of the brain anatomical structure for a better visualization. This approach is designated volume-based visualization, and its images can be displayed in a plane (e.g. sagittal, coronal, axial) or a 3D model. To allow a better understanding of the data displayed, details such as the nature of the statistical map, the threshold used to create the image, the source of the underlying anatomical image, as well as any additional operations that have been applied to the map, should always be attached to the image.

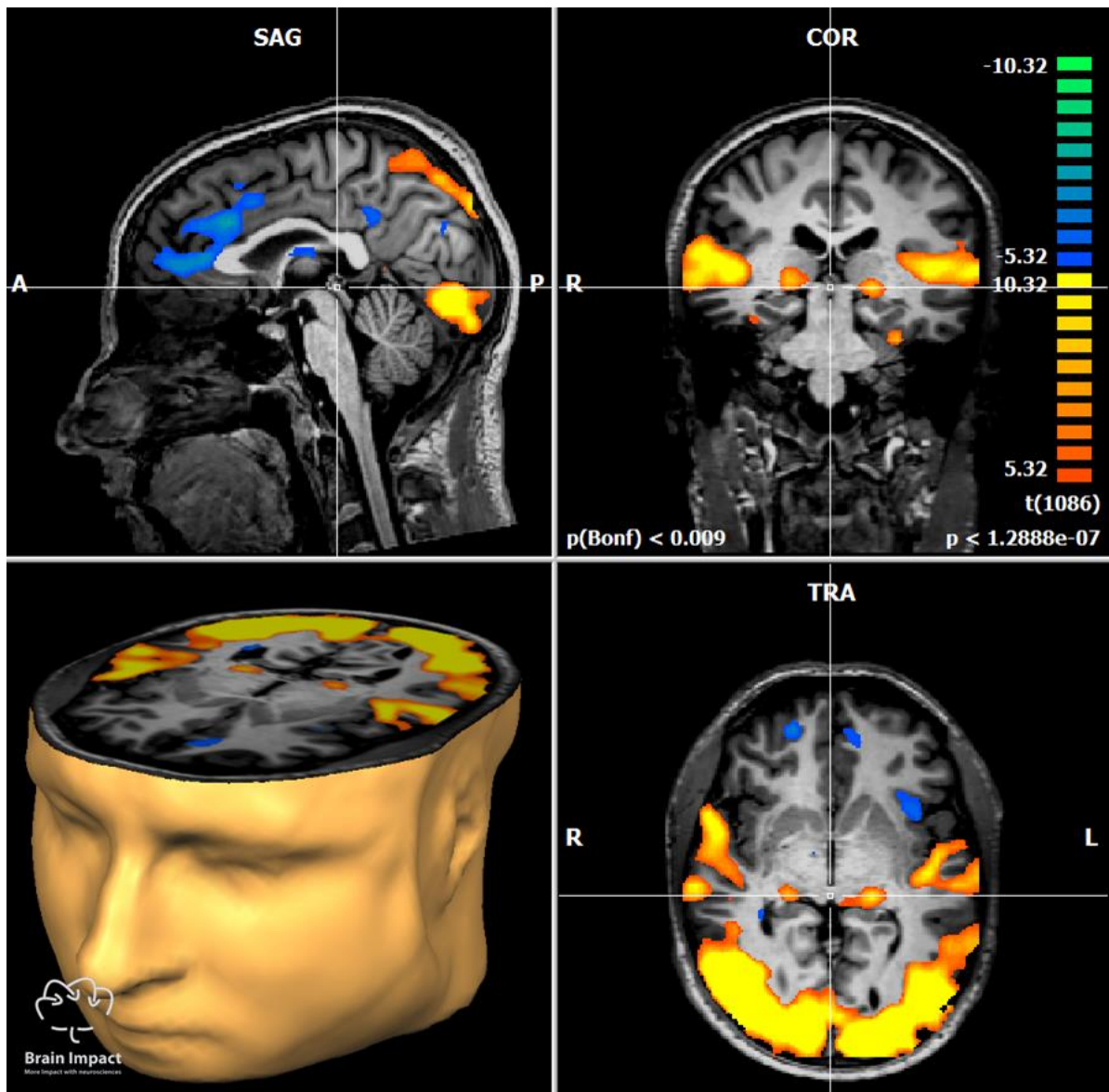


Figure 21: Activation map visualization in different planes [261].

Many researchers advocate for surface-based normalization approaches, also known as cortical flattening. In these, the cerebral cortex, which is effectively just a large ~5 mm-thick sheet folded into a complex, convoluted topography, is unfolded and “blown up” into a balloon shape. This is achieved by segmenting the different brain structures from an anatomical MRI and reconstructing the cortical surface based on the border between gray and white matter. The reconstructed cortex is then inflated into a smooth 3D surface and/or unfolded onto a 2D sheet. Therefore, it allows the cortical

surface (either whole or part) and its connections to be visualized more easily as a single entity [173]. Surface-based approaches can have significant advantages in separating activations that are near to each other in volume space but not near each other in neural space (e.g., activation from voxels on opposite sides of a sulcus), especially if functional SNR is high [43].

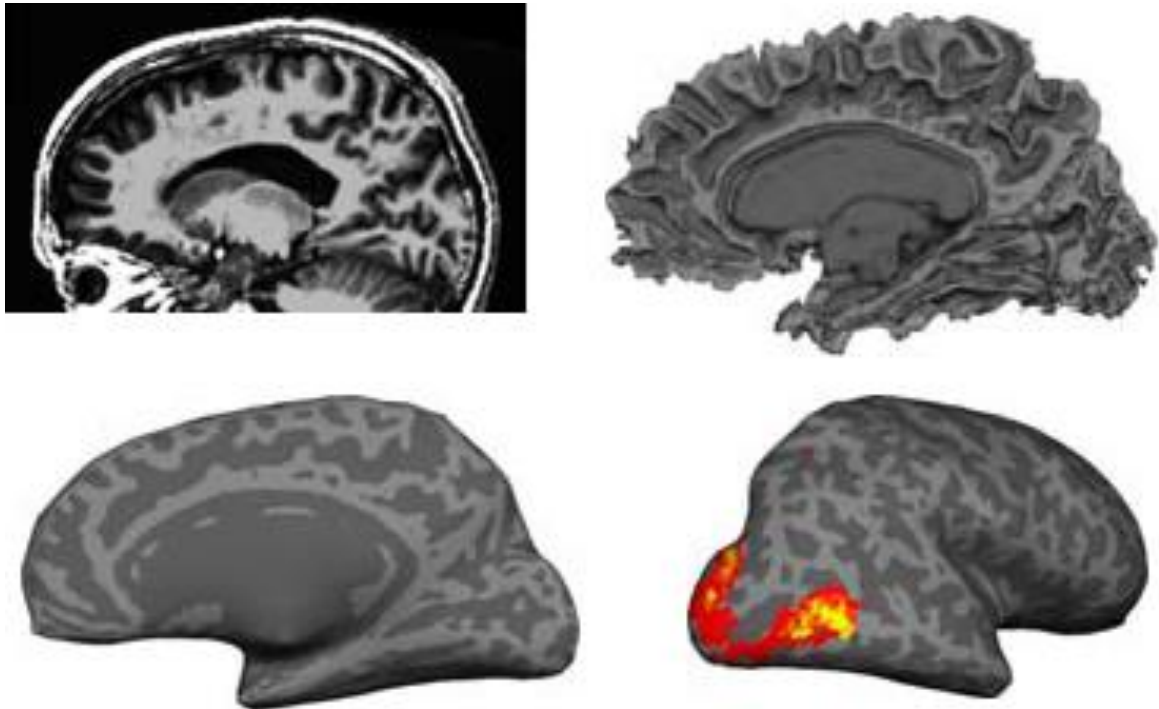


Figure 22: Surface based visualization. Images adapted from "Visualization and quantification of fMRI results" [262].

In connectivity studies, common types of visualizations are node-link diagrams, which display links between nodes as lines of arbitrary orientations, matrices, in which nodes comprise the rows and columns while the matrix entries correspond to links, and circle view, in which nodes are arranged in a circular way with links between them. The node-link diagrams are overlaid on the 2D or 3D anatomical model. For a better visualization, many software packages now render these models as maximum intensity projections, also known as "*glass brains*". The Connectome Visualization Utility is a tool that allows the visualization of the mentioned views in an interactive way.

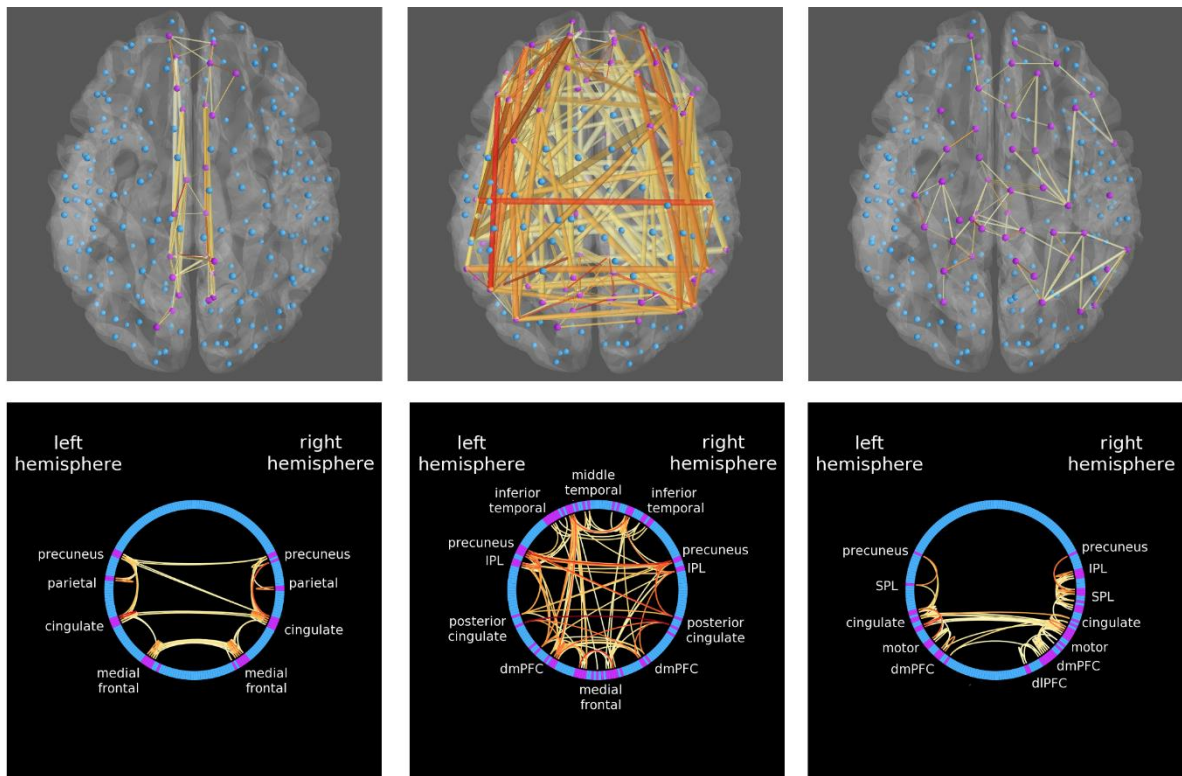


Figure 23: 3D node link and circle representation of a RSN. Nodes corresponding most closely to the network in question are isolated and represented in purple while the others are shown in blue. Stronger connections are shown in red while weaker connections are shown in yellow [225].

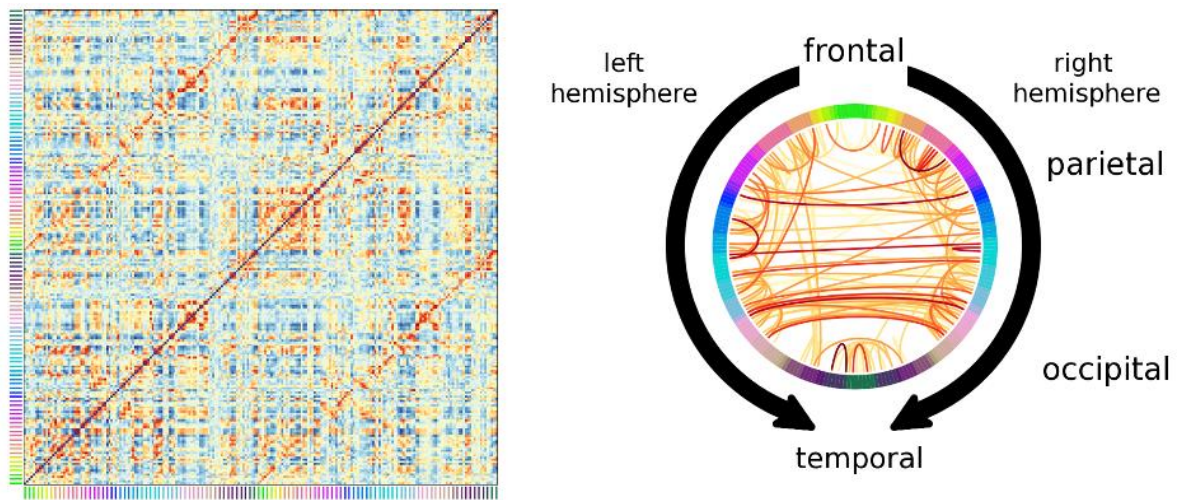


Figure 24: Connectivity matrix and corresponding circle view. Stronger connections are shown in orange while weaker connections are shown in blue [225].

9 - Multimodal Neuroimaging

Multimodal neuroimaging typically combines two or more data sets acquired with different imaging instruments. By using complementary physical and physiological sensitivities, it aims to improve the understanding of the structure and function of the brain. In a broader sense, multimodal neuroimaging also refers to the fusion of data modalities obtained with the same physical instrument [232].

The main neuroimaging modalities are MRI/fMRI, PET, functional Near-Infrared Spectroscopy (fNIRS), EEG and MEG. These modalities are based on biophysical signals related to either brain electrophysiology (EEG and MEG) or hemodynamics/metabolism (fMRI, PET, and fNIRS). PET uses radiolabeled compounds that are integrated into a biologically relevant molecule and injected into or inhaled by the subject. It then concentrates in specific brain areas according to the molecule's function and the brain's metabolic and blood flow demands. These areas are detected when γ -rays are emitted as a result of the annihilation of positrons with electrons (radioactive β -decay of radiolabeled compounds). Optical imaging methods, including fNIRS, measure changes in light scattering and absorption properties of the tissue following neuronal activity. EEG and MEG passively record electric and magnetic changes induced by extra- and intracellular electric currents associated with neuronal activity [232-234].

Strengths and limitations of these modalities depend largely upon the spatiotemporal characteristics of the measured "source" signals in relation to neuronal activity, as well as from the many diverse sensing and imaging methods applied to individual modalities [233]. Hereunder a brief review of fMRI strengths and limitations and a spatiotemporal resolution comparison with the main neuroimaging techniques is presented.

9.1 - Strengths and limitations of fMRI

The main strength of fMRI lies in its relatively high spatial resolution and availability. In addition from being readily available to both clinical and academic researchers, it is safe, painless, noninvasive, and as it does not involve ionizing radiation inherent to other scanning methods, there are no limits on the number of scans,

allowing for repeated measurements. Furthermore, a standard fMRI experiment generates many thousands of measures in one scan, being this mass recording also a significant advantage of fMRI. It provides not only the signal change associated with brain activity but also, in the same session, high-resolution anatomic scans which can be used for activation localization, vessel identification, or establishment of white matter connectivity maps through the use DTI [100][46].

There are several limitations of the fMRI technique that need to be correctly taken into account to make fMRI the extraordinarily powerful and versatile advanced neuroimaging method that it is recognized to be. A significant limitation is its low temporal resolution. Being limited by the nature of the hemodynamic response it is poor comparatively to the electrical signals that define neuronal communication. Temporal smoothing makes it difficult to determine the precise moment of activity. In fact, the image reflects an average over many seconds, which makes it challenging to study highly dynamic mental events – fast neural processes are simply blurred [46].

The signal dropout and/or geometric distortion caused by the ~9 ppm difference in magnetic susceptibility at interfaces between air and tissue can result in an erroneous lack of BOLD signal in ventral, temporal and prefrontal cortex regions critical in many cognitive studies. Furthermore, the reliability is reduced when there are significant subject motions or physiologically related variations. The small BOLD effect limits the sensitivity, requiring fMRI experiments to perform multiple samplings of brain responses [100].

The BOLD signal is an indirect measure of neural activity and is, therefore, susceptible to influences of non-neural changes in the body. For example, the impact of the variations in the blood levels of some substances likely to affect the BOLD signal, such as glucose, caffeine, nicotine, or of hormones such as estrogen, is not well documented. Aging and impaired cerebrovascular supply are also likely to influence the magnitude of the BOLD response [46].

The scanner's loud noise associated with the switching magnetic fields can cause confounds in studies of audition and resting state networks. Furthermore, the confined environment in which subjects lie in MRI scanner and the high motion susceptibility constrain the experiments that can be performed [100].

9.2 - Comparison with other functional imaging modalities

FMRI can be quickly compared to other functional neuroimaging methods regarding spatial and temporal resolution. The primary alternatives are PET, fNIRS, EEG and MEG.

9.2.1 - Spatial Resolution

It is important to consider that for fMRI the nominal spatial resolution is defined by the FOV in k-space (or voxel size in the image space). However, its effective spatial resolution can be considerably lower due to the physiological spread of the hemodynamic response and the specific vascular weighting of the fMRI sequence [232]. The typical fMRI voxel size is 3-4 mm, although with higher field magnets (7T) a size of 500 microns or less may be readily achieved [100]. The spatial resolution of PET is typically $\geq 4-5$ mm, being limited by the positron-electron annihilation range and the size of the gamma ray detectors [234]. The NIRS spatial resolution is low (10–20 mm) and limited mainly by the strong dispersion and attenuation of IR photons, which also restricts the depth of cortex that can be imaged within a banana-shaped region connecting the NIRS optodes [100]. The resolution in EEG and MEG is also limited to $> 10-20$ mm because unique reconstructions of dipoles are not possible from scalp based measurements of electrical or magnetic distributions. Unlike EEG, MEG does not suffer from scalp recordings being spatially distorted by heterogeneous electrical conduction paths within the brain/skull [100].

9.2.2 - Temporal Resolution

As for temporal resolution in fMRI, the nominal resolution is given by the repetition rate time TR, but the effective resolution is lower due to the slow evolution of the hemodynamic response [232]. BOLD response has its peak occurring $\sim 5-6$ s after the onset of a brief neural stimulus. As this response is much slower than the underlying neural processes, the temporal information becomes heavily blurred. However, by jittering event-related stimuli and using appropriate analysis methods, temporal inferences in the 100ms resolution range can be achieved. PET scans require some minutes to complete because of the low count rates of injected radionuclides, so changes in neural activity can only be studied by repeated scanning. NIRS reports

changes in blood oxygenation and, aggravated by the low SNR of NIR photons in the brain, has temporal limitations similar to those of fMRI [100]. EEG and MEG methods typically have a nominal temporal resolution in the millisecond range. However, statistical detectability and the slow evolution of neuronal field potentials can rather limit the effective resolution to the order of tens or hundreds of milliseconds [232].

9.3 - Multimodal data integration

It is possible to understand from this comparison that some modalities have an excellent temporal resolution but poor spatial resolution and vice-versa. Therefore, data integration of different modalities seems almost has a natural progress in the enhanced functional and structural understanding of the human brain.

There are several advantages of multimodal setups compared to unimodal measurements, as it will exploit the complementary information from multiple data sources. A good example of the application of the multimodal approach is in epilepsy treatment, where high temporal resolution is needed to detect the temporal dynamics of epileptic activity and at the same time high spatial resolution is required to localize the origin of the seizure. The EEG-fMRI approach is, in this case, an effective solution. While typically the unimodal techniques do not have both high temporal and spatial resolution, the multimodal methods combine the advantages of single modalities to provide a view of brain activity with an unprecedented spatiotemporal resolution. Moreover, multimodal methods can enhance the understanding of how neural activity is reflected in each of the single imaging modalities [235].

There is a growing interest and implementation of EEG-fMRI recordings, combining fMRI's good spatial resolution with the EEG's excellent temporal resolution. Furthermore, this combination overcomes the limitations of fMRI in situations where pathological conditions or drugs regionally alter the neurovascular coupling [53]. Likewise of fMRI, the EEG of the resting human brain exhibits different spontaneous rhythms. Seeking to understand better the significance of the RSNs, some studies have focused on the relationships between the BOLD oscillations, characteristic of RS-fMRI, and EEG rhythms. The EEG-fMRI approach provides valuable perceptions into the

effects of disease on these networks involved in human brain functions, and extends the applications of EEG-fMRI to uncooperative or unconscious patients [53]. To note that additional safety and artifact prevention considerations need to be taken into account when performing simultaneous neuroimaging multimodal recordings [236].



Figure 25: EEG-fMRI recording hardware setup [263].

Recording and analyzing data that often reside in different dimensional spaces and measured at different time scales has historically proven to be quite challenging. Multimodal imaging typically requires specialized post-processing tools to merge data from the modalities because the “space” of meaningful qualities imaged is mostly different for each modality. A necessary condition for this integration is that the data are transformed into the same dimensional space. Data can be separately recorded and processed but interpreted together in the same template space, or data can be separately recorded (from the same subject and with the same paradigm) and jointly processed. If the data of interest is the average responses to a task and those are presumed to be predictable, then multimodal data can be acquired sequentially. If, however, the responses to the same task and corresponding images are state-

dependent and vary with context, then it is mandatory that the data are simultaneously acquired. Simultaneous recording often includes degraded data quality regarding SNR and increased artifacts compared to separate recording [232].

Many solutions to this data integration challenge have been proposed, which makes both the comparison of results, as well as the choice of the right method to handle the data, a difficult task. In a general sense, multimodal methods can be categorized as asymmetric and symmetric, though some methods cannot be clearly assigned to one of these categories [235]. In asymmetric integration approaches, information from one modality is given higher importance or lower uncertainty than the other. For example considering data acquired from one modality as the cause of the other modality (using the time–frequency of EEG as a predictor in fMRI General Linear Modeling) [232]. In symmetric data fusion, both modalities are treated equally, with appropriate concern for their spatial and temporal resolution and, possibly, their indirect correlation to neuronal activity and the uncertainty about that correlation. Model-driven symmetric fusion is implemented using generative model inversion, which has the potential to incorporate, both the physiological and spatiotemporal complementarities of different modalities, explicitly. A generative model is a dynamical model that has a physiologically and physically realistic description of the sequence of events from neuronal activity to the observed data. Currently, the most prominent form of generative modeling in neuroimaging is Dynamic Causal Modeling [235].

Multimodal methods have become a mainstay of neuroscientific research and clinical application. Although the combined efforts of the community have solved most technical limitations associated with concurrent recordings of electrophysiological and metabolic views on brain activity there is still no gold standard analysis framework [235].

10 - Results interpretation

fMRI allows a functional assessment of neural activation, mainly by measuring the hemodynamic changes assumed to be associated with neural activity. By far the most influential fMRI technique is BOLD, measuring the local intravascular T2*-sensitive hemodynamic variations in response to neuronal activity, meaning that its results are an indirect detection of this activity. Important questions raise on what can be extrapolated from the fMRI BOLD signal variations. What does it mean when an fMRI study results of a certain brain region being more active when associated to a certain task? Does the activation of this area mean that it is truly involved in that task? How confident can a researcher be of its conclusions? There are several factors to be taken into account in interpreting the results.

The complex mechanisms of the neurovascular coupling are still not totally understood. In addition, several studies have reported that it is potentially affected by respiration (CO₂ levels), drugs and hormones (e.g. caffeine, nicotine, estrogen), age and brain pathology, attention, and regional neurovascular coupling differences (e.g. white matter vs. gray matter) [32]. Moreover the fMRI BOLD signal may potentially confuse excitation and inhibition, complicating the functional interpretations of the BOLD responses, or simply not detect the neuronal activity resulting from an excitatory/inhibitory equilibrium, which might only show minor hemodynamic alterations despite having a functional role [237]. These possible confounds need to be taken into account, and excluded, as far as possible, from the study.

To successfully interpret fMRI results, it is necessary to understand the underlying hemodynamics, physiology, and organization of the human brain. The smallest fMRI unit, the voxel, covers millions of dynamically interconnected neurons, therefore, the activity detected is not at the neuron resolution, but rather the average differential activity of functional subunits and their joint (e.g. blobs) or conditional activation (e.g. brain connectivity networks). The hemodynamic response is then sensitive to the size of the activated population of neurons and, due to the nature of the hemodynamic response, it reflects the integration of several seconds of neural activity, making it challenging for the fMRI signal to accurately reflect differences among brain regions or tasks within the same region [237].

The identification of primary and secondary sensorimotor areas is relatively straightforward because anatomical, functional and cytoarchitectonic labels are highly related. The situation is less straightforward and more controversial in many other brain areas, especially those involved in higher cognitive functions [238]. One would assume that complex psychological states or processes (e.g. speech, feelings, memory) depend on neural circuitry widely distributed throughout the brain and not in one restrained area. This organization results in sparse contributions to the hemodynamic responses (e.g., instantiated in the activity of a very small number of neurons) that overlap with those of other activity, making it challenging to deduce the exact role of that area in the task at hand [237]. Additionally, the significant variability in brain anatomy between individuals, cause uncertainty in localization. This limits the effective resolution of functional imaging, especially for brain areas involved in higher cognitive function [238].

In the neuroimaging literature, there is a historical tendency to interpret discrete areas of activation as reflecting specialized, independent modules that are responsible for a particular cognitive function - the colored "blobs" represent a "pleasure center", an "art center" and even sometimes a "love center". Researchers often support these structure-function deductions [239] with previous studies finding similar activation and inferring that the same cognitive function is engaged in their study. This neurocentrist perspective seems to oversimplify the complexity of the human brain function, by disregarding its true distributed nature [66] and often devaluating the powerful role of the social-cultural context as well as psychological and environmental factors, in shaping our mental contents and behavior.

In recent years, the study of RSNs is revealing several interesting observations on how spontaneous connectivity patterns are altered in different conditions. However the concrete meaning of these underlying processes, seemingly fundamental to the human neural functional architecture, remains vague [66].

The number of potential confounds, together with the multiple possibilities of experimental design, data acquisition, data analysis, data visualization and reporting implies that there is no unequivocal fMRI approach and no 'perfect' fMRI study. To help

the fMRI researcher from publishing spurious results and allow for study replication some guidelines have been created and should be followed [231, 240-243].

To conclude, the neuroscientist should be careful while interpreting the fMRI results. A localized BOLD activation should not be simply interpreted as a specific area responsible for a given cognitive task (although this perspective may be sufficient for primary motor and sensory areas). Rather it reflects the localized neurovascular coupling of the underlying neuronal architecture that performs a specific computation. Hence, the neuronal network involved may be active in various cognitive tasks and may spatially overlap with various other networks [32].

11 - The Future of fMRI

fMRI is a technology that has revolutionized neuroimaging, being now a widely available and used pillar of cognitive neuroscience, where it has primarily been used as a tool to localize brain activity. It has, as well increasingly importance in clinical neuroscience research [244, 245]. Though BOLD-based fMRI has now matured and proliferate, the wide range of new approaches and technical developments, easily induce the belief that fMRI is far from its technical limits. If the pace of the advances from the last 25 years is kept, then the future of fMRI is an even more exciting place to be.

For Russel A. Poldrack [246] the future of fMRI in cognitive neuroscience will encompass an increasing emphasis on connectivity and pattern analysis, a greater focus on selective inference supported by open databases, and wide use of ontologies and computational models to describe underlying processes. Sharing of fMRI data in large scale databases will become increasingly common, providing a unique resource to, for example, testing the power of reverse inference (e.g., "the anterior cingulate is active, thus the subject must be experiencing conflict") across a much larger set of tasks. More data to process and more complex paradigms will require more computational power. The development of high-performance computing clusters based on commodity hardware has begun to provide such resources, which dramatically reduces the processing times [246].

According to Alan Koretsky [247], the development of MRI techniques to measure brain function more directly will help sustain the design of molecular imaging tools and increasingly sophisticated studies of neural function. Recent progress has been made to directly measure membrane potentials, the effects of action potential propagation using MRI (see chapter 3.4 SEEP), and to develop fluorescent based protein indicators of fast membrane potential. Another approach is founded on the principle that some genes increase expression in response to neural activity. Monitoring the expression of these genes has the potential to be a substitute for monitoring neural activity. MRI approach so far was used to express a protein that can alter magnetic resonance properties, as the example of some studies using creatine kinase (and

subsequently the related arginine kinase) to alter metabolites that could be detected by magnetic resonance [247].

The field of “imaging genetics” is giving its first steps, and as described by Andreas Meyer-Lindenberg [248], it is a research approach in which genetic information and fMRI data from the same subjects are combined to define neuromechanisms linked to genetic variation, in a search to better understand human neurobiology and disease. If made possible it will enable to map genetic effects of high penetrance (proportion of individuals with the mutation who exhibit clinical symptoms) while simultaneously being relatable to the behavioral phenotypes that neuropsychiatrists study, also promising a much-needed impetus to speed up drug development in psychiatry [248].

Although the direct benefit of fMRI to individual patients with brain disorders has so far been minimal, Ed Bullmore [245] considers that fMRI studies will bring considerable impact on the understanding of neurological and psychiatric disorders. He believes that the integration of genetic data or concepts into imaging study designs will play a significant role on it. To date, the most familiar example of clinical fMRI is the use of simple activation paradigms to map cortical areas for the motor, sensory and language functions in patients preparing for neurosurgery. Surgical teams have used fMRI maps to plan operational procedures that will minimize the impact on non-diseased but functionally important areas. He believes that future clinical application will include measuring the interaction between a drug and the genetic variation in its target, which will allow to predict more reliably if the new drug will have effects on the brain networks implicated in several disorders [245].

An expected evolution of fMRI will be driven by the increase of the magnetic field strength, improving the study of both the brain's function and structure, as it provides increases in sensitivity, contrast, and resolution. Jeff Duyn [249] predicts that in the near future, human-ready systems of 12 T and possibly even 14 T will become available, offering the prospect of the ability to visualize new features in the brain. Currently, field increases beyond these levels appear prohibitively difficult due to physical, technological and physiological limitations [249]. Though, this advance has a cost, as high-field fMRI is associated with greater field homogeneity challenges and

higher sensitivity to head-motion artifacts. Furthermore, greater spatial resolution means more voxels, which pose a greater statistical challenge [250].

For Stephen M. Smith [199] raising the field strength continues to be of increasing value, possibly more than expected, for RS-fMRI. Resting and task-fMRI at 7 T already sees spectacular gains in spatial resolution and/or effective SNR. Additionally, several groups are producing exciting new work on accelerated fMRI, with the ability to achieve sub-second whole-brain imaging. He foresees that clinical applications of fMRI connectivity will clearly going to be a huge growth area, based on the current evidence that links changes in connectivity to different diseases [251]. RS-fMRI (and fMRI connectivity in general) should hopefully become a powerful clinical marker, albeit the quantitative and biological issues associated with the simpler functional connectivity measures [199]. The advent and development of the connectivity paradigm opens up fMRI to clinical groups, such as patients with dementia or in a coma, who are difficult to assess by the activation paradigm, using fMRI to support decision-making about the level of consciousness and the probability of recovery of patients in a persistent vegetative state [60, 245].

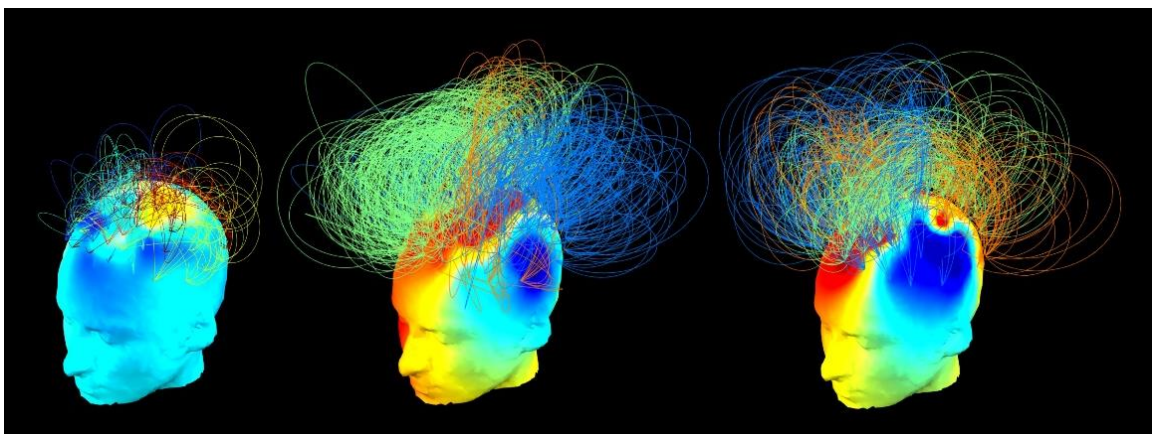


Figure 26: The colour-coded lines represent distinct functional networks of patients in vegetative state. Data collected from three different patients with distinct degrees of consciousness are displayed [264].

Finally, Uri Hasson [252] defends that there should be a tendency towards more ecologically valid fMRI experiments. Shifting from studying cognitive functions in isolation within controlled laboratory environments to studying the same functions within more natural settings – real life cognition. Emphasizing that as most of the cognitive faculties emerge from interactions among individuals, a comprehensive understanding of an individual's brain cannot be achieved without studying the ways in which brains couple together. New discoveries will not be limited by the spatiotemporal resolution of the BOLD signal, which is continuously improving, but rather to the precision of the hypotheses and the creativity of the methods for testing them. He is also convinced that the future of fMRI will embrace combining fMRI with other imaging techniques [252].

12 - Practical example of fMRI studies

To validate the proposed guide two cases were analyzed, with real data, one with task stimulation and one for resting-state fMRI, being all the workflow details considered from the fMRI study definition to the final results reported here. For the preprocessing and statistical analysis, the two most popular software were used. SPM for the task study and FSL for the resting state, being that the GUI was used for the first and the command line for the second.

12.1- Task fMRI

In this study the goal is to identify the areas involved in working memory.

12.1.1 - Participants

For this study 12 healthy volunteers were selected. The inclusion criteria was being more than 50 years old. One subject was excluded (SW00866C) after preprocessing and first-level analysis as there was a substantial artifact identified.

Table 3: Participants demographic data

	Number of participants	Age (years) min/max/average/SD
females	7	52/70/60,5/4,3
males	5	52/68/61,4/4,5
total	12	52/70/60,9/6,5

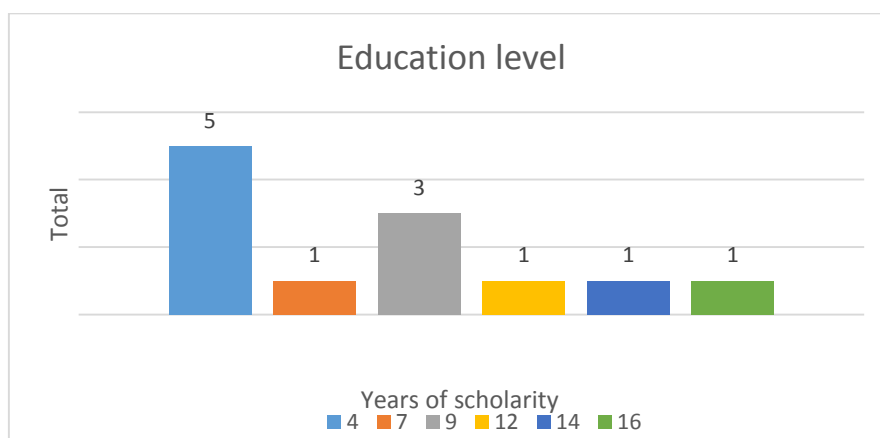


Figure 27: Participants education level

12.1.2 - Paradigm

The n-back task, a standard executive working memory measure in cognitive neuroscience and in fMRI [253], was used to investigate the task-induced activations. In this study, a modified version of this task was used. This version contained four different conditions: rest, 0-Back, 1-Back and 2-Back.

A block design was used (Chapter 4.3), in which four blocks of each condition were presented, randomly distributed along the experiment. Each block was composed by an instruction card (600 ms) that indicated the condition of the block, followed by 16 trial cards and a pause card (10 000 ms) at the end. In each trial card a letter was presented for 500 ms (letters included were b/c/d/p/t/w) followed by a fixation cross presented for 2000 ms. Responses were allowed during the presentation of the letter and trial cards.

- In rest blocks, trial cards consisted in consecutive presentations of the letter 'X' and participants were instructed to remain still, looking at the screen, without pressing any button. Defined in the GLM as "nbfix".
- In the 0-Back blocks (control condition), the instruction card presented a target letter and participants were instructed to press a button whenever the trial card presented the same letter as the target letter. Defined in the GLM as "nb0".
- In 1-Back (low working memory load condition) blocks, participants were instructed to press the button whenever the trial card letter matched the letter presented one trial before. Defined in the GLM as "nb1".
- In 2-Back blocks (high working memory load condition), participants were instructed to press the button whenever the trial card letter matched the letter presented two trials before. Each block of the 0-Back, 1-Back and 2-Back conditions had four target trials. Defined in the GLM as "nb2".

12.1.3 - Image acquisition

Imaging was performed at Hospital de Braga on a clinical approved 1.5 T Siemens Magnetom Avanto MRI scanner (Siemens, Erlangen, Germany) using the Siemens 12-channel receive-only head coil.

The imaging session included one structural T1 high-resolution anatomical sequence, 3D MPRAGE (magnetization prepared rapid gradient echo). This protocol was performed with the following scan parameters: TR/TE=2.730/3.48ms, 176 sagittal slices with no gap, FA=7°, in-plane resolution=1.0mm×1.0mm and slice thickness = 1.0 mm with an Interleaved acquisition order.

Acquisition of BOLD sensitive, gradient echo T2* weighted EPI images was performed with the following parameters: TR/TE=2000/30ms, 30 axial slices with slice gap=4.8mm, FA=90°, in-plane resolution=3.5×3.5mm², slice thickness=4mm with an Interleaved acquisition order, FOV=1344x1344mm² and 456 volumes.

12.1.4 - Preprocessing

- **Software**

Software used for preprocessing and statistical analysis was SPM12 (6685), MATLAB R2016a (9.0.0.341360) running on Windows 8.1 Pro 64-bit.

The first step is to start MATLAB, and in the MATLAB command window type: *addpath [SPM directory path]* and then *spm_fmri*

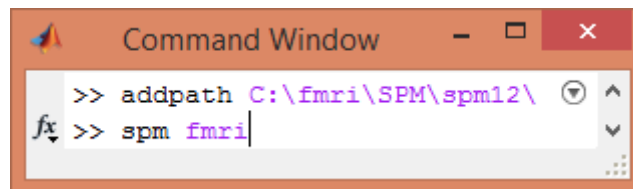


Figure 28: MATLAB Command Window

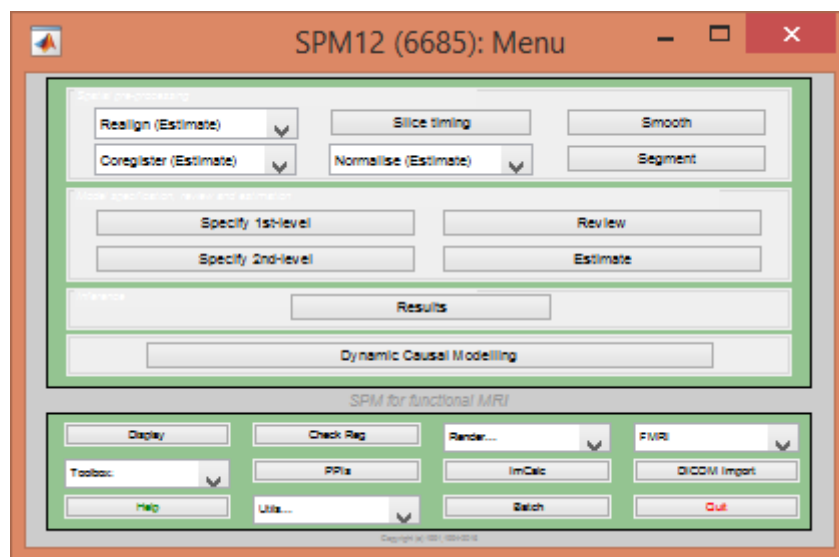


Figure 29: SPM12 Menu window

- **Batch Editor**

The “Batch Editor” in SPM is a powerful tool that allows to automatize the different preprocessing and analysis steps, saving time and reducing the possibility of errors, as the exact same preprocessing configuration will be applied to the all the images of the study. In addition, by saving the “Batch” file, it provides a way to document the preprocessing order and configuration used. Although the job is automatized it is important not to forget to verify the outcome of each individual step as part of data QA. A “DEP” (dependency) can be selected so the input of one step is the output of a previous step.

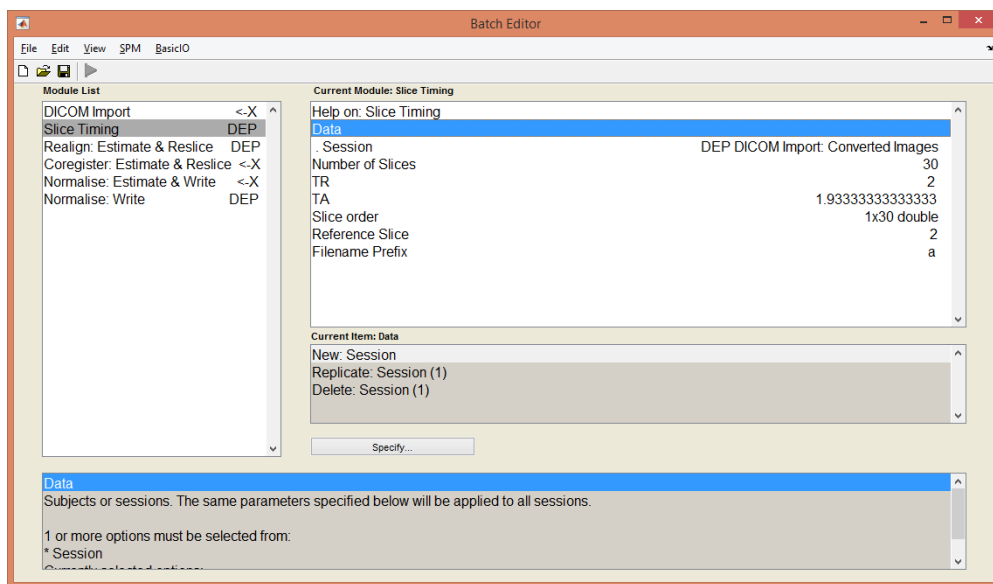


Figure 30: SPM12 – Batch Editor

- **File format conversion**

Use “DICOM Import” to convert, for each subject, the DICOM images to Single NIfTI file (.nii), without ICEDims in filename.

- **Slice Timing**

Slice Timing

Number of Slices=30
 TR=2
 TA=2-(2/30)
 Slice Order= 2:2:30 1:2:30
 Reference Slice=2
 Filename Prefix=a

- **Motion Correction**

SPM corrects for the linear effects of motion by realigning the images. In this case the option selected was Estimate & Reslice. In Reslice Options, "Mean Image Only" was selected, as the functional images will be resliced later in the Normalization step. In general, unnecessary reslicing should be avoided, because every time it is performed, the images lose some spatial resolution. Configure with the following options:

Realign (Estimate & Reslice)

Data: output from the Slice timing preprocessing step

<p><i>Estimation Options:</i></p> <p>Quality= 0.9 Separation= 4 Smoothing (FWHM)= 5 Num Passes: Register to Mean Interpolation: 4th Degree B-Spline Wrapping: No wrap Weighting: 0 files</p>	<p><i>Reslice Options:</i></p> <p>Reslice Images: Mean-Image Only Interpolation: 4th Degree B-Spline Wrapping: No Wrap Masking: Mask images Filename Prefix: r</p>
---	---

Once the "Realign: Estimate & Reslice" is finished a graph describing the estimated 6 degree transformation applied the source image is displayed. It is important to verify this information for all images as part of data QA.

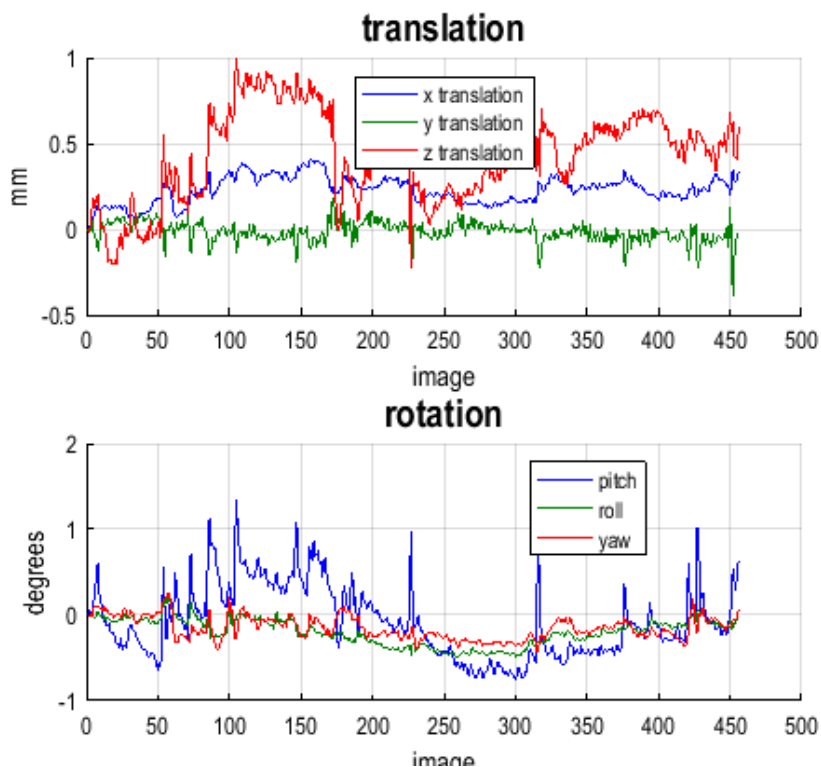


Figure 31: Motion correction parameters plots.

- **Coregistration**

The Coregistration approach used was to coregister the anatomical image to the mean functional image.

Coregister (Estimate & Reslice)

Reference Image: mean functional image created in the realign preprocessing step

Source Image: structural image

Other Images: none

Estimation Options:

Objective Function: Normalised Mutual Information

Separation: default [4 2]

Tolerances: default (1x12 double)

Histogram Smoothing: default [7 7]

Reslice Options:

Interpolation: 4th Degree B-Spline

Wrapping: No Wrap

Masking: don't mask images

Filename Prefix: r

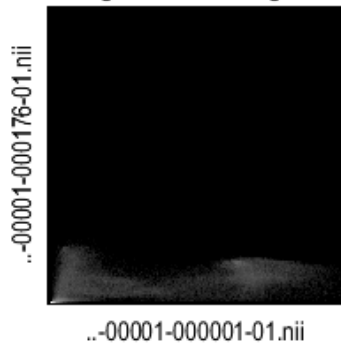
Normalised Mutual Information Coregistration

$$X1 = -0.000 \cdot X - 0.009 \cdot Y - 0.286 \cdot Z + 59.706$$

$$Y1 = -0.281 \cdot X + 0.049 \cdot Y - 0.002 \cdot Z + 65.047$$

$$Z1 = 0.038 \cdot X + 0.220 \cdot Y - 0.007 \cdot Z - 29.583$$

Original Joint Histogram



Final Joint Histogram

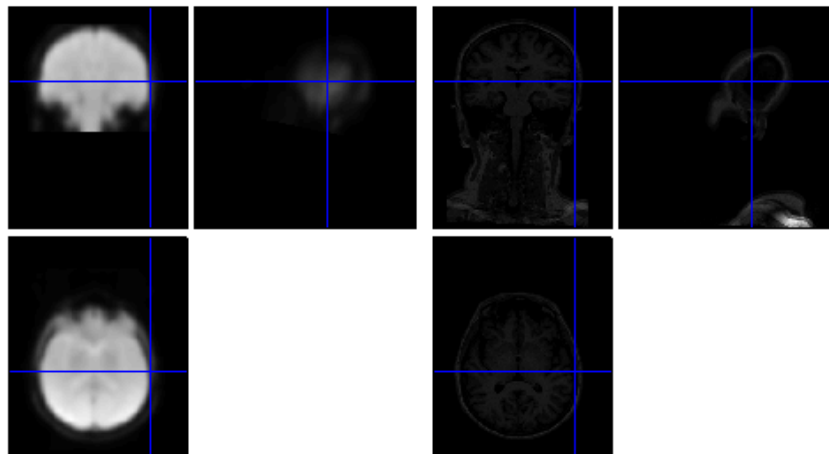
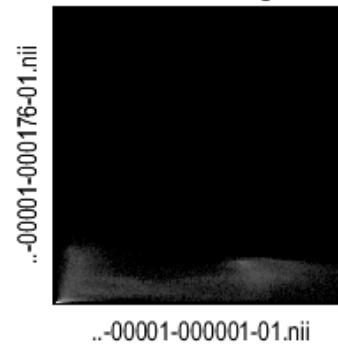


Figure 32: Normalised Mutual Information Histograms.

At the end of the coregister preprocessing step it is important to verify the quality of the coregistration by clicking on the edges of the brain from the source image and verify whether they correspond to the edges of the brain from reference image. The "Check Reg" function of SPM can and should also be used to verify the coregistration of multiple images.

- **Normalization**

The strategy used for the Normalization, was a two-step Normalization. First the coregistered and resliced anatomical image was normalized to the ICBM (International Consortium for Brain Mapping) stereotaxic space using the "ICBM space template-European brains" and then the estimated parameters (deformation field) were used to normalize the slice-timed, realigned, and coregistered functional images.

First step - Normalise (Estimate & Write)

Image to Align: coregistered and resliced anatomical image

Images to Write: coregistered and resliced anatomical image

Estimation Options:

Bias regularization: very light regularization (0.0001)

Bias FWHM: 60mm cutoff

Tissue probability map: .\SPM\spm12\tpm\TPM.nii

Affine Regularisation: ICBM space template-European brains

Warping Regularisation: default (1x5 double)

Smoothness: 0

Sampling distance: 3

Writing Options:

Bounding box: default (2x3 double)

Voxel sizes: [2 2 2]

Interpolation: 4th Degree B-Spline

Filename prefix: w

Second step - Normalise (Write)

Deformation field: the deformation parameters file ("y_rs*") created in the first step

Images to write: slice-timed, realigned, and coregistered functional images.

Writing Options:

Bounding box: default (2x3 double)

Voxel sizes: [2 2 2]

Interpolation: 4th Degree B-Spline

Filename Prefix: w

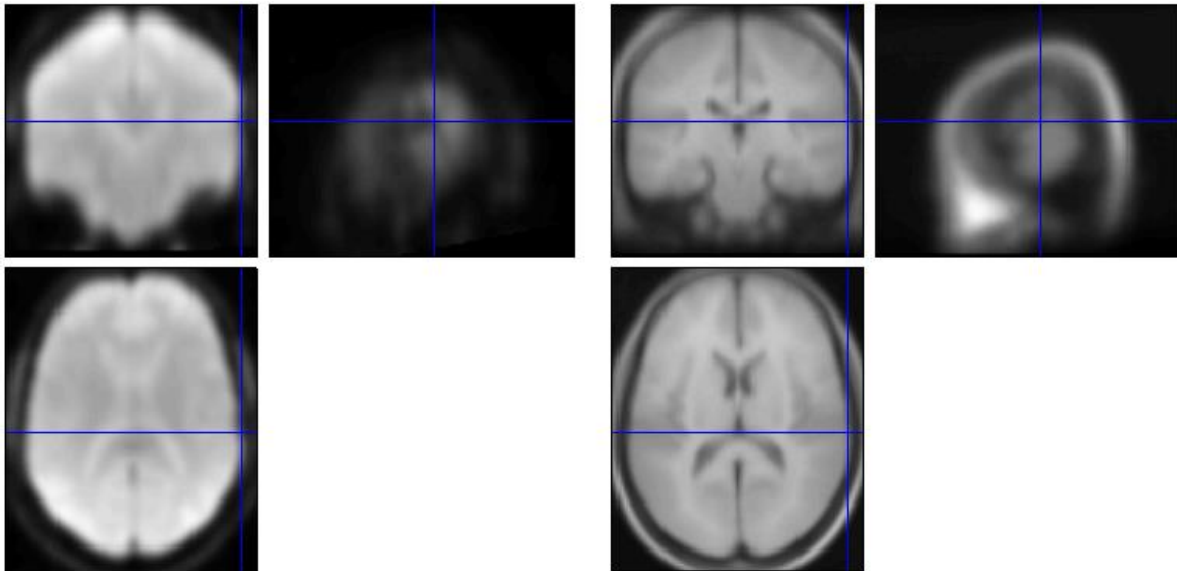


Figure 33: SPM - Check Registration. On the left the subject's image and on the left an MNI template.

At the end of the normalization preprocessing step it is important to verify its quality by clicking on the edges of the brain from the normalized functional images and verify whether they correspond to the edges of a brain in an already normalized image. This should be done for each subject.

- **Smoothing**

The functional images are spatially smoothed with a Gaussian Kernel that is approximately twice the voxel dimensions.

Smooth

Images to Smooth: the normalized functional images.

FWHM: [8 8 8]

Data type: SAME

Implicit masking: No

Filename Prefix: s

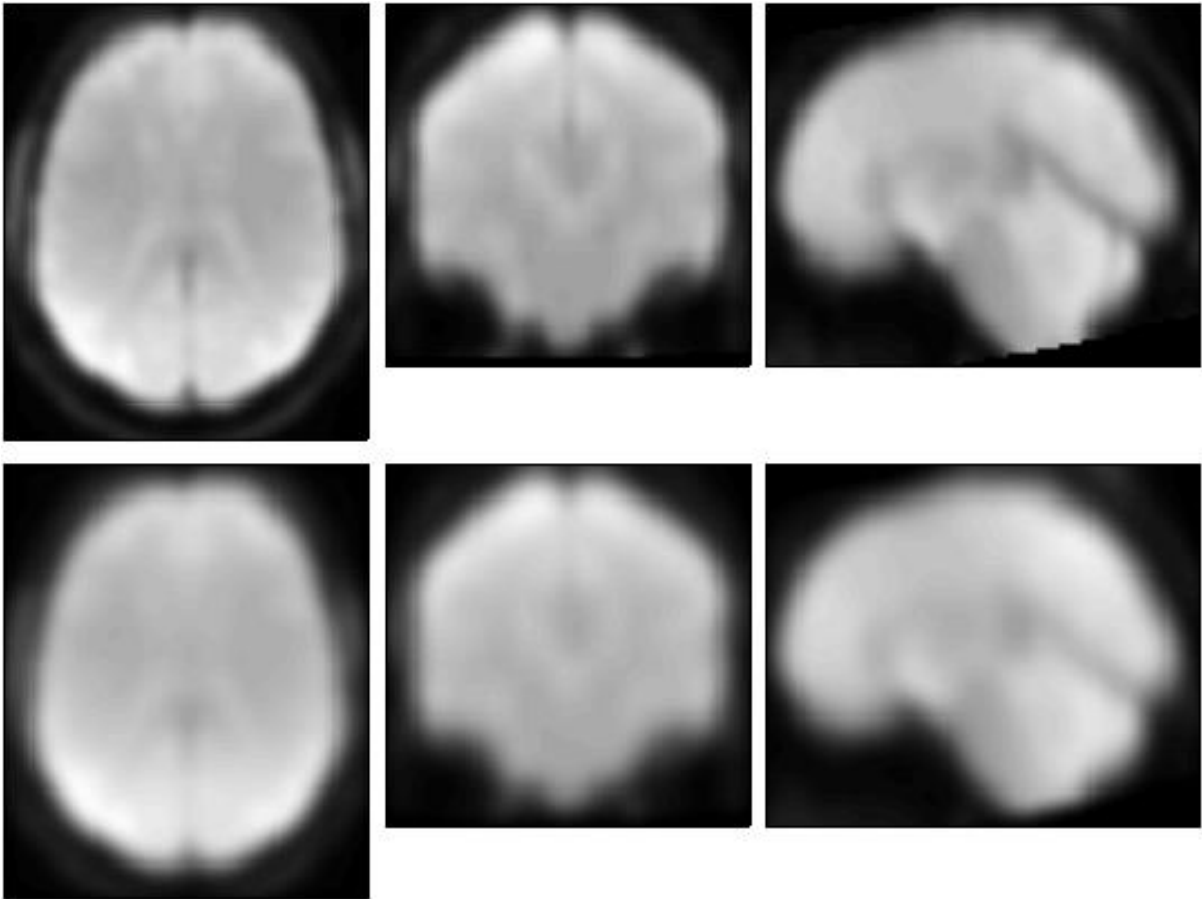


Figure 34: Before Smoothing (top) vs After Smoothing (bottom)

- **Structural Image Preprocessing**

In SPM, the unified segmentation approach [254] combines/optimizes bias correction, segmentation, and normalization all in one, such as the prior probability of a voxel to belong to a tissue class is determined using a tissue probabilistic atlas.

Removal of the skull and other non-brain tissue like dura and eyes from anatomical images, improves coregistration and normalization steps. Skull stripping in SPM can be achieved by segmenting the anatomical scan, and using a thresholded version of the sum of grey and white matter probability maps to mask out the bias corrected structural scan.

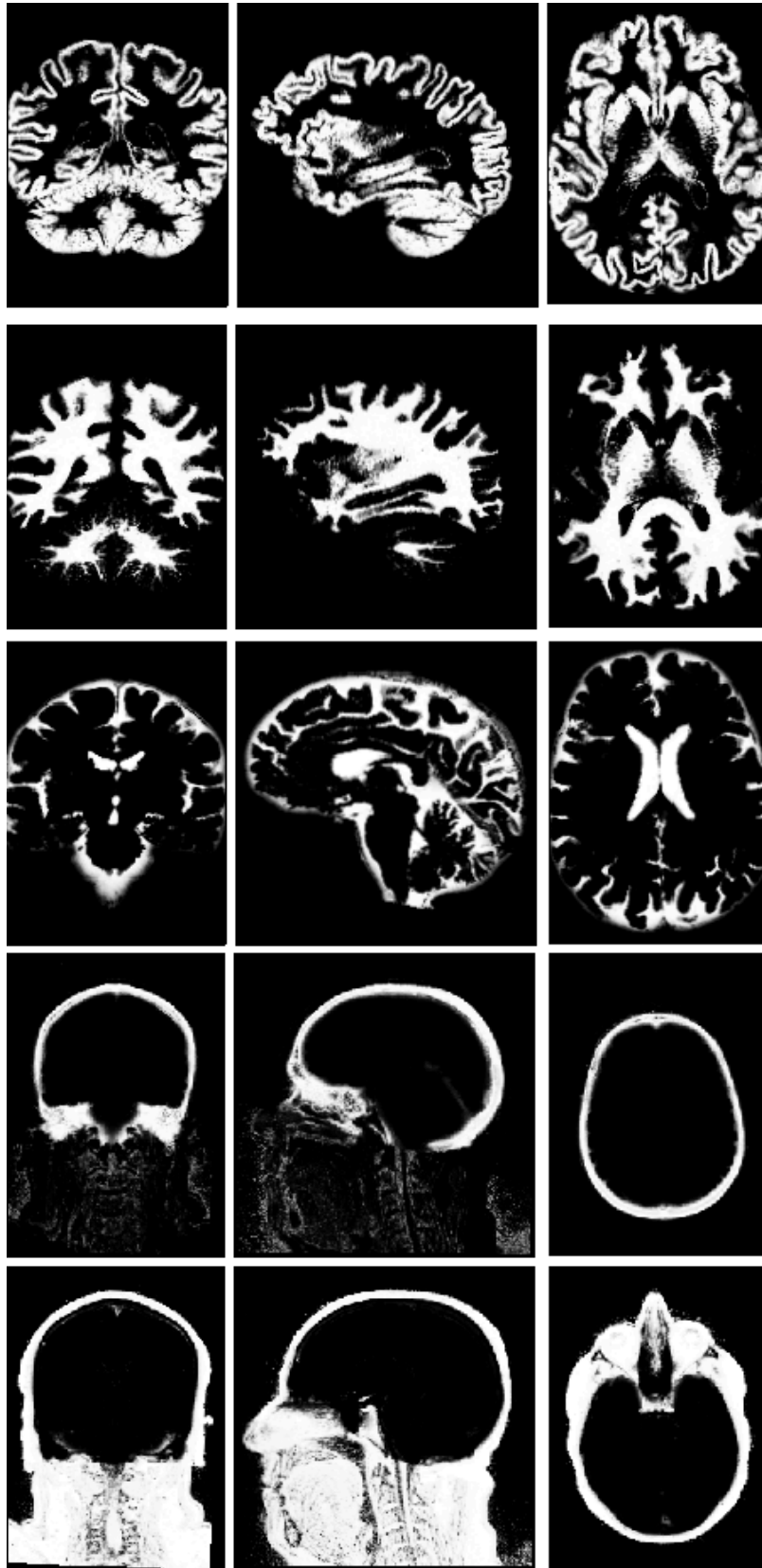


Figure 35: Segmentation of structural T1 image. From top to bottom: GM; WM; CSF; Bone; soft-tissue.

- **Image Calculator (ImCalc)**

ImCalc is a SPM tool that allows algebraic manipulation on a set of images, with the result being written as an image. Combining the segmented images of Gray Matter and White Matter, it is possible to extract the brain (removing bone, CSF, soft tissue, air) from the original picture.

ImCalc

Input Images: c1*.nii (i1), c2*.nii (i2), original structural image (i3).

Output Filename: e.g. "justbrain"

Output directory: same directory where the structural image is saved.

Expression: $[i3.*(i1+i2)]$

Data Matrix: No

Masking: No implicit zero mask

Interpolation: Trilinear

Data Type: INT16 – signed short

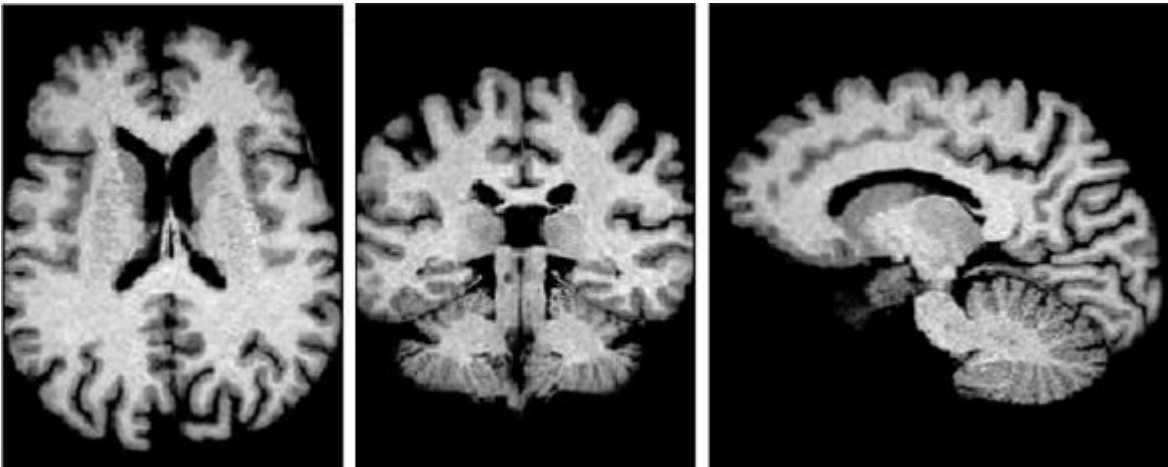


Figure 36: Image resulting from combination of GM and WM of one subject.

- **Surface extraction**

Using SPM it is possible to render 3D surface models of brains, having as input the segmented images of White and Gray Matter.

Surface Extraction

In the SPM Menu select Render -> Extract Surface.

Select c1*.nii and c2*.nii images

Save Rendering and Surface



Figure 37: 3D surface model extracted from GM and WM images.

12.1.5 - Statistical Analysis

At the first-level, one General Linear Model (GLM) was set modelling the four conditions individually (i.e. one regressor for each condition) with blocks of 40 s duration with onset on the first trial card of the corresponding block. Additionally, six regressors of no interest were included corresponding to the six motion parameters estimated during preprocessing (realign).

Specify 1st-level:

Timing parameters:

Units for design: Seconds
Interscan interval: 2
Microtime Resolution: 30
Microtime onset: 2

Data&Design:

Scans: preprocessed functional images

Condition:

Name: nb0
Onsets: from the synchronization system
Durations: 40
Time modulation: no time modulation
Orthogonalise modulations: Yes

Condition:

Name: nb2
Onsets: from the synchronization system
Durations: 40
Time modulation: no time modulation
Orthogonalise modulations: Yes

Condition:

Name: nb1
Onsets: from the synchronization system
Durations: 40
Time modulation: no time modulation
Orthogonalise modulations: Yes

Condition:

Name: nbfix
Onsets: from the synchronization system
Durations: 40
Time modulation: no time modulation
Orthogonalise modulations: Yes

Multiple regressors: rp_af*.txt file created during the realign preprocessing step.
High-pass: 800

Basis Functions: Canonical HR
Model derivatives: No derivatives
Model Interactions (Volterra): Do not model interactions

Global normalisation: None
Masking threshold: 0.8
Serial correlations: AR(1)

After the definition of the GLM it is important to review it using the "Review" function in SPM.

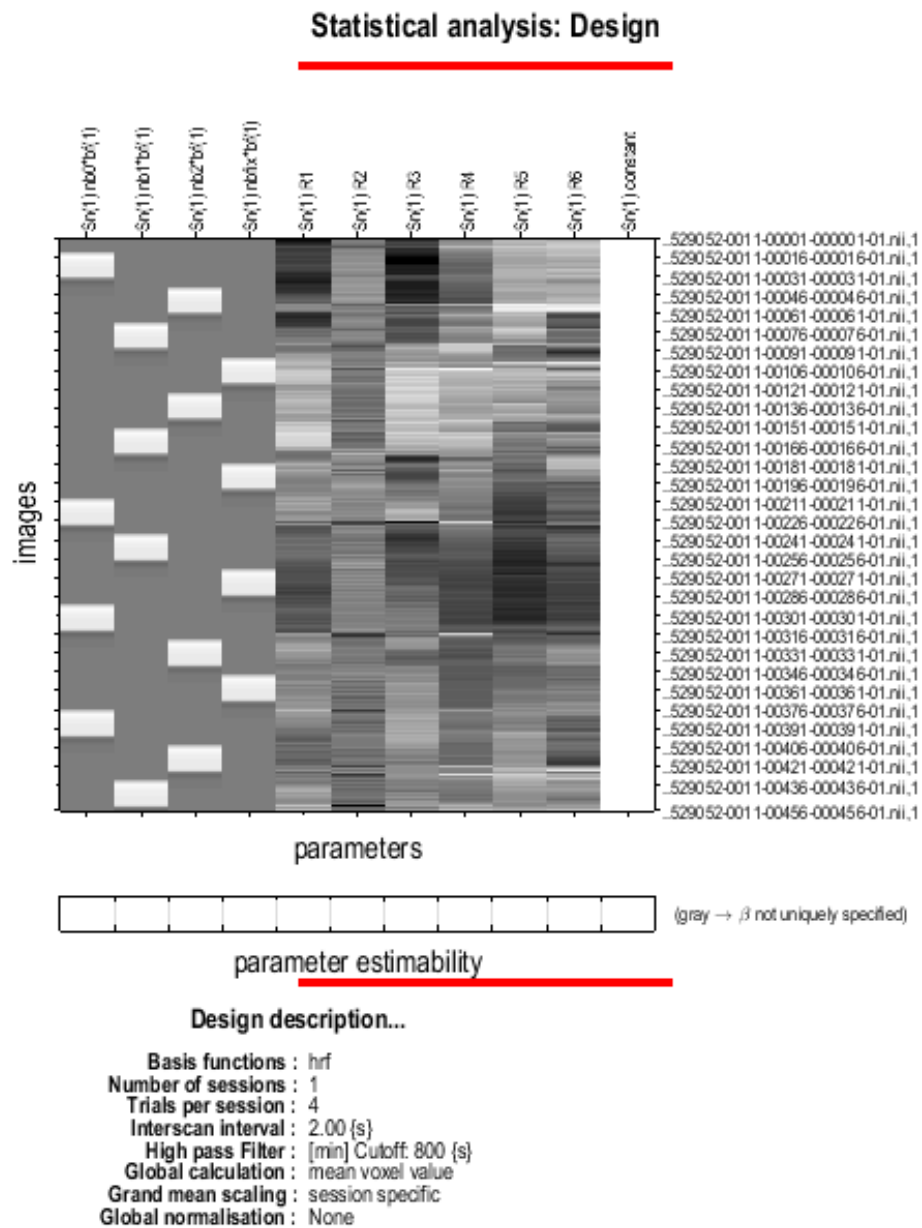


Figure 38: Review of study design

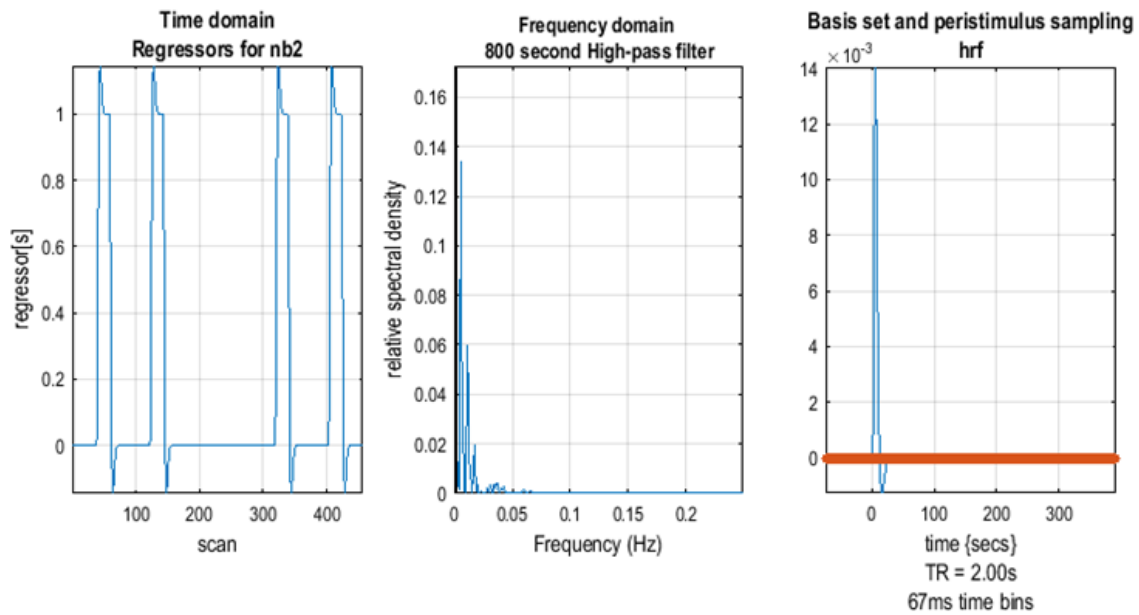


Figure 39: Review of parameters.

- **Model Estimation**

Estimate

Select SPM.mat: SPM.mat containing GLM defined in "Specify 1st-level"

Write residuals: No

Method: Classical

Once the model estimate is finished then the results can be viewed through the "Results" function in SPM. The first thing to do before visualizing results is to define the contrasts of interest. In this study the following t contrasts were defined:

Results

nb1>nb0: contrast weights vector [-1 1 0 0 0 0 0 0 0]

nb2>nb0: contrast weights vector [-1 0 1 0 0 0 0 0 0]

Apply masking: none

p value (FWE): 0.05

&extent threshold {voxels}: 80

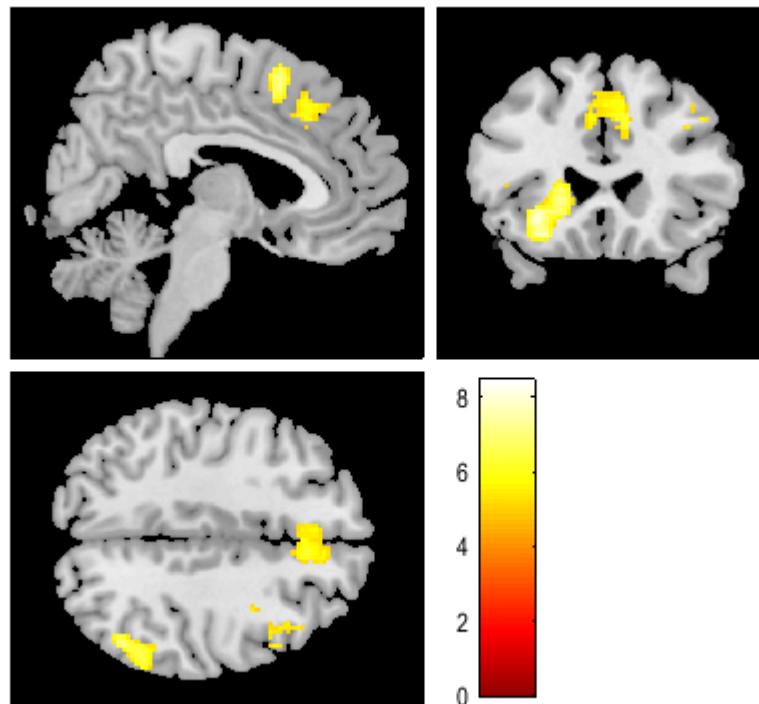
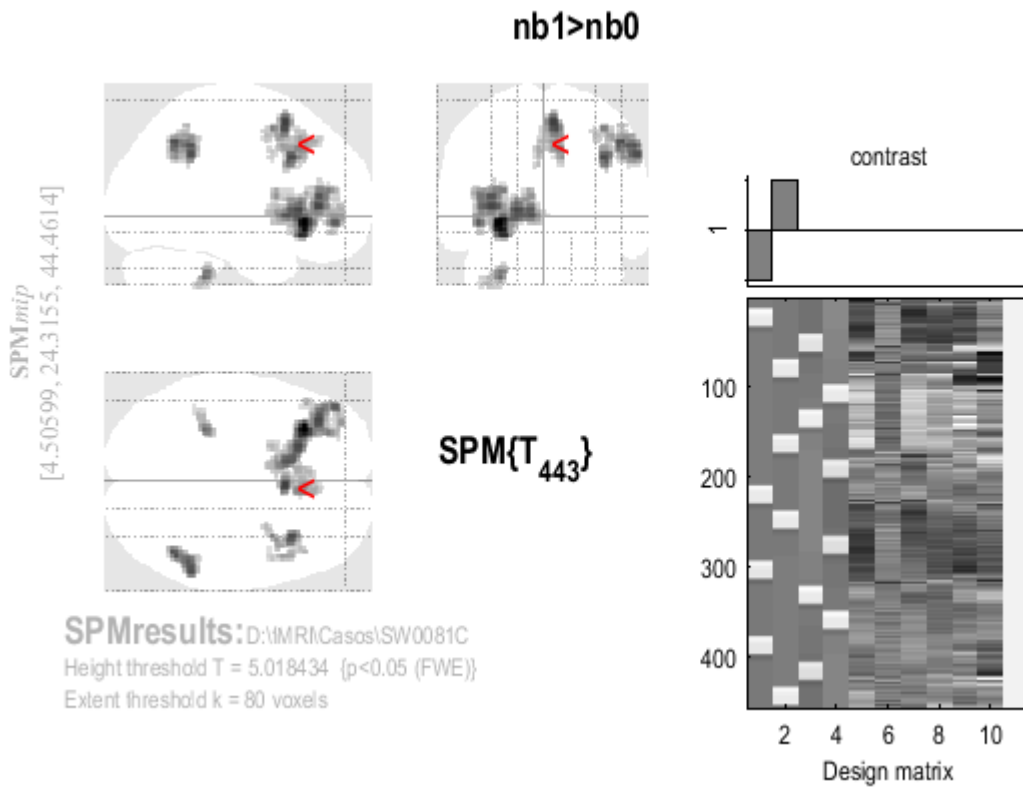


Figure 40: Brain regions of subject SW0081C in which local volume was significantly related with working memory. Clusters (>80voxels), significant at $p < 0.05$ (FWE corrected), are projected on coronal, axial and sagittal sections. The color bar represents the t values.

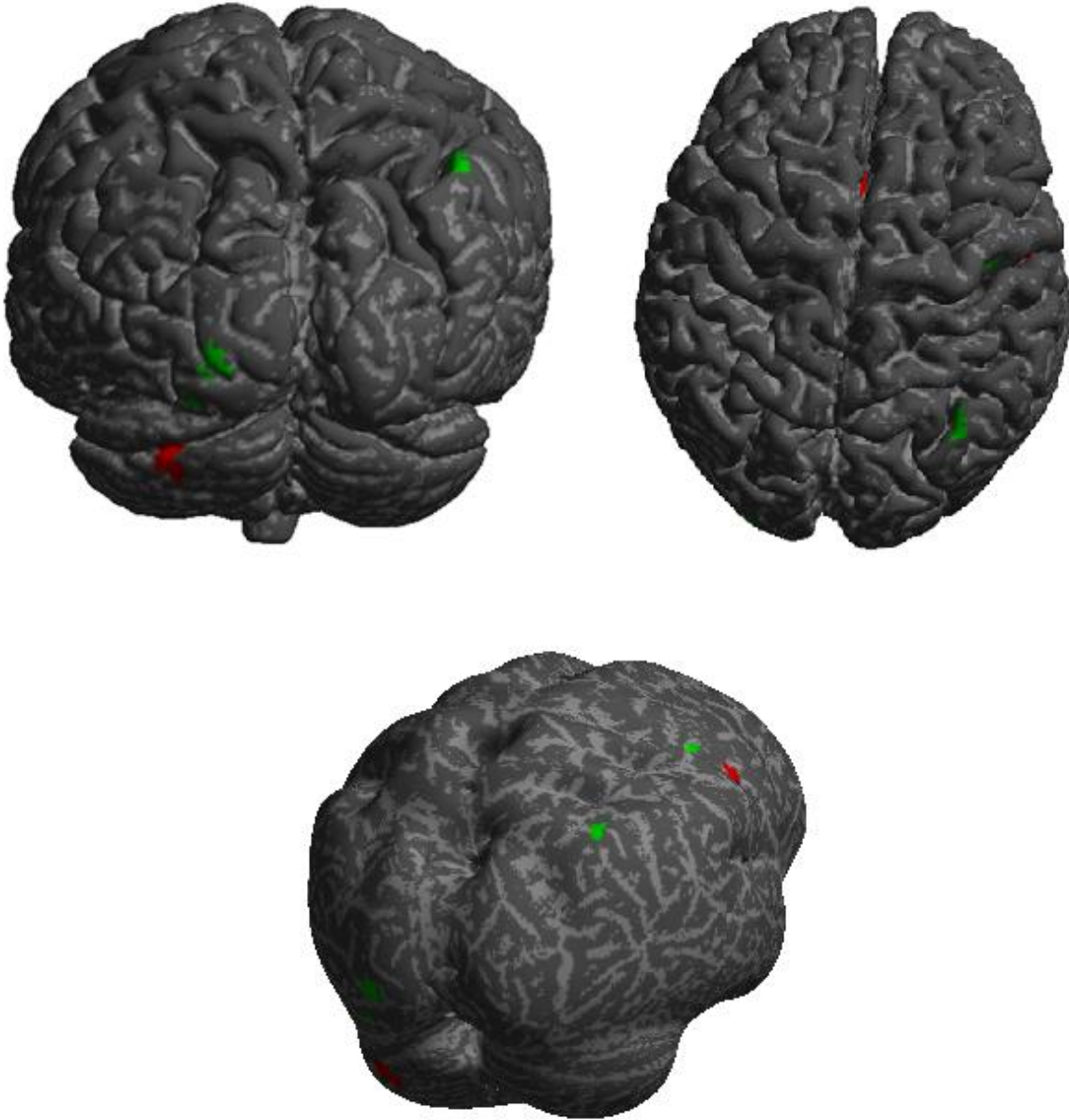


Figure 41: 3D surface model of a single subject overlaid with its individual statistical map with two contrasts. Red: $nb1 > nb0$. Green: $nb2 > nb0$. The bottom image is an inflated version of the surface model.

- **Group Analysis**

For the group analysis a summary statistics approach was used. Here the contrast images from each subject first-level analysis were used for a second-level analysis where a one-sample t-test was performed to infer about the results of all the subjects in the group.

Specify 2nd-level:

Design: One-sample t-test

Scans: the contrast images from each subject first-level analysis. (e.g. con_001.nii)

Threshold masking: None

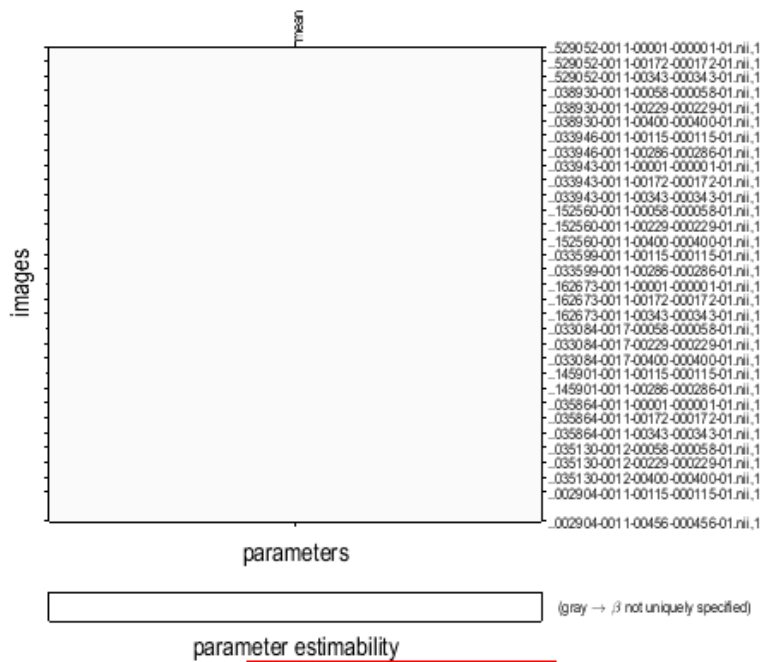
Implicit Mask: Yes

Overall grand mean scaling: No

Normalisation: None

The result of the design will look like an “empty” design because there is only one condition.

Statistical analysis: Design



Design description...

- Design :** One sample t-test
- Global calculation :** omit
- Grand mean scaling :** <no grand Mean scaling>
- Global normalisation :** <no global normalisation>
- Parameters :** 1 condition, +0 covariate, +0 block, +0 nuisance
1 total, having 1 degrees of freedom
leaving 5471 degrees of freedom from 5472 images

Figure 42: SPM – Review Design.

The next step is to run the model estimate. Once this step is finished then the results can be viewed through the "Results" function in SPM. The first thing to do before visualizing results is to define the contrasts of interest. In this study the following contrasts were defined:

Results

Positive Contrast: contrast weights vector [1]
Negative Contrast: contrast weights vector [-1]
Apply masking: image (AAL2 atlas)
Nature of mask: inclusive*
P value adjustment to control: none
Threshold {T or p value}: 0.001
& extent threshold {voxels}: 89

*the inclusive masking with AAL2 atlas will include only gray matter activations.

Using the AAL2 toolbox [255] it is possible to perform an automated anatomical labeling of activations in SPM using a macroscopic anatomical parcellation of the MNI MRI single-subject brain [256]. Combining the labeling information with the p-values table for whole brain one can build results tables (see table 4 and 5).

Toolbox: aal

Automated Anatomical Labeling 2(AAL2): Local Maxima Labeling

Labelised Atlas: spm12\toolbox\aal\ROI_MNI_V5.nii

positive contrast (masked [incl.] by AAL2.nii)

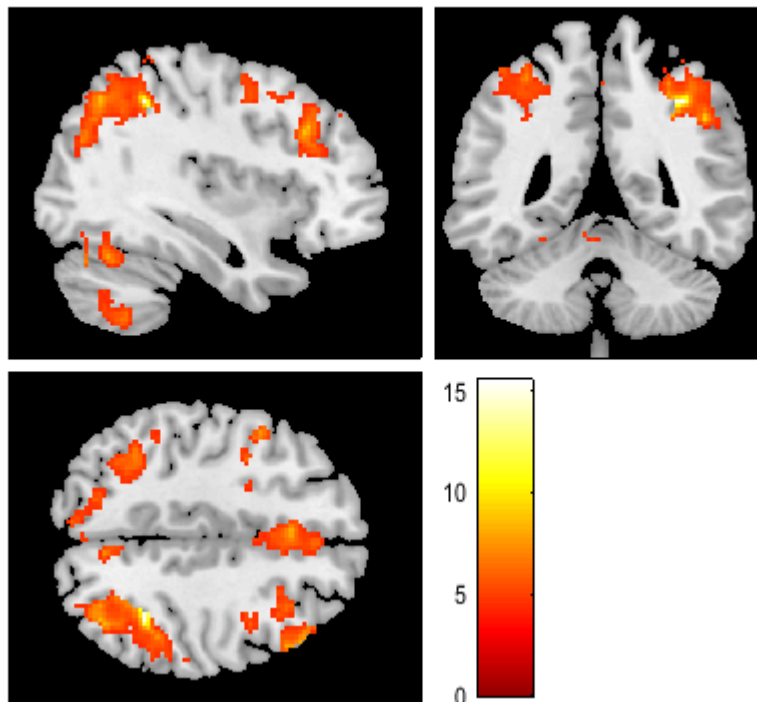
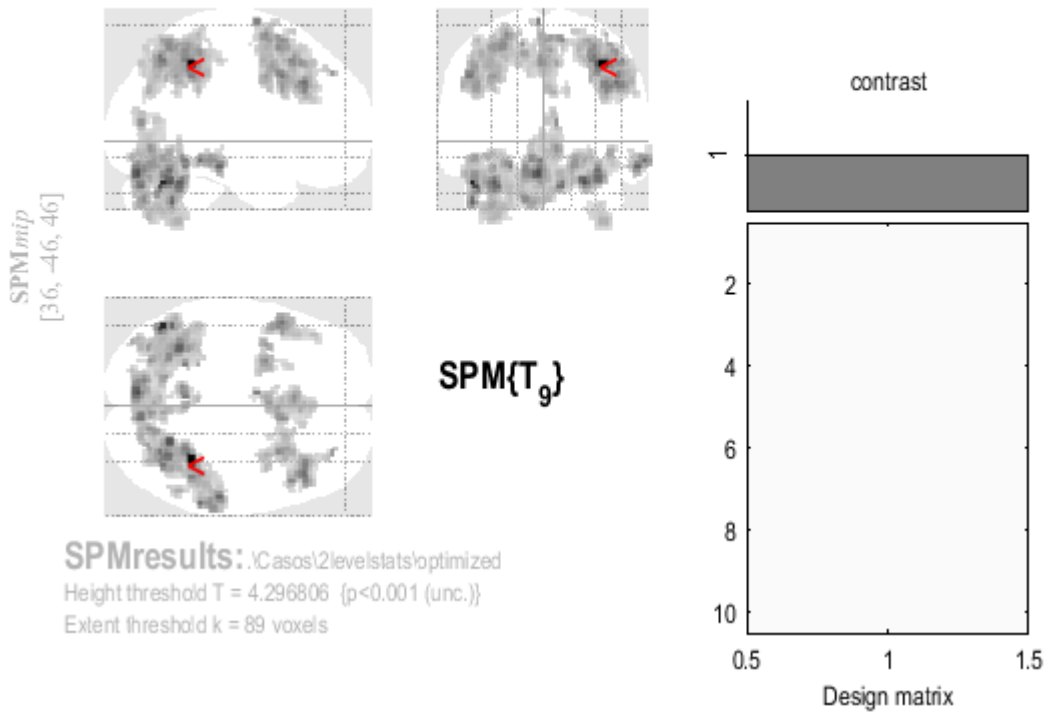


Figure 43: Brain regions from all subjects in the group in which local volume was significantly related with working memory ($nb1 > nb0$). Clusters (>89 voxels), significant at $p < 0.001$ (uncorrected), are projected on coronal, axial and sagittal sections of a template. The color bar represents the t values.

positive contrast (masked [incl.] by AAL2.nii)

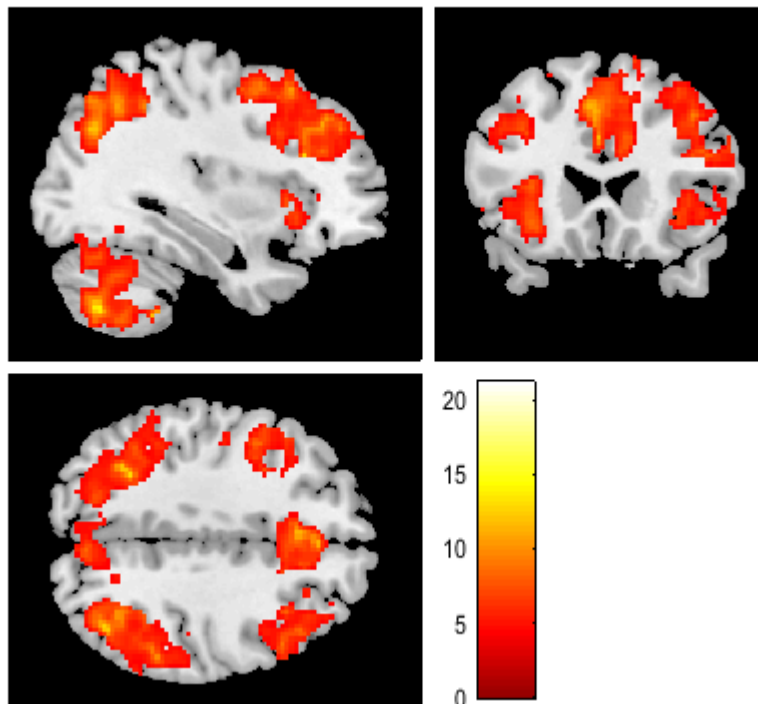
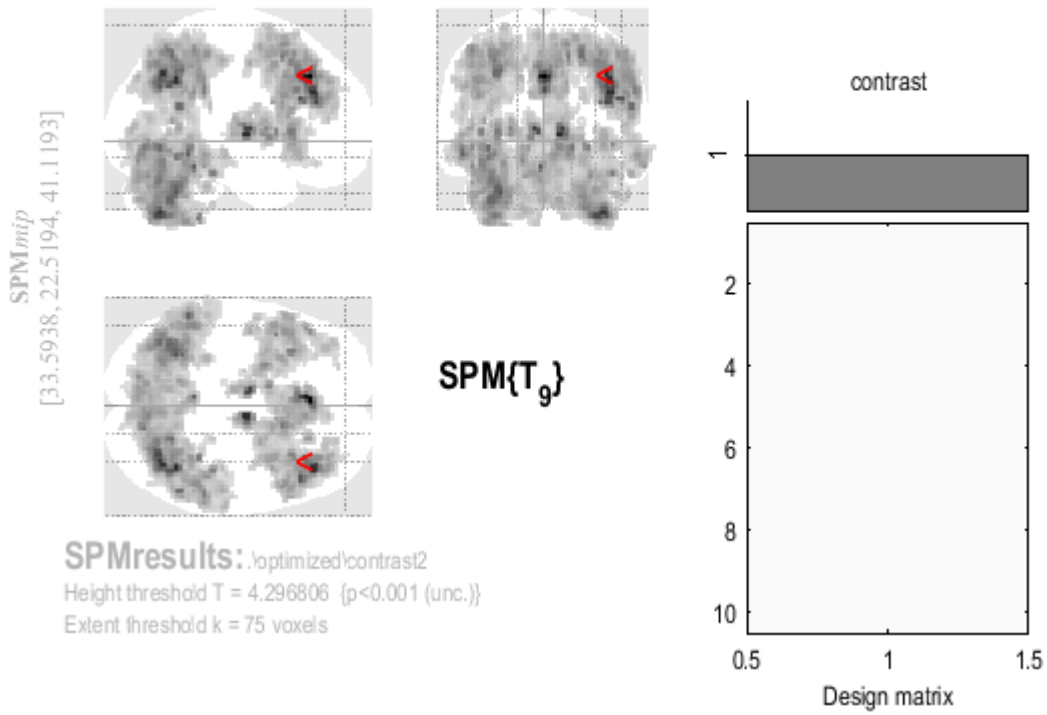


Figure 44: Brain regions from all subjects in the group in which local volume was significantly related with working memory ($nb2 > nb0$). Clusters (>75 voxels), significant at $p < 0.001$ (uncorrected), are projected on coronal, axial and sagittal sections of a template. The color bar represents the t values.

Table 4: Grey matter regions showing a positive correlation with working memory (nb1>nb0). Each cluster's coordinates in MNI space (x, y, z), maximum Z-value and size are given. From clusters (>89voxels), significant at $p<0.001$ (uncorrected) different brain regions were automatically labeled using AAL2 toolbox for SPM with the ROI_MNI_V5 anatomical parcellation database.

Condition	Regions	Peak MNI coordinates (x,y,z) mm	Cluster size (voxels)	Maximum Z-score
nb1 > nb0	Parietal Inferior (Right)	36 -46 46	1732	5.35
	Angular (Right)	38 -64 48		4.51
	Parietal Superior (Right)	30 -66 50		4.49
	Cerebellum Crus I (Left)	-48 -64 -28	3994	5.09
	Cerebellum Crus I (Left)	-6 -80 -22		4.82
	Cerebellum VI (Right)	24 -60 -28		4.80
	Temporal Inferior (Right)	58 -28 -18	239	4.65
	Temporal Mideal Right	62 -40 -14		4.58
	Temporal Mideal Right	54 -36 -8		3.36
	Frontal Mideal II (Right)	44 26 34	1857	4.58
	Supplementary motor area (Left)	-6 -4 72		4.45
	Frontal Mideal II (Right)	48 18 48		4.36
	Frontal Mideal II (Left)	-50 12 38	360	4.49
	Precentral (Left)	-48 6 44		4.13
	Frontal Mideal II (Left)	-42 20 38		3.72
	Cerebellum IV V (Left)	-4 -50 -14	89	4.46
	Vermis III	-2 -42 -14		3.76
	Lingual (Left)	-10 -54 -4		3.66
	Parietal Superior (Left)	-28 -60 58	1043	4.32
	Parietal Superior (Left)	-16 -62 58		4.20
	Parietal Superior (Left)	-34 -48 56		4.17
	Frontal Superior II (Left)	-26 2 64	377	4.30
	Precentral (Left)	-36 2 38		4.11
	Precentral (Left)	-38 0 48		3.94

Table 5: Grey matter regions showing a positive correlation with working memory (nb2>nb0). Each cluster's coordinates in MNI space (x, y, z), maximum Z-value and size are given. From clusters (>75voxels), significant at $p<0.001$ (uncorrected) different brain regions were automatically labeled using AAL2 toolbox for SPM with the ROI_MNI_V5 anatomical parcellation database.

Condition	Regions	Peak MNI coordinates (x,y,z) mm	Cluster size (voxels)	Maximum Z-score
nb2 > nb0	Frontal Superior Medial (Left)	-2 30 38	5693	5.82
	Frontal Inferior Triangularis (Right)	40 32 28		5.51
	Frontal Inferior Triangularis (Right)	46 24 24		5.25
	Thalamus (Right)	8 -10 2	317	5.54
	Thalamus (Right)	10 -18 12		4.25
	Thalamus (Right)	12 -8 14		4.00
	Angular (Right)	40 -56 36	6904	5.51
	Angular (Right)	38 -64 40		5.47
	Occipital Mideal (Right)	38 -66 32		5.20
	Cerebellum VIIIb (Right)	36 -66 -46	11308	5.44
	Cerebellum VI (Left)	-30 -56 -34		5.21
	Cerebellum III (Left)	-4 -44 -18		5.15
	Thalamus (Left)	-8 -8 6	3220	5.37
	Insula (Left)	-32 18 4		4.86
	Insula (Left)	-42 8 4		4.78
	Pallidum (Right)	14 6 0	132	4.78
	Pallidum (Right)	22 2 0		4.21
	Pallidum (Right)	20 -4 6		3.90
	Temporal Inferior (Right)	50 -16 -26	76	4.01
	Temporal Inferior (Right)	58 -14 -26		3.64
Cingulum Anterior (Right)	8 42 12	75	3.97	
Cingulum Anterior (Right)	8 42 22		3.50	

Another possibility is to make inferences based on between-subject comparisons. One example for this study is to compare the activations of female vs male. For that in SPM one can use a two-sample t-test.

Specify 2nd level

Directory: where the SPM.mat file containing the specified design matrix will be written

Design: Two-sample t-test

Group 1 scans: Select the appropriate contrast con_000* files from the individual subject folders corresponding to females. (In this case 6 files)

Group 2 scans: Select the appropriate contrast con_000* files from the individual subject folders corresponding to males. (In this case 5 files)

Independence: Yes

Implicit Mask: Yes

Variance: Unequal

Global Calculation: Omit

Grand mean scaling: No

Overall Grand mean scaling: No

ANCOVA: No

Normalization: None

Estimate

Select SPM.mat defined in the previous step

Write residuals: No

Method: Classical

Results:

Define t-contrast: [1 -1]

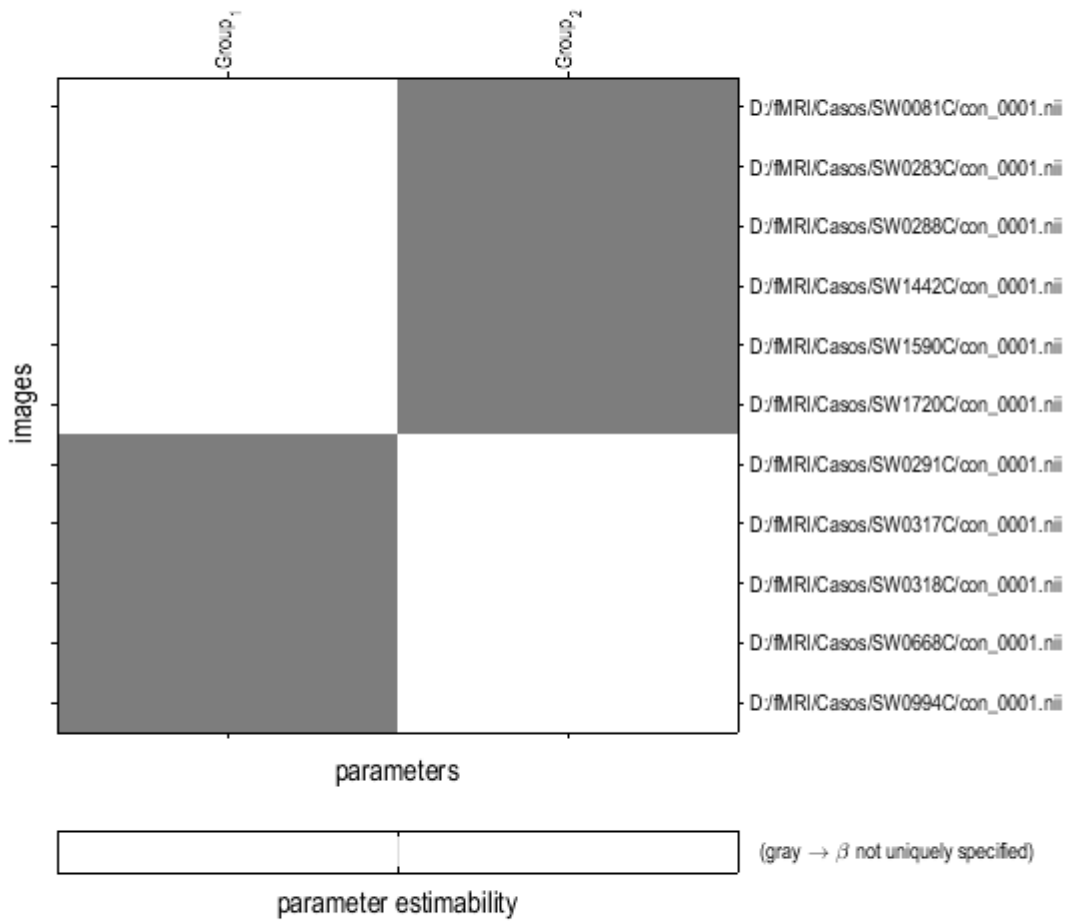
Apply masking: none

p value (FWE): 0.05

&extent threshold {voxels}: 0

Applying the t-contrast with FWE correction at $p > 0.05$ results in no suprathreshold voxels. With uncorrected threshold a very small population of voxels appear as having being active in females but not in males, though due to their sparsity those are most likely false positive results. (see figure 45)

Statistical analysis: Design



Design description...

Design : Two-sample t-test
Global calculation : omit
Grand mean scaling : <no grand Mean scaling>
Global normalisation : <no global normalisation>
Parameters : 2 condition, +0 covariate, +0 block, +0 nuisance
 2 total, having 2 degrees of freedom
 leaving 9 degrees of freedom from 11 images

Figure 45: Study design of two-sample t-test. Group 1: female subjects. Group 2: male subjects

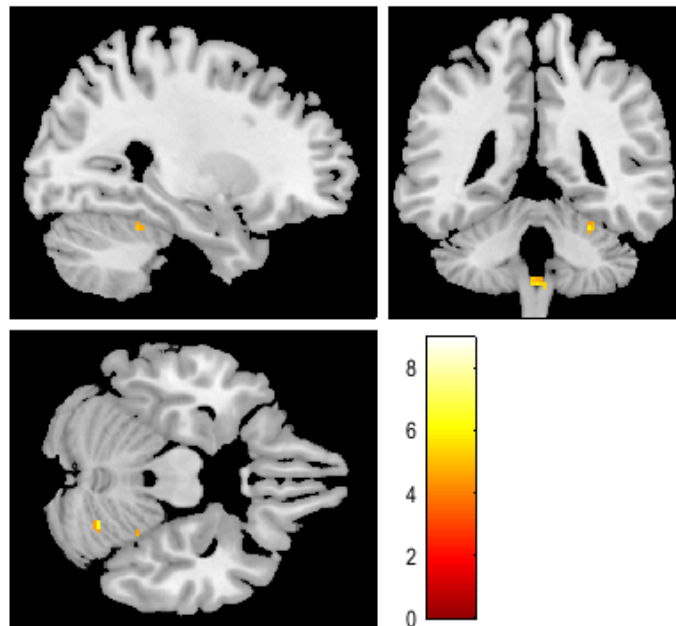
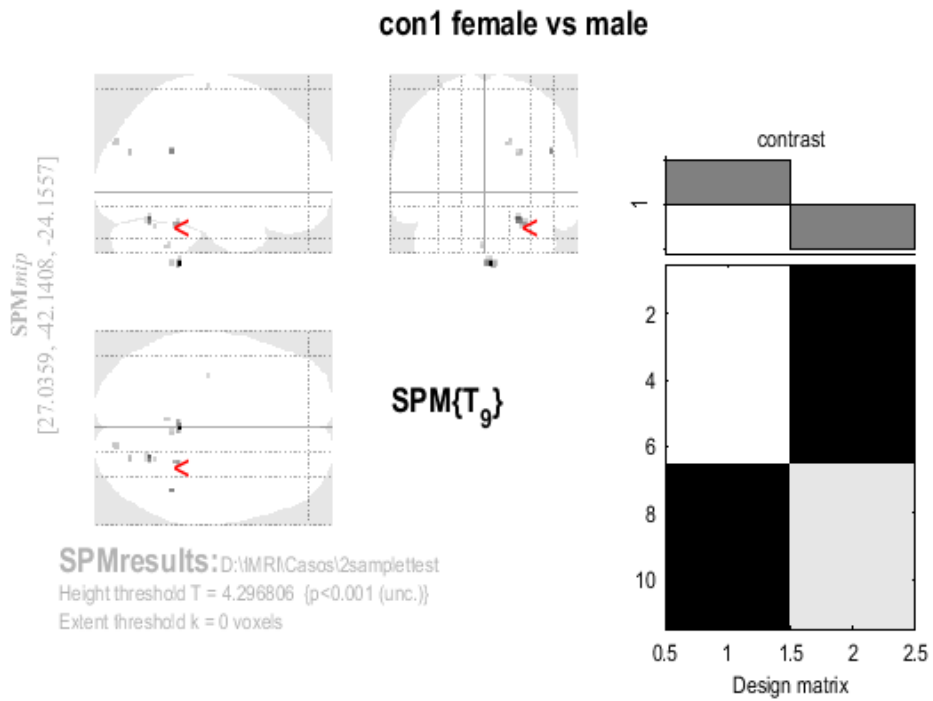


Figure 46: Brain regions in which local volume from female group was more significantly related with working memory than male group. Voxel significant at $p < 0.001$ (uncorrected), are projected on coronal, axial and sagittal sections of a template. The color bar represents the t values.

12.1.6 - Results Interpretation

Regions where significant activations were found for the defined contrasts are in accordance with findings of similar working memory studies [253, 257] which validates the pipeline used in this study.

12.2 - Resting State Study

In this study the goal is to identify Resting State Networks.

12.2.1 - Participants

For this study 15 healthy volunteers were selected. The inclusion criteria was being more than 50 years old.

Table 6: Participants demographic data

	Number of participants	Age (years) min/max/average/SD
females	6	55 / 82 / 68,8 / 8,6
males	9	58 / 77 / 64,7 / 7,8
total	15	55 / 82 / 66,3 / 8,1

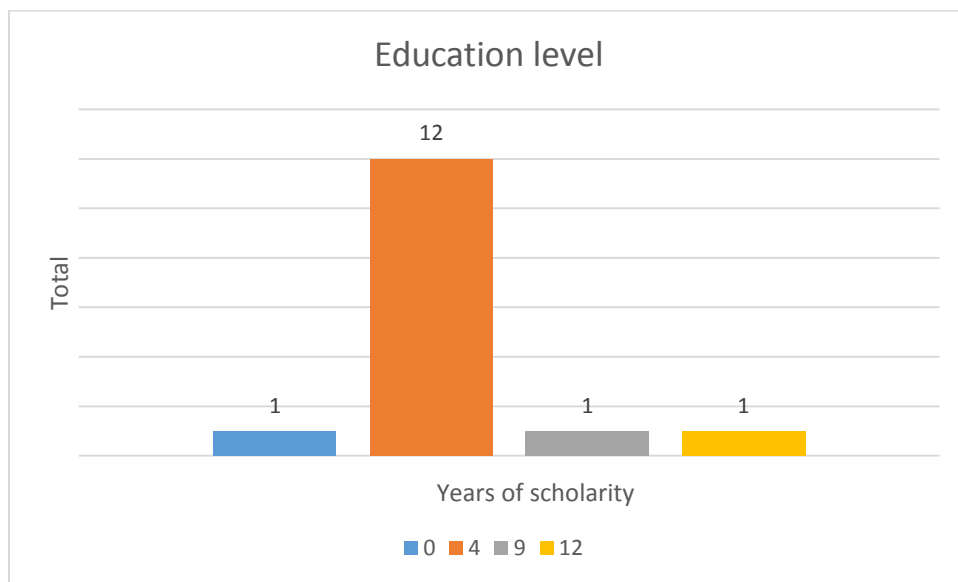


Figure 47: Participants education level

12.2.2 - Image acquisition and Paradigm

Imaging was performed at Hospital de Braga on a clinical approved 1.5 T Siemens Magnetom Avanto MRI scanner (Siemens, Erlangen, Germany) using the Siemens 12-channel receive-only head coil.

The imaging session included one structural T1 high-resolution anatomical sequence, 3D MPRAGE (magnetization prepared rapid gradient echo). This protocol was performed with the following scan parameters: TR/TE=2.730/3.48ms, 176 sagittal slices with no gap, FA=7°, in-plane resolution=1.0mm×1.0mm and slice thickness = 1.0 mm with an Interleaved acquisition order.

Acquisition of BOLD sensitive, gradient echo T2* weighted EPI images was performed with the following parameters: TR/TE=2000/30ms, 30 interleaved axial slices with slice gap=0.48mm, FA=90°, in-plane resolution=3.5×3.5mm², slice thickness=3.5mm, FOV=224x224mm² and 180 volumes. During the resting state scan, the subjects were instructed to remain still, awake, with their eyes closed, as motionless as possible and to think of nothing in particular. None of the participants fell asleep during the acquisition.

12.2.3 - Preprocessing

The preprocessing of the structural and functional images was performed using an optimized pipeline developed by the researchers at ICVS, based on the one applied in the BrainCAT software package [226].

- **Software**

Software used for preprocessing and statistical analysis was FSL 5.0.9 included in FSLVm6_64 image running on VMware® Workstation 12 Player 12.1.0 build-3272444 on a Windows 8.1 Pro 64-bit.

- **Bash**

For this example the command line was used. Here the commands are typed in the bash terminal. By typing just the command, the syntax for usage of the command plus a list of all the different options of each command is displayed.

```

fsl@fslvm6:~
File Edit View Search Terminal Help
[fsl@fslvm6 ~]$ bet

Usage:    bet <input> <output> [options]

Main bet2 options:
-o        generate brain surface outline overlaid onto original image
-m        generate binary brain mask
-s        generate approximate skull image
-n        don't generate segmented brain image output
-f <f>    fractional intensity threshold (0->1); default=0.5; smaller values
-g <g>    vertical gradient in fractional intensity threshold (-1->1); defau
-r <r>    head radius (mm not voxels); initial surface sphere is set to half
-c <x y z> centre-of-gravity (voxels not mm) of initial mesh surface.
-t        apply thresholding to segmented brain image and mask
-e        generates brain surface as mesh in .vtk format

Variations on default bet2 functionality (mutually exclusive options):
(default) just run bet2
-R        robust brain centre estimation (iterates BET several times)
-S        eye & optic nerve cleanup (can be useful in SIENA)
-B        bias field & neck cleanup (can be useful in SIENA)
-Z        improve BET if FOV is very small in Z (by temporarily padding end

```

Figure 48: Screenshot of a Bash session with FSL command "bet" instructions

- **File Conversion**

Convert images from DICOM format to NiftI format (.nii) using the dcm2nii tool from MRICron. Note that the variables \$DIR and \$i correspond to the directory and folder where the images for each subject are stored. \$i corresponds as well to the subject id (e.g. SW00081C)

```

dcm2nii -d N -x Y -o $DIR/$i/MRI $DIR/$i/MRIDCM/*0001.dcm
dcm2nii -d N -x N -o $DIR/$i/FMRI $DIR/$i/FMRIDCM/*0001.dcm

Options:
-d Date in filename: Y or N (Yes or No)
-x Reorient and crop 3D NIfTI images: Y or N (Yes or No)
-o Output Directory

```

The -x function will reorient the image to the canonical space (only structural image should be reoriented as reorienting fMRI data can disrupt slice timing correction). In addition it will crop the image function to remove excess air surrounding the brain as well as parts of the neck below the cerebellum. It will add the suffix *co* to the filenames. It creates three .nii files. One with name of the original image, one with the prefix "o" (reoriented) and another with prefix "co" (cropped and reoriented)

As QA step FSLView should be used to visually inspect the reoriented and cropped images. Typing the command `fs/view` will launch the GUI of FSLview.

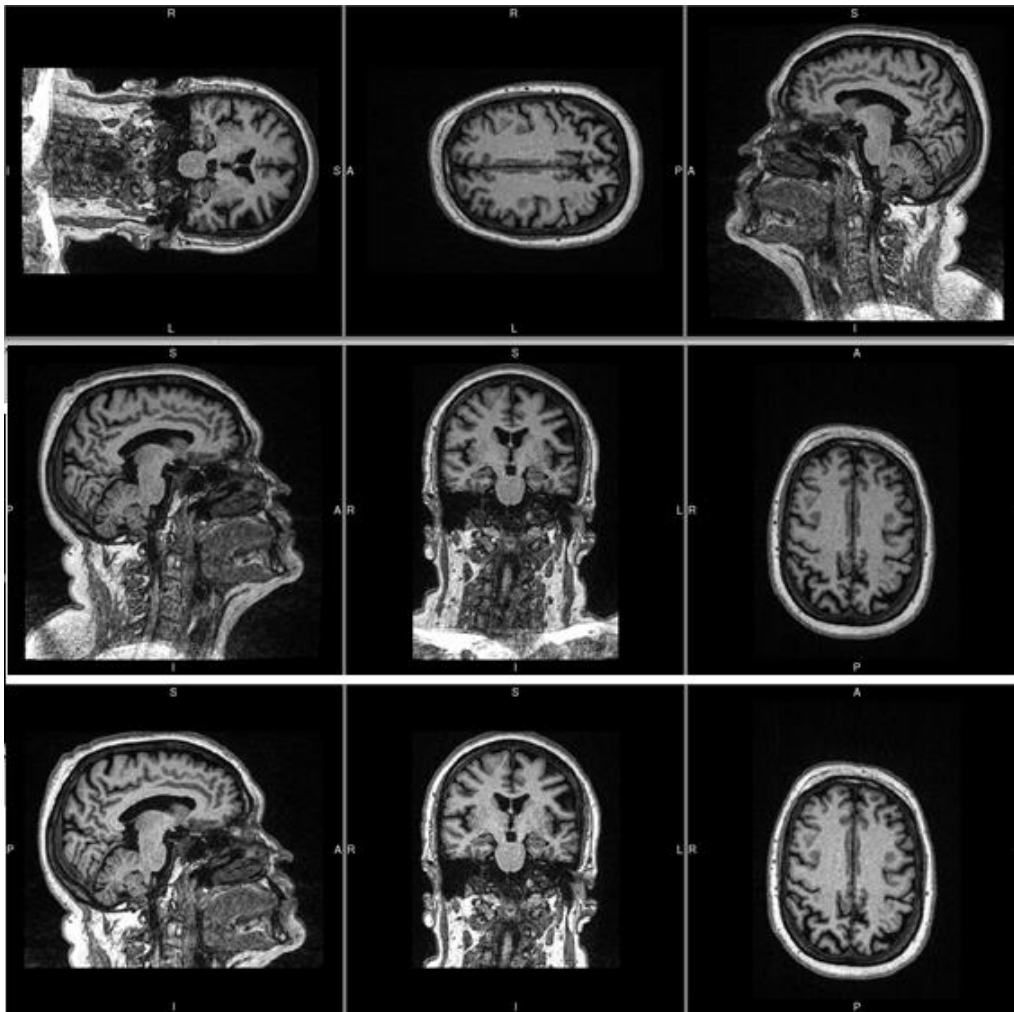


Figure 49: On the top the original structural image, in the middle the oriented version, and on the bottom the cropped (part of the neck was removed) and oriented image.

- **Rename files**

Rename the .nii files such that they include in their name the subject id (\$i), "_str_crop" for structural and cropped images and "_fnc" for functional images to ease its identification.

```
mv $DIR/$i/MRI/"co"*.nii.gz $DIR/$i/MRI/$i"_str_crop.nii.gz"  
mv $DIR/$i/FMRI/*.nii.gz $DIR/$i/FMRI/$i"_fnc.nii.gz"
```

12.2.3.1 - Structural images Preprocessing

- **Skull stripping**

Remove bone from the structural image to allow for a better registration and generate a mask of brain without bone.

```
bet $DIR/$i/MRI/$i"_str_crop.nii.gz"  
$DIR/$i/MRI/$i"_str_crop"_bet -m -f 0.35 -R
```

Options:

```
-m generate binary brain mask  
-f <f> fractional intensity threshold. For the images of this  
study <f> =0.35 was found to be a good starting point.  
-R This option runs more "robust" brain center estimation
```

At the end of the Skull Stripping it is important to verify the quality, using fslview.

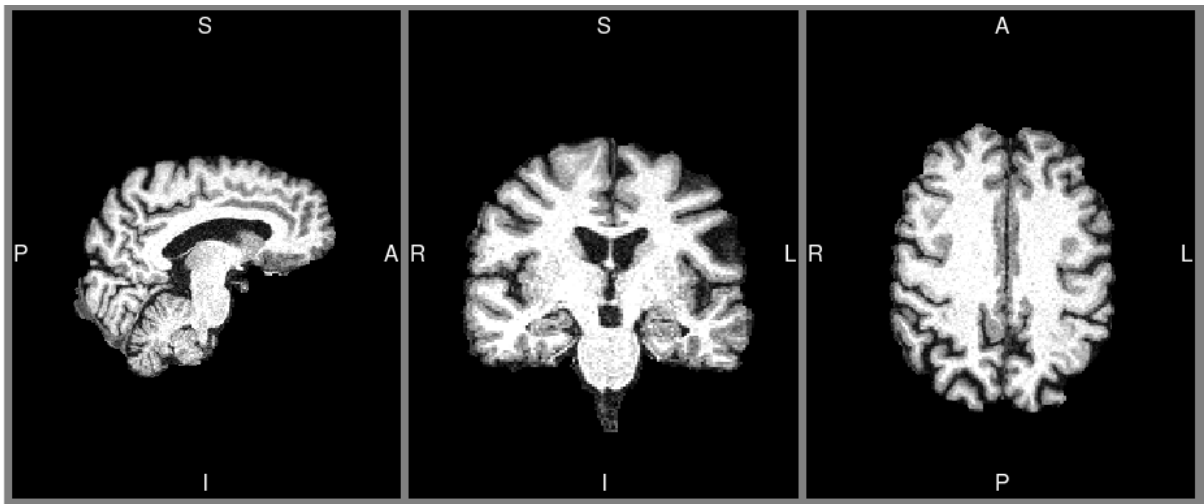


Figure 50: Skull stripped structural image.

A further quality check is achieved by overlaying a mask of the skull stripped brain on the original structural image, using the following command.

```
fslview $DIR/$SUB/MRI/$SUB""_str_crop.nii.gz  
$DIR/$SUB/MRI/$SUB""_str_crop_bet_mask.nii.gz
```

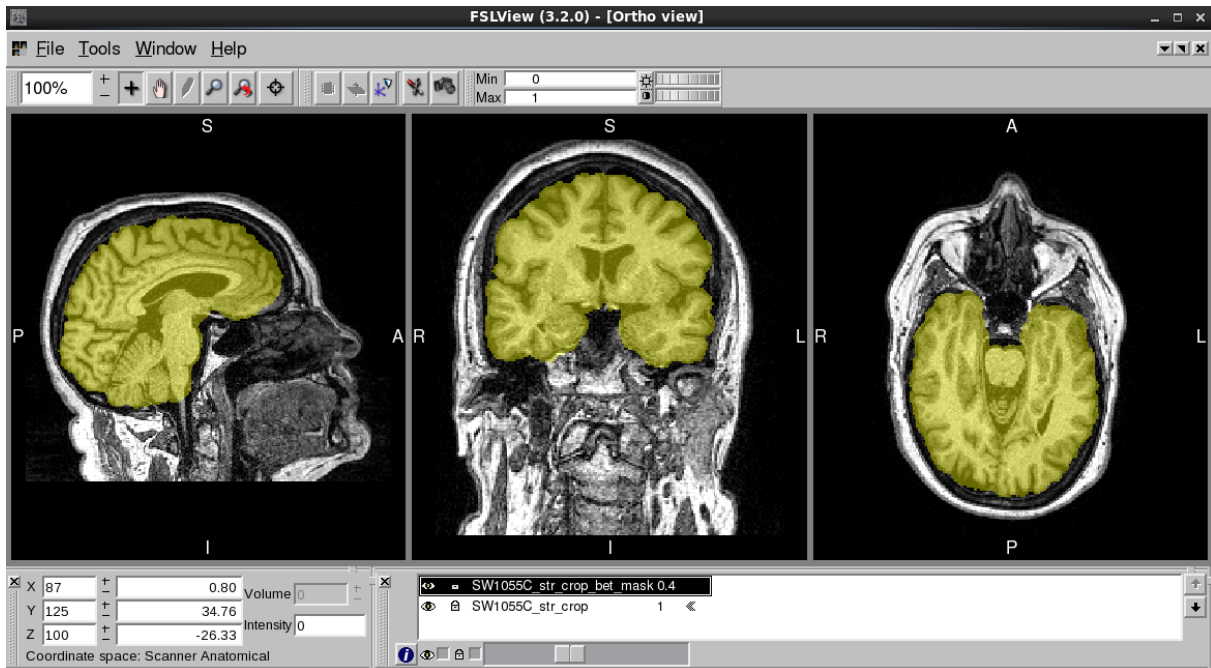



Figure 51: Overlay of brain mask on the original structural image.

Colored yellow with 50% transparency (Figure 50) is the mask which is overlaid on the structural image. It is recommended to visualize different coordinates to check the overall quality of the skull stripping step. If the skull stripping is not optimized then this step should be repeated, adjusting the fractional intensity threshold $-f$ and/or providing estimated brain center coordinates.

```
bet $DIR/$SUB/MRI/$SUB""_str_crop.nii.gz
$DIR/$SUB/MRI/$SUB""_str_crop_bet -m -f $3 -R -c $4 $5 $6
```

Options:

```
-m generate binary brain mask
-f <f> fractional intensity threshold. For the images of this study
<f> of 0.35 was found to be a good starting point. Stored in
variable $3
-R This option runs more "robust" brain center estimation
-c <x y z> center-of-gravity (voxels not mm) of initial mesh
surface. Stored in variables $4 $5 $6
```

At the end of this step verify again with fslview and repeat the process if needed until acceptable quality is reached.

- **Normalize Structural image**

The approach taken here to normalize the structural image to the MNI stereotaxic space involves 3 steps. First apply a linear registration algorithm (FLIRT) to the structural image. Second step is to apply the calculated affine transformation matrix as an initial guess to a non-linear registration algorithm (FNIRT). The final step is to apply the estimated transformation parameters to the structural image.

FLIRT

FLIRT (FMRIB's Linear Image Registration Tool) is a fully automated robust and accurate tool for linear (affine) intra- and inter-modal brain image registration. It performs a linear registration, meaning that it will translate, rotate, zoom and shear one image to match it with another.

```
flirt -searchrx -180 180 -searchry -180 180 -searchrz -180 180 -  
dof 12 -cost normcorr -in $DIR"/$i"/MRI/$i"_str_crop_bet.nii.gz  
-ref $FSLDIR/data/standard/MNI152_T1_1mm_brain.nii.gz -omat  
$DIR"/$i"/MRI/$i"_str_2mni.mat
```

Options:

-search select the angular range over which the initial optimization search stage is performed. *rx*, *ry*, *rz* are the rotation angles in radians (for the matrices *Rx*, *Ry* and *Rz* respectively).

-dof Degrees of freedom. In this case 12 degrees of freedom were used because the images being registered are of different subjects (registering to standard space)

-cost is the Cost Function used. In this case Normalised Correlation "*normcorr*"

-in is the input file volume

-ref is the reference volume

-omat the calculated affine transformation that registers the input to the reference which is saved as a 4x4 affine matrix

FNIRT

FNIRT (FMRIB's Non-Linear Image Registration Tool) is used for cases where the 12 DoF offered by linear registration are not sufficient to achieve a good registration.

```
fnirt --in=$DIR"/$i"/MRI/$i"_str_crop.nii.gz --  
aff=$DIR"/$i"/MRI/$i"_str_2mni.mat --  
cout=$DIR"/$i"/MRI/$i"_str_warp --config=T1_2_MNI152_2mm
```

Options:

--in= input file

--aff= Name of text-file with affine starting guess. The output from the previous step (FLIRT).

--cout= file where thfsolve transformation coefficient-field output is stored.

--config= a configuration file is a text file containing some or all of the parameters that can be specified for fnirt. In this case *T1_2_MNI152_2mm* was used, which is an optimized parameter configuration to register a good quality T1-weighted 3D acquisition to the MNI152 template.

APPLYWARP

```
applywarp --ref=$FSLDIR/data/standard/MNI152_T1_2mm_brain --  
in=$DIR"/$i"/MRI/$i"_str_crop_bet.nii.gz --  
warp=$DIR"/$i"/MRI/$i"_str_warp.nii.gz --  
out=$DIR"/$i"/MRI/$i"_str_crop_bet_mni.nii.gz
```

Options:

--ref= reference image. In this case the MNI template

--in= input image. In this case the cropped and skull stripped structural image.

--warp= the transformation coefficients. The output from the previous step (FNIRT)

--out= output file.

As part of QA, use fslview to verify the structural image normalization.

12.2.3.2 - Functional images preprocessing

- **Remove the first 5 volumes**

The first 5 volumes (10s) of the functional images acquisition are removed to account for initial scanner instability.

```
fslroi $DIR"/$i"/FMRI/$i"_fnc.nii.gz
$DIR"/$i"/FMRI/$i"_fnc_vol 5 175
Usage: fslroi <input> <output> <tmin> <tsize>
```

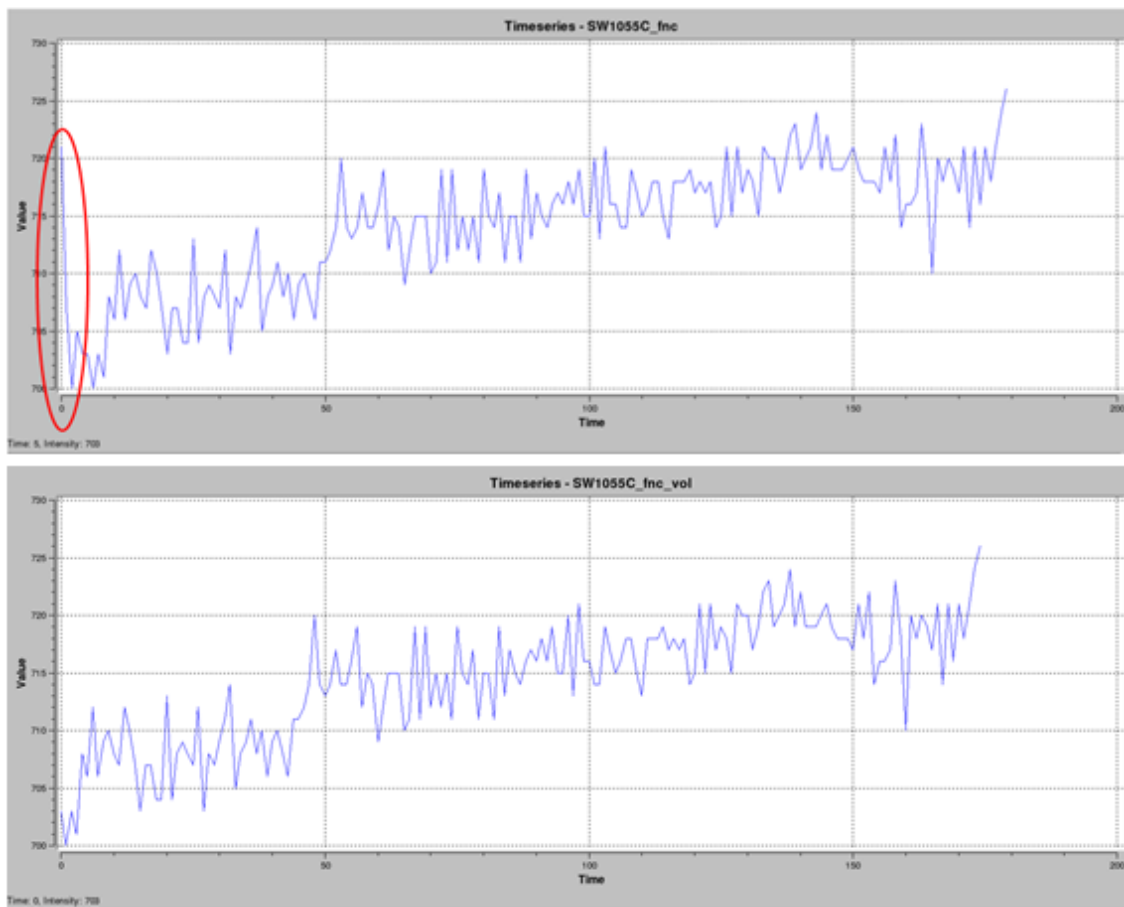


Figure 52: Time series of one voxel.

In Figure 51, the time series on the top are from before the 5 volumes removal, and the ones on the bottom are after this step. Highlighted in red is an intensity “spike” which is removed by this step.

- **Slice-timing**

```
slicetimer -i $DIR"/$i"/FMRI/$i"_fnc_vol.nii.gz -o
$DIR"/$i"/FMRI/$i"_fnc_vol_stime -r 2 --
ocustom=/home/neuroimg/Scripts/slicetimings
```

options:

```
-i input timeseries. In this case is the output of the previous
step.
-o output file
-r Specify TR of data. In this case TR=2
--ocustom filename of single-column custom interleave order file
(first slice is referred to as 1 not 0)
```

- **Motion correction (realign)**

The approach here is to correct for the linear effects of motion by realigning all the functional images to its mean. The first step is then to calculate the mean of the functional images:

```
fslmaths $DIR"/$i"/FMRI/$i"_fnc_vol_stime.nii.gz -Tmean
$DIR"/$i"/FMRI/$i"_fnc_vol_stime_mean
```

Options:

```
-Tmean mean across time
```

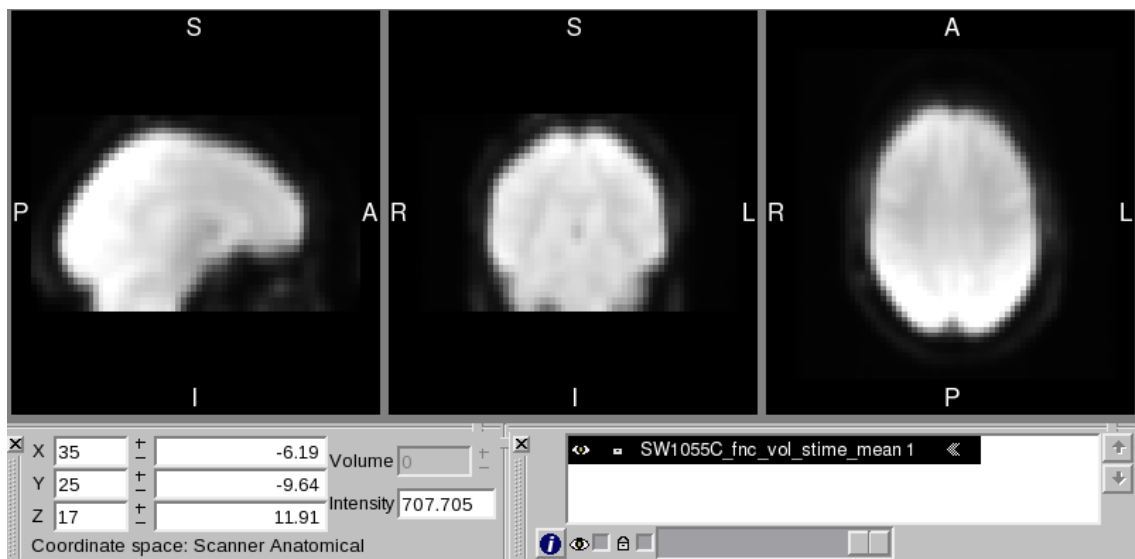


Figure 53: Mean of functional images.

Once the mean of the functional images is calculated then the realignment can be performed. MCFLIRT is an intra-modal motion correction tool designed for use on fMRI time series and based on optimization and registration techniques used in FLIRT. MCFLIRT loads the time series and will reference to the middle volume as an initial template image. A coarse 8mm search for the motion parameters is then carried out using the cost function specified followed by two subsequent searches at 4mm using increasingly tighter tolerances. All optimizations use trilinear interpolation.

```
mcflirt -in $DIR"/$i"/FMRI/$i"_fnc_vol_stime.nii.gz -r
$DIR"/$i"/FMRI/$i"_fnc_vol_stime_mean.nii.gz -stages 4 -plots
```

Options:

```
-in Input file.
-r use a separate 3d image file as the target for registration
-stages 4 specifies final (internal) sinc interpolation
-plots save transformation parameters in file outputfilename.par
```

As part of QA, after the realignment step it is important to verify the result by plotting the estimated motion parameters (rotation and translation).

```
fsl_tsplot -i $DIR"/$i"/FMRI/$i"_fnc_vol_stime_mcf.par -t
'Headmovement - rotation(rad)' --start=1 --finish=3 -a x,y,z -o
$DIR"/$i"/FMRI/$i"_fnc_vol_stime_rot.png
```

```
fsl_tsplot -i $DIR"/$i"/FMRI/$i"_fnc_vol_stime_mcf.par -t
'headmovement - translation(mm)' --start=4 --finish=6 -a x,y,z -o
$DIR"/$i"/FMRI/$i"_fnc_vol_stime_trans.png
```

Options:

```
-i input file
-t plot title
--start position of the first column to plot
--finish Position of final column to plot
-a comma separated list of labels
-o output filename for the PNG file
```

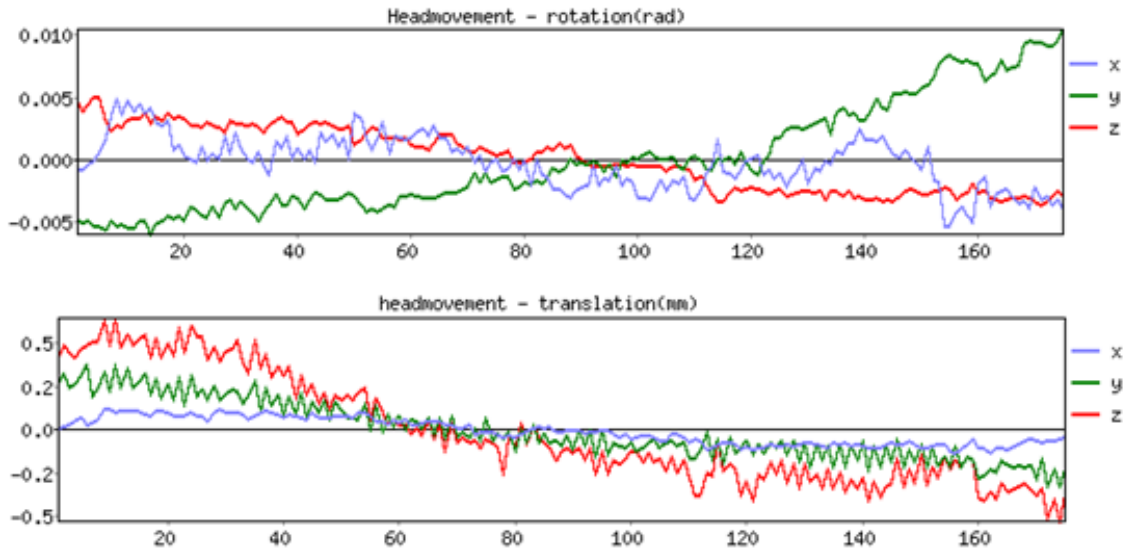


Figure 54: Motion correction parameter plots. The middle volume is used as reference.

An alternative way to visually inspect data for head movement is to use the movie mode (cycles through volumes in multi-volume images) of FSLview. One can run it before and after the motion correction and assess its effectiveness.

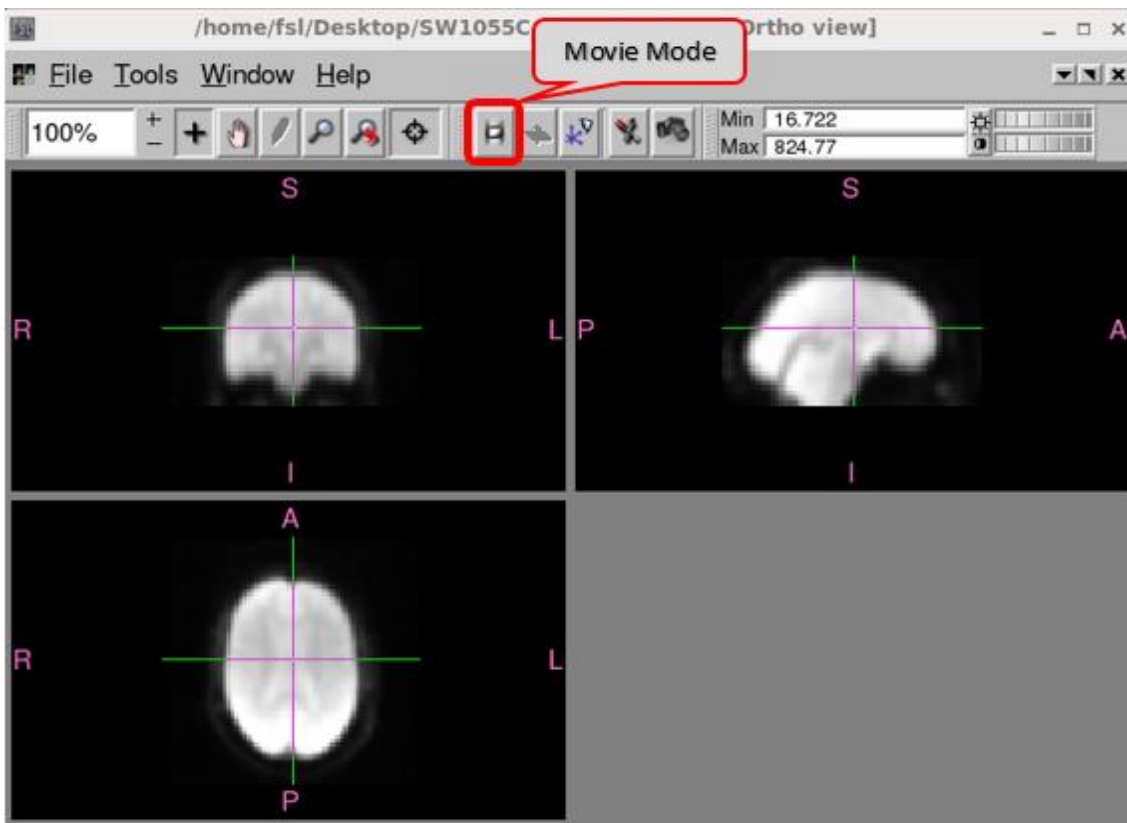


Figure 55: FSLview GUI – Movie Mode

- **Skull Stripping of the functional image**

For an optimized skull stripping the mean of the functional images is recalculated to account for the motion correction.

```
fslmaths $DIR"/$i"/FMRI/$i"_fnc_vol_stime_mcf.nii.gz -Tmean  
$DIR"/$i"/FMRI/$i"_fnc_vol_stime_mcf_mean
```

The skull stripping involves two steps. The first removes the skull of the mean functional image.

```
bet2 $DIR"/$i"/FMRI/$i"_fnc_vol_stime_mcf_mean.nii.gz  
$DIR"/$i"/FMRI/$i"_fnc_vol_stime_mcf_mean_bet -m -f 0.35
```

Options:

-m generate binary brain mask

-f <f> fractional intensity threshold. For the images of this study <f> of 0.35 was found to be a good starting point.

-R This option runs more "robust" brain center estimation

The second step is then to apply the mask from the previous step to all functional images.

```
fslmaths $DIR"/$i"/FMRI/$i"_fnc_vol_stime_mcf.nii.gz -mas  
$DIR"/$i"/FMRI/$i"_fnc_vol_stime_mcf_mean_bet.nii.gz  
$DIR"/$i"/FMRI/$i"_fnc_vol_stime_mcf_bet
```

Usage: fslmaths [-dt <datatype>] <first_input> [operations and inputs] <output> [-odt <datatype>]

Options:

-dt sets the datatype used internally for calculations (default float)

-odt sets the output datatype (default is float)

-mas use (following image>0) to mask current image

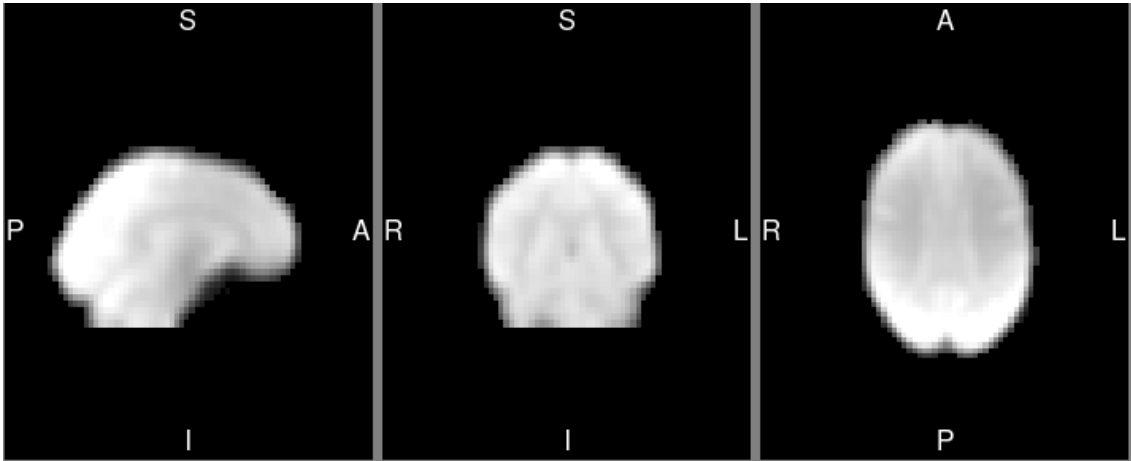


Figure 56: Skull Stripped functional image.

- **Co-registration**

A mean of the functional images is recalculated to account for the skull stripping

```
fslmaths $DIR"/$i"/FMRI/$i"_fnc_vol_stime_mcf_bet.nii.gz -Tmean
$DIR"/$i"/FMRI/$i"_fnc_vol_stime_mcf_bet_mean
```

The mean of the functional images is then co-registered to the structural image with the linear registration algorithm (Flirt)

```
flirt -searchrx -180 180 -searchry -180 180 -searchrz -180 180 -dof 6 -
cost corratio -in $DIR"/$i"/FMRI/$i"_fnc_vol_stime_mcf_bet_mean.nii.gz
-ref $DIR"/$i"/MRI/$i"_str_crop_bet.nii.gz -omat
$DIR"/$i"/FMRI/$i"_fnc_2str.mat
```

Options:

-*search* select the angular range over which the initial optimization search stage is performed. *rx*, *ry*, *rz* are the rotation angles in radians (for the matrices *Rx*, *Ry* and *Rz* respectively).

-*dof* Degrees of freedom. In this case 6 degrees of freedom were used because the images being registered are from the same subject.

-*cost corratio* is the Cost Function used. In this case Correlation Ratio.

-*in* is the input file volume

-*ref* is the reference volume

-*omat* the calculated affine transformation that registers the input to the reference which is saved as a 4x4 affine matrix

- **Normalization**

For the normalization of the functional image, the matrix from co-register and the warp parameters from structural image normalization are applied to the functional images.

```
applywarp --ref=$FSLDIR/data/standard/MNI152_T1_2mm_brain --  
in=$DIR"/$i"/FMRI/$i"_fnc_vol_stime_mcf_bet.nii.gz --  
warp=$DIR"/$i"/MRI/$i"_str_warp.nii.gz --  
premat=$DIR"/$i"/FMRI/$i"_fnc_2str.mat --  
out=$DIR"/$i"/FMRI/$i"_fnc_vol_stime_mcf_bet_mni
```

Options:

--ref= reference image. In this case the a MNI template

--in= input image. In this case the skull stripped functional image.

--warp= the transformation coefficients. The output from the structural image normalization.

--premat filename for pre-transform (affine matrix). The output from the co-register step.

--out= output file.

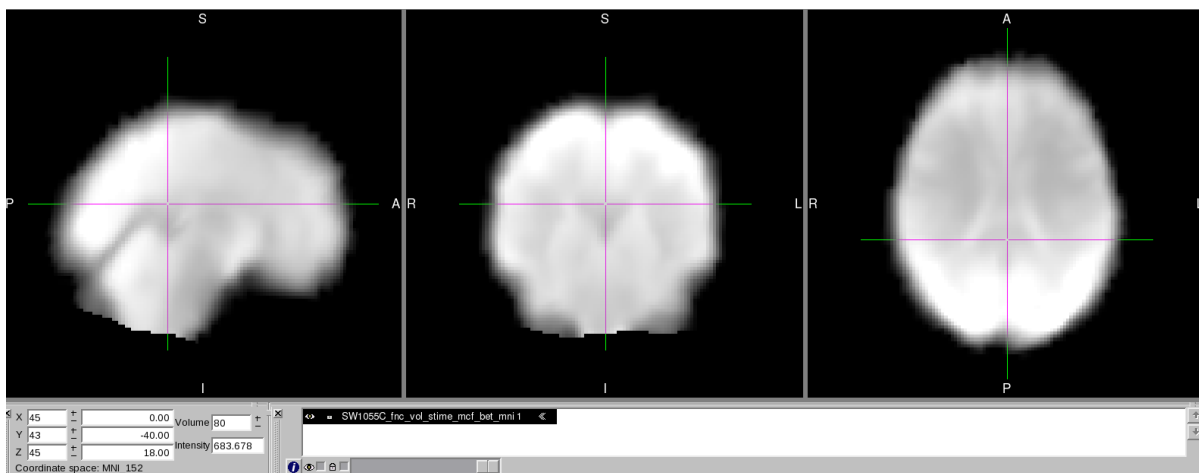


Figure 57: Functional image normalized to MNI space.

- **Spatial Smoothing**

The functional images are spatially smoothed with an 8mm Gaussian kernel.

```
fslmaths $DIR"/$i"/FMRI/$i"_fnc_vol_stime_mcf_bet_mni.nii.gz  
-kernel gauss 3.397 -fmean -mas  
$FSLDIR/data/standard/MNI152_T1_2mm_brain_mask  
$DIR"/$i"/FMRI/$i"_fnc_vol_stime_mcf_bet_mni_smooth
```

Options:

-kernel gauss <sigma>: gaussian kernel (sigma in mm, not voxels). For Gaussian distribution $FWHM=2.355\sigma$ so for an 8mm FWHM smoothing kernel $\sigma=3.397$. ($\sigma=8/2.355=3.397$)

-fmean Mean filtering, kernel weighted (conventionally used with gauss kernel)

-mas use (following image>0) to mask current

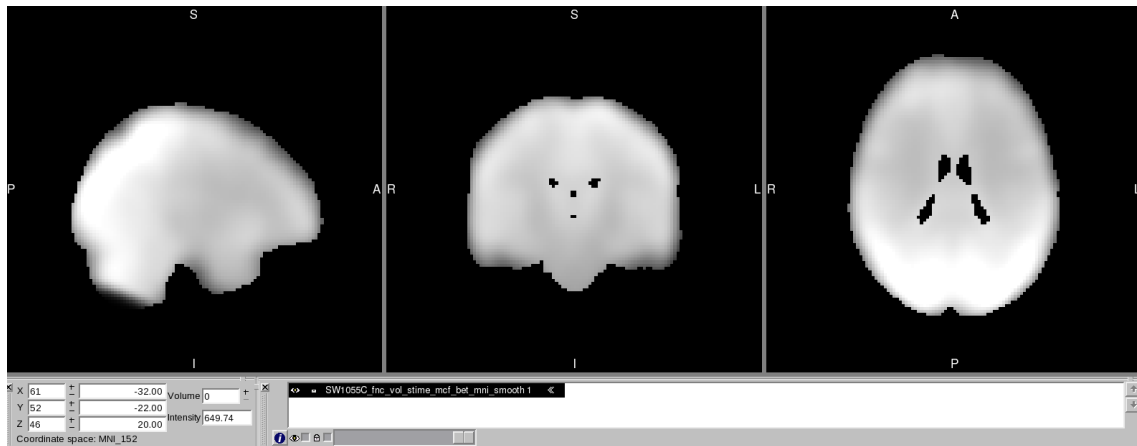


Figure 58: Spatially Smoothed Functional Image

- **Grand Mean Scalling**

This step normalizes signal intensity to values around 10000 to facilitate comparisons between subjects.

```
factor=$(bc <<< "scale=10;10000/`fslstats
"$DIR"/"$i"/FMRI/"$i"_fnc_vol_stime_mcf_bet_mni.nii.gz -k
$FSLDIR/data/standard/MNI152_T1_2mm_brain_mask -p 50`)
echo $factor
```

Options:

```
-k <mask>      : use the specified image (filename) for masking
-p <n>         : output nth percentile (n between 0 and 100)
```

- **Multiply image**

```
fslmaths $DIR"/"$i"/FMRI/"$i"_fnc_vol_stime_mcf_bet_mni.nii.gz -
mul $factor $DIR"/"$i"/FMRI/"$i"_fnc_vol_stime_mcf_bet_mni_scaled
```

Options:

```
-mul      : multiply current image by following input
```

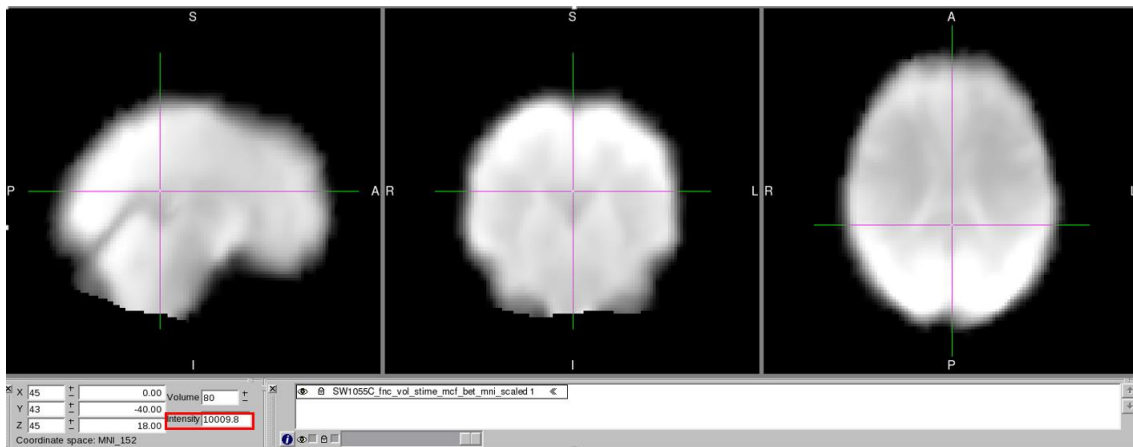


Figure 59: Functional image with normalized intensities.

By comparing images in Figure 56 and Figure 58, it is possible to verify that intensity of the selected voxel in Figure 58 is 10009, while the same voxel before this step had intensity 683.

- **Temporal filtering**

In this step a pass band filter 0.01-0.08Hz is applied, as resting state networks signal were described to vary within this frequency range [140].

```
fslmaths $DIR"/$i"/FMRI/$i"_fnc_vol_stime_mcf_bet_mni_scaled.nii.gz
-bptf 25.000000 3.125000
$DIR"/$i"/FMRI/$i"_fnc_vol_stime_mcf_bet_mni_scaled_filter
```

Usage: fslmaths [-dt <datatype>] <first_input> [operations and inputs] <output> [-odt <datatype>]

Options:

-bptf <hp_sigma> <lp_sigma> : (-t in ip.c) Bandpass temporal filtering; nonlinear highpass and Gaussian linear lowpass (with sigmas in volumes, not seconds)

For the temporal bandpass filter applied in this command sigma at FWHM corresponds to half the Period. Therefore the sigma calculation is:

High-pass sigma:

Period=1/0.01=100seconds

Sigma at FWHM=100/2=50seconds

Sigma in volumes (TR=2s): 50/2 = 25 volumes

Low-pass sigma:

Period=1/0.08=12.5seconds

Sigma at FWHM=12.5/2=6.25 seconds

Sigma in volumes (TR=2s): 6.25/2 = 3.125 vol

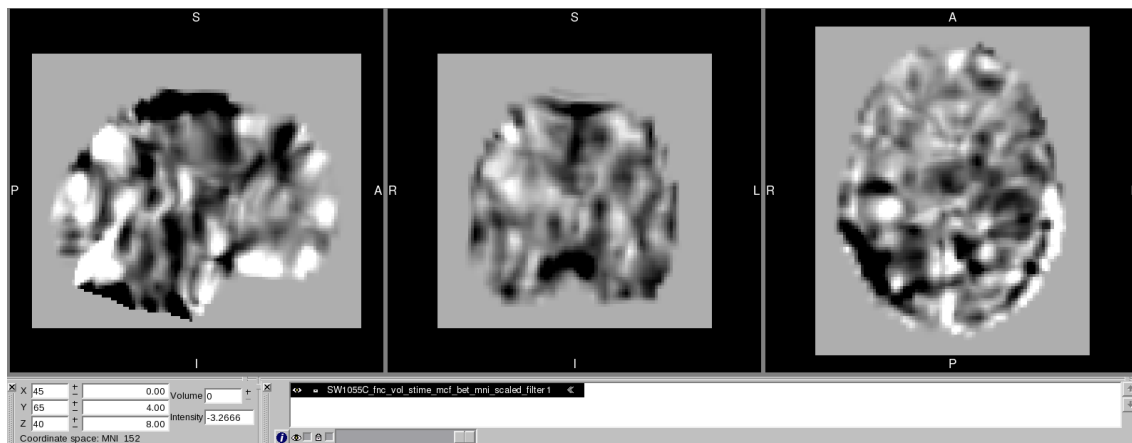


Figure 60: Temporally filtered functional image.

12.2.4 - Statistical Analysis

Here a data-driven group analysis is performed searching for RSNs using ICA.

```
melodic -i <filename> -o /mnt/disk2/GroupICA -v --nobet -a
concat --tr=2 --report --
mask=/usr/share/fsl/5.0/data/standard/MNI152_T1_2mm_brain_mas
k.nii.gz
```

Usage: melodic -i <filename> <options>

Input will be the functional images of each subject after preprocessing. Example:
SW1055C_fnc_vol_stime_mcf_bet_mni_scaled_filter.nii.gz

Options:

- o output directory name
- v switch on diagnostic messages
- nobet switch off BET
- a approach for decomposition *concat*
- tr TR in seconds
- report generate Melodic web report
- mask file name of mask for thresholding

In this study 22 independent components were found for this group of subjects. One can find the results and logfile of the *melodic* command at [/GroupICA_X/report/00index.html](#)

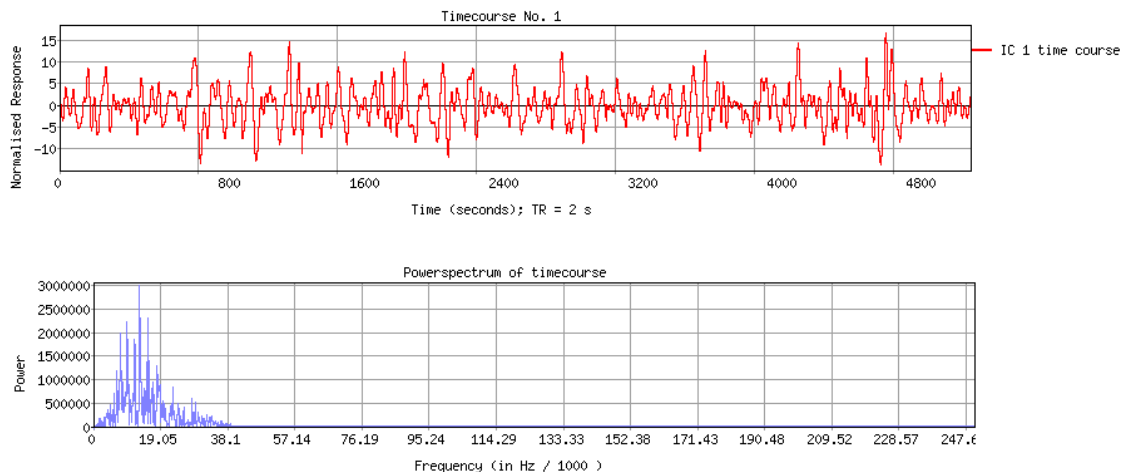


Figure 61: Independent Component Number 1 timecourse and Powerspectrum of timecourse.

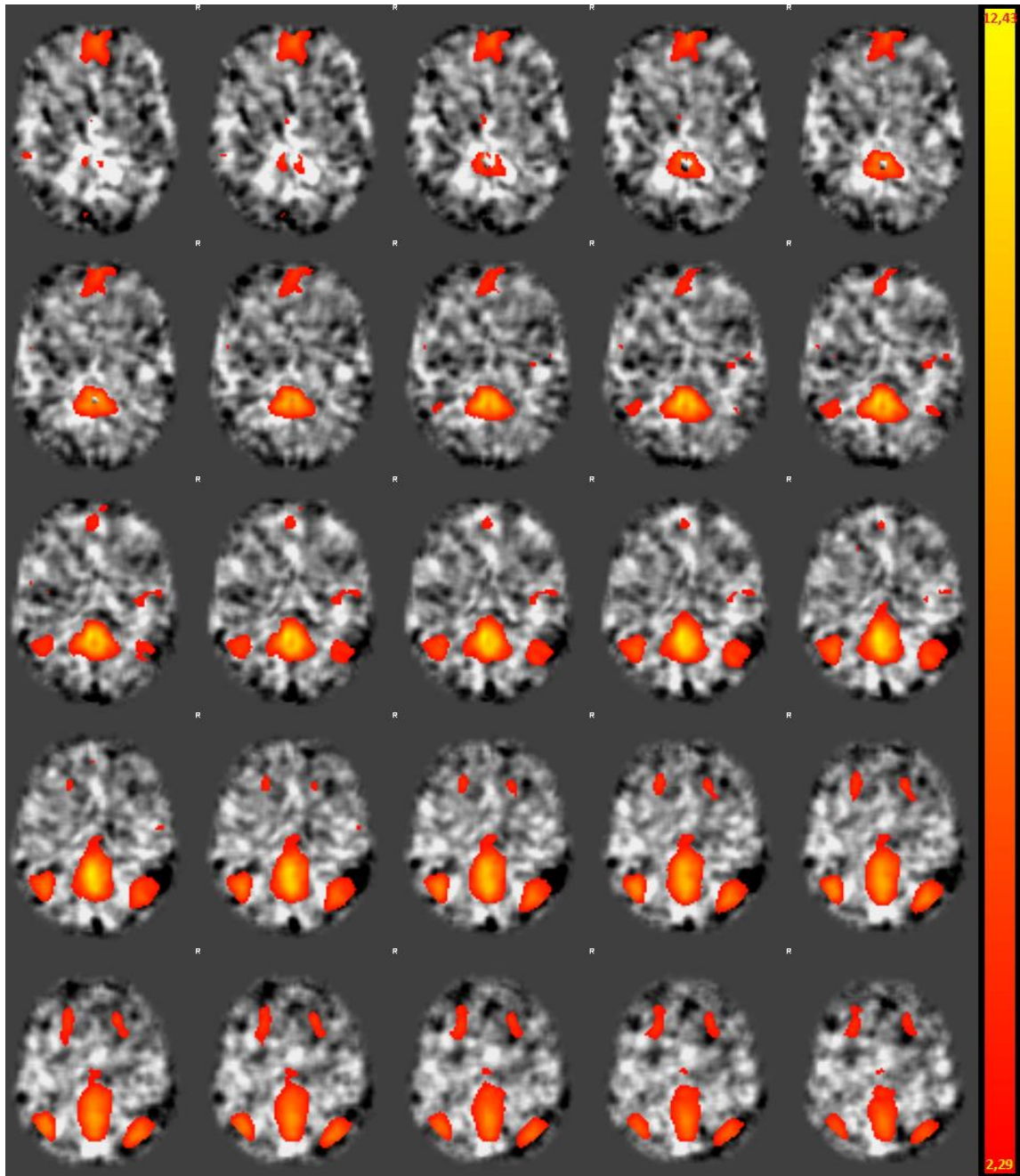


Figure 62: Component No. 1 – thresholded IC map. Alternative hypothesis test at $p > 0.5$

Each of the 22 resulting Independent Components should then be visually compared with the most common RSNs described in literature, allowing to separate noise from RSNs. The pattern highlighted in Figure 61 fits what is commonly described in the literature as the Default Mode Network [209].

13 - Conclusion and future work

fMRI has revolutionized and expanded the functional neuroimaging field. Supported by its superior spatial resolution with whole brain coverage, non-invasiveness and availability, it is a safe and powerful tool used for mapping the organization and functioning of the human brain.

Although it is a technology that has greatly improved and matured since its inception in 1990, it still has many pitfalls that limit its clinical application, being thus mostly used for research purposes. During these years many different approaches were developed to overcome the limitations and improve the quality of the results, though there is still no standard on how to perform an fMRI study.

This guide provides crucial information and essential references for understanding the basic fundamentals of brain physiology and signals, fMRI physics, statistical analysis, and results interpretation. In addition the limitations and pitfalls are discussed referencing the state of the art approaches to overcome them. It is then a valuable tool for the fMRI beginner researcher, or clinician, to set an fMRI study with optimized workflow and data quality. To validate the guide two examples of fMRI studies were analyzed, with real data, obtaining results according to similar studies literature.

A recommendation for future work includes a deeper focus on high field fMRI, brain anatomy and multimodal functional imaging which can improve scope and value of this guide. It can also be updated as newly valuable techniques and tools become available.

14 - References

- [1] A. T. Bui and R. K. Taira, *Medical Imaging Informatics*: Springer, 2010.
- [2] J. P. Hornak. (2011). *The Basics of MRI*. Available: <https://www.cis.rit.edu/htbooks/mri/chap-1/chap-1.htm>
- [3] F. Bloch, "Nuclear Induction," *Physical Review*, vol. 70, pp. 460-474, 1946.
- [4] F. Bloch, W. W. Hansen, and M. Packard, "The Nuclear Induction Experiment," *Physical Review*, vol. 70, pp. 474-485, 1946.
- [5] E. M. Purcell, H. C. Torrey, and R. V. Pound, "Resonance Absorption by Nuclear Magnetic Moments in a Solid," *Physical Review*, vol. 69, pp. 37-38, 1946.
- [6] P. C. Lauterbur, "Image Formation by Induced Local Interactions: Examples Employing Nuclear Magnetic Resonance," *Nature*, vol. 242, pp. 190-191, 1973.
- [7] A. N. Garroway, P. K. Grannell, and P. Mansfield, "Image formation in NMR by a selective irradiative process," *Journal of Physics C: Solid State Physics*, vol. 7, p. L457, 1974.
- [8] R. W. Brown, "Magnetic Resonance Imaging," in *Magnetic Resonance Imaging*, ed: John Wiley & Sons Ltd, 2014, pp. 1-17.
- [9] A. Kumar, D. Welti, and R. R. Ernst, "NMR Fourier zeugmatography," *Journal of Magnetic Resonance (1969)*, vol. 18, pp. 69-83, 1975.
- [10] P. Mansfield, "Multi-planar image formation using NMR spin echoes," *Journal of Physics C: Solid State Physics*, vol. 10, p. L55, 1977.
- [11] S. Ogawa, T. M. Lee, A. R. Kay, and D. W. Tank, "Brain magnetic resonance imaging with contrast dependent on blood oxygenation," *Proceedings of the National Academy of Sciences of the United States of America*, vol. 87, pp. 9868-9872, 1990.
- [12] K. Smith, "Brain imaging: fMRI 2.0," *Nature* vol. 484, pp. 24-26, 2012.
- [13] M. Ullsperger, *Simultaneous EEG and fMRI*, 2010.
- [14] D. Stansbury. (2012). *fMRI In Neuroscience: The Basics*. Available: <https://theclevermachine.wordpress.com/2012/11/23/fmri-in-neuroscience-the-basics/>
- [15] K. Uludag, D. J. Dubowitz, and R. B. Buxton, "Basic principles of functional MRI," *Clinical MRI. Elsevier, San Diego*, pp. 249-287, 2005.
- [16] P. A. Bandettini, E. C. Wong, R. S. Hinks, R. S. Tikofsky, and J. S. Hyde, "Time course EPI of human brain function during task activation," *Magnetic Resonance in Medicine*, vol. 25, pp. 390-397, 1992.
- [17] A. M. Blamire, S. Ogawa, K. Ugurbil, D. Rothman, G. McCarthy, J. M. Ellermann, *et al.*, "Dynamic mapping of the human visual cortex by high-speed magnetic resonance imaging," *Proceedings of the National Academy of Sciences of the United States of America*, vol. 89, pp. 11069-11073, 1992.
- [18] M. Nijboer, J. Borst, H. van Rijn, and N. Taatgen, "Single-task fMRI overlap predicts concurrent multitasking interference," *NeuroImage*, vol. 100, pp. 60-74, 2014.
- [19] S. E. Petersen and J. W. Dubis, "The mixed block/event-related design," *NeuroImage*, vol. 62, pp. 1177-1184, 2012.
- [20] A. Vallesi, S. Arbula, M. Capizzi, F. Causin, and D. D'Avella, "Domain-independent neural underpinning of task-switching: An fMRI investigation," *Cortex*, vol. 65, pp. 173-183, 2015.
- [21] B. Biswal, F. Zerrin Yetkin, V. M. Haughton, and J. S. Hyde, "Functional connectivity in the motor cortex of resting human brain using echo-planar mri," *Magnetic Resonance in Medicine*, vol. 34, pp. 537-541, 1995.
- [22] T. A. Carlson, P. Schrater, and S. He, "Patterns of activity in the categorical representations of objects," *J Cogn Neurosci*, vol. 15, pp. 704-17, 2003.

- [23] M. D. Fox and M. E. Raichle, "Spontaneous fluctuations in brain activity observed with functional magnetic resonance imaging," *Nat Rev Neurosci*, vol. 8, pp. 700-711, 2007.
- [24] M. D. Fox, A. Z. Snyder, J. L. Vincent, M. Corbetta, D. C. Van Essen, and M. E. Raichle, "The human brain is intrinsically organized into dynamic, anticorrelated functional networks," *Proceedings of the National Academy of Sciences of the United States of America*, vol. 102, pp. 9673-9678, 2005.
- [25] M. E. Raichle, "A Paradigm Shift in Functional Brain Imaging," *The Journal of Neuroscience*, vol. 29, pp. 12729-12734, 2009.
- [26] M. E. Raichle, "The Restless Brain," *Brain Connectivity*, vol. 1, pp. 3-12, 2011.
- [27] S. M. Smith, K. L. Miller, G. Salimi-Khorshidi, M. Webster, C. F. Beckmann, T. E. Nichols, *et al.*, "Network modelling methods for fMRI," *NeuroImage*, vol. 54, pp. 875-891, 2011.
- [28] J. Carp, "On the Plurality of (Methodological) Worlds: Estimating the Analytic Flexibility of fMRI Experiments," *Frontiers in Neuroscience*, vol. 6, p. 149, 2012.
- [29] R. B. Buxton, *Introduction to Functional Magnetic Resonance Imaging: Principles and Techniques*, Second Edition ed.: Cambridge, 2009.
- [30] T. Davis and R. A. Poldrack, "Measuring neural representations with fMRI: practices and pitfalls," *Annals of the New York Academy of Sciences*, vol. 1296, pp. 108-134, 2013.
- [31] S. H. Faro and F. B. Mohamed, *BOLD fMRI: A Guide to Functional Imaging for Neuroscientists*: Springer, 2010.
- [32] S. Haller and A. Bartsch, "Pitfalls in fMRI," *European Radiology*, vol. 19, pp. 2689-2706, 2009.
- [33] K. J. Bangen, K. Restom, T. T. Liu, A. J. Jak, C. E. Wierenga, D. P. Salmon, *et al.*, "Differential age effects on cerebral blood flow and BOLD response to encoding: associations with cognition and stroke risk," *Neurobiol Aging*, vol. 30, pp. 1276-87, 2009.
- [34] R. Deichmann, *fMRI Techniques and Protocols* vol. 41: Humana Press, 2009.
- [35] D. G. Norris, "Principles of magnetic resonance assessment of brain function," *Journal of Magnetic Resonance Imaging*, vol. 23, pp. 794-807, 2006.
- [36] R. A. Poldrack, J. A. Mumford, and T. E. Nichols, *Handbook of Functional MRI Data Analysis*: Cambridge, 2011.
- [37] T. Aue, L. A. Lavelle, and J. T. Cacioppo, "Great expectations: What can fMRI research tell us about psychological phenomena?," *International Journal of Psychophysiology*, vol. 73, pp. 10-16, 2009.
- [38] J. D. Van Horn and R. A. Poldrack, "Functional MRI at the crossroads," *International Journal of Psychophysiology*, vol. 73, pp. 3-9, 2009.
- [39] P. Bandettini, "Functional MRI today," *International Journal of Psychophysiology*, vol. 63, pp. 138-145, 2007.
- [40] P. A. Bandettini, "Twenty years of functional MRI: The science and the stories," *NeuroImage*, vol. 62, pp. 575-588, 2012.
- [41] S. M. Smith, "Overview of fMRI analysis," *The British Journal of Radiology*, vol. 77, pp. S167-S175, 2004.
- [42] S. Ulmer, *fMRI - Basics and Clinical Applications*, Second Edition ed.: Springer, 2013.
- [43] S. A. Huettel, A. W. Song, and G. McCarthy, *Functional Magnetic Resonance Imaging*, Second Edition ed.: Sinauer Associates, Inc, 2009.
- [44] J. A. Bobholz, S. M. Rao, A. J. Saykin, and N. Pliskin, "Clinical Use of Functional Magnetic Resonance Imaging: Reflections on the New CPT Codes," *Neuropsychology review*, vol. 17, pp. 189-191, 2007.

- [45] J. J. Pillai, "The Evolution of Clinical Functional Imaging during the Past 2 Decades and Its Current Impact on Neurosurgical Planning," *American Journal of Neuroradiology*, vol. 31, pp. 219-225, 2010.
- [46] J. C. Gore, "Principles and practice of functional MRI of the human brain," *Journal of Clinical Investigation*, vol. 112, pp. 4-9, 2003.
- [47] M. Gabriel, N. P. Brennan, K. K. Peck, and A. I. Holodny, "Blood Oxygen Level Dependent Functional Magnetic Resonance Imaging for Presurgical Planning," *Neuroimaging Clinics of North America*, vol. 24, pp. 557-571, 2014.
- [48] S. G. Hushek, *Interventional Magnetic Resonance Imaging*, 2012.
- [49] E. A. DeYoe and R. V. Raut, "Visual Mapping Using Blood Oxygen Level Dependent Functional Magnetic Resonance Imaging," *Neuroimaging Clinics of North America*, vol. 24, pp. 573-584, 2014.
- [50] J. L. Ulmer, A. P. Klein, W. M. Mueller, E. A. DeYoe, and L. P. Mark, "Preoperative Diffusion Tensor Imaging: Improving Neurosurgical Outcomes in Brain Tumor Patients," *Neuroimaging Clinics of North America*, vol. 24, pp. 599-617, 2014.
- [51] N. Fujiwara, K. Sakatani, Y. Katayama, Y. Murata, T. Hoshino, C. Fukaya, *et al.*, "Evoked-cerebral blood oxygenation changes in false-negative activations in BOLD contrast functional MRI of patients with brain tumors," *NeuroImage*, vol. 21, pp. 1464-1471, 2004.
- [52] Malte Ottenhausen, Sandro M. Krieg, Bernhard Meyer, and Florian Ringel, "Functional preoperative and intraoperative mapping and monitoring: increasing safety and efficacy in glioma surgery," *Neurosurgical Focus*, vol. 38, p. E3, 2015.
- [53] P. Vitali, C. Di Perri, A. E. Vaudano, S. Meletti, and F. Villani, "Integration of multimodal neuroimaging methods: a rationale for clinical applications of simultaneous EEG-fMRI," *Functional Neurology*, vol. 30, pp. 9-20, 2015.
- [54] U. J. Chaudhary and J. S. Duncan, "Applications of Blood-Oxygen-Level-Dependent Functional Magnetic Resonance Imaging and Diffusion Tensor Imaging in Epilepsy," *Neuroimaging Clinics of North America*, vol. 24, pp. 671-694, 2014.
- [55] M. C. G. Vlooswijk, J. F. A. Jansen, M. C. de Krom, H. J. M. Majoie, P. A. M. Hofman, W. H. Backes, *et al.*, "Functional MRI in chronic epilepsy: associations with cognitive impairment," *The Lancet Neurology*, vol. 9, pp. 1018-1027, 2010.
- [56] J. Chang and A. Narayana, "Functional MRI for Radiotherapy of Gliomas," *Technology in Cancer Research & Treatment*, vol. 9, pp. 347-358, 2010.
- [57] A. Narayana, J. Chang, S. Thakur, W. Huang, S. Karimi, B. Hou, *et al.*, "Use of MR spectroscopy and functional imaging in the treatment planning of gliomas," *The British Journal of Radiology*, vol. 80, pp. 347-354, 2007.
- [58] M. Wang, H. Ma, X. Wang, Y. Guo, X. Xia, H. Xia, *et al.*, "Integration of BOLD-fMRI and DTI into radiation treatment planning for high-grade gliomas located near the primary motor cortexes and corticospinal tracts," *Radiation Oncology (London, England)*, vol. 10, p. 64, 2015.
- [59] R. Piperno, A. Battistini, D. Cevolani, M. Maffei, M. Leonardi, and R. Agati, "fMRI Activation with an "Affective Speech" Paradigm in Vegetative and Minimally Conscious States: Applicability and Prognostic Value," *The Neuroradiology Journal*, vol. 25, pp. 289-299, 2012.
- [60] S. Laureys, A. M. Owen, and N. D. Schiff, "Brain function in coma, vegetative state, and related disorders," *The Lancet Neurology*, vol. 3, pp. 537-546, 2004.
- [61] A. M. Owen, M. R. Coleman, M. Boly, M. H. Davis, S. Laureys, and J. D. Pickard, "Detecting Awareness in the Vegetative State," *Science*, vol. 313, p. 1402, 2006.

- [62] A. M. Owen, N. D. Schiff, and S. Laureys, "A new era of coma and consciousness science," in *Progress in Brain Research*. vol. Volume 177, N. D. S. Steven Laureys and M. O. Adrian, Eds., ed: Elsevier, 2009, pp. 399-411.
- [63] S. Laureys and N. D. Schiff, "Coma and consciousness: Paradigms (re)framed by neuroimaging," *NeuroImage*, vol. 61, pp. 478-491, 2012.
- [64] M. D. Rosenberg, E. S. Finn, D. Scheinost, X. Papademetris, X. Shen, R. T. Constable, *et al.*, "A neuromarker of sustained attention from whole-brain functional connectivity," *Nat Neurosci*, vol. advance online publication, 2015.
- [65] M. H. Lee, C. D. Smyser, and J. S. Shimony, "Resting state fMRI: A review of methods and clinical applications," *AJNR. American journal of neuroradiology*, vol. 34, pp. 1866-1872, 2013.
- [66] D. M. Cole, S. M. Smith, and C. F. Beckmann, "Advances and Pitfalls in the Analysis and Interpretation of Resting-State FMRI Data," *Frontiers in Systems Neuroscience*, vol. 4, p. 8, 2010.
- [67] S. Lang, N. Duncan, and G. Northoff, "Resting-state functional magnetic resonance imaging: review of neurosurgical applications," *Neurosurgery*, vol. 74, pp. 453-64; discussion 464-5, 2014.
- [68] A. Panigrahy, M. Borzage, and S. Blüml, "Basic Principles and Concepts Underlying Recent Advances in Magnetic Resonance Imaging of the Developing Brain," *Seminars in Perinatology*, vol. 34, pp. 3-19, 2010.
- [69] L. R. Ment and B. R. Vohr, "Preterm birth and the developing brain," *The Lancet Neurology*, vol. 7, pp. 378-379, 2008.
- [70] D. Wang, R. L. Buckner, M. D. Fox, D. J. Holt, A. J. Holmes, S. Stoecklein, *et al.*, "Parcellating cortical functional networks in individuals," *Nat Neurosci*, vol. advance online publication, 2015.
- [71] A. B. Bruhl, "Making sense of real-time functional magnetic resonance imaging (rtfMRI) and rtfMRI neurofeedback," *Int J Neuropsychopharmacol*, vol. 18, 2015.
- [72] R. C. deCharms, F. Maeda, G. H. Glover, D. Ludlow, J. M. Pauly, D. Soneji, *et al.*, "Control over brain activation and pain learned by using real-time functional MRI," *Proceedings of the National Academy of Sciences of the United States of America*, vol. 102, pp. 18626-18631, 2005.
- [73] N. Weiskopf, "Real-time fMRI and its application to neurofeedback," *NeuroImage*, vol. 62, pp. 682-692, 2012.
- [74] L. Subramanian, J. V. Hindle, S. Johnston, M. V. Roberts, M. Husain, R. Goebel, *et al.*, "Real-Time Functional Magnetic Resonance Imaging Neurofeedback for Treatment of Parkinson's Disease," *The Journal of Neuroscience*, vol. 31, pp. 16309-16317, 2011.
- [75] D. E. J. Linden, I. Habes, S. J. Johnston, S. Linden, R. Tatineni, L. Subramanian, *et al.*, "Real-Time Self-Regulation of Emotion Networks in Patients with Depression," *PLoS ONE*, vol. 7, p. e38115, 2012.
- [76] W. I. Dewiputri and T. Auer, "Functional magnetic resonance imaging (FMRI) neurofeedback: implementations and applications," *Malays J Med Sci*, vol. 20, pp. 5-15, 2013.
- [77] N. Weiskopf, R. Sitaram, O. Josephs, R. Veit, F. Scharnowski, R. Goebel, *et al.*, "Real-time functional magnetic resonance imaging: methods and applications," *Magn Reson Imaging*, vol. 25, pp. 989-1003, 2007.
- [78] A. Caria, R. Sitaram, and N. Birbaumer, "Real-time fMRI: a tool for local brain regulation," *Neuroscientist*, vol. 18, pp. 487-501, 2012.

- [79] J. Sulzer, S. Haller, F. Scharnowski, N. Weiskopf, N. Birbaumer, M. L. Belfari, *et al.*, "Real-time fMRI neurofeedback: progress and challenges," *Neuroimage*, vol. 76, pp. 386-99, 2013.
- [80] C. A. Hanlon, K. J. Hartwell, M. Canterbury, X. Li, M. Owens, T. LeMatty, *et al.*, "Reduction of cue-induced craving through realtime neurofeedback in nicotine users: The role of region of interest selection and multiple visits," *Psychiatry Research: Neuroimaging*, vol. 213, pp. 79-81, 2013.
- [81] R. Sperling, "The potential of functional MRI as a biomarker in early Alzheimer's disease," *Neurobiology of aging*, vol. 32, pp. S37-S43, 2011.
- [82] J. S. Paulsen, J. L. Zimelman, S. C. Hinton, D. R. Langbehn, C. L. Leveroni, M. L. Benjamin, *et al.*, "fMRI Biomarker of Early Neuronal Dysfunction in Presymptomatic Huntington's Disease," *American Journal of Neuroradiology*, vol. 25, pp. 1715-1721, 2004.
- [83] E. P. Duff, W. Vennart, R. G. Wise, M. A. Howard, R. E. Harris, M. Lee, *et al.*, "Learning to identify CNS drug action and efficacy using multistudy fMRI data," *Science Translational Medicine*, vol. 7, pp. 274ra16-274ra16, 2015.
- [84] T. D. Wager and C.-W. Woo, "fMRI in analgesic drug discovery," *Science Translational Medicine*, vol. 7, pp. 274fs6-274fs6, 2015.
- [85] D. Borsook, L. Becerra, and R. Hargreaves, "A role for fMRI in optimizing CNS drug development," *Nat Rev Drug Discov*, vol. 5, pp. 411-425, 2006.
- [86] R. G. Wise and C. Preston, "What is the value of human FMRI in CNS drug development?," *Drug Discovery Today*, vol. 15, pp. 973-980, 2010.
- [87] D. Borsook, R. Hargreaves, and L. Becerra, "Can Functional Magnetic Resonance Imaging Improve Success Rates in CNS Drug Discovery?," *Expert opinion on drug discovery*, vol. 6, pp. 597-617, 2011.
- [88] P. Schweinhardt, C. Bountra, and I. Tracey, "Pharmacological FMRI in the development of new analgesic compounds," *NMR Biomed*, vol. 19, pp. 702-11, 2006.
- [89] A. J. Schwarz, L. Becerra, J. Upadhyay, J. Anderson, R. Baumgartner, A. Coimbra, *et al.*, "A procedural framework for good imaging practice in pharmacological fMRI studies applied to drug development #1: processes and requirements," *Drug Discov Today*, vol. 16, pp. 583-93, 2011.
- [90] D. Borsook, D. Bleakman, R. Hargreaves, J. Upadhyay, K. F. Schmidt, and L. Becerra, "A 'BOLD' experiment in defining the utility of fMRI in drug development," *NeuroImage*, vol. 42, pp. 461-466, 2008.
- [91] U. S. NIH. (2015, 1/12/2015). *ClinicalTrials.gov* Available: <https://www.clinicaltrials.gov/>
- [92] C. Rachul and A. Zarzeczny, "The rise of neuroskepticism," *International Journal of Law and Psychiatry*, vol. 35, pp. 77-81, 2012.
- [93] D. D. Langleben and J. C. Moriarty, "Using Brain Imaging for Lie Detection: Where Science, Law and Research Policy Collide," *Psychology, public policy, and law : an official law review of the University of Arizona College of Law and the University of Miami School of Law*, vol. 19, pp. 222-234, 2013.
- [94] N. L. MRI. *No Lie MRI*. Available: <http://www.noliemri.com/>
- [95] E. Rusconi and T. Mitchener-Nissen, "Prospects of functional magnetic resonance imaging as lie detector," *Frontiers in Human Neuroscience*, vol. 7, p. 594, 2013.
- [96] J. R. Simpson, "Functional MRI Lie Detection: Too Good to be True?," *Journal of the American Academy of Psychiatry and the Law Online*, vol. 36, pp. 491-498, 2008.
- [97] F. B. Mohamed, S. H. Faro, N. J. Gordon, S. M. Platek, H. Ahmad, and J. M. Williams, "Brain Mapping of Deception and Truth Telling about an Ecologically Valid Situation: Functional

- MR Imaging and Polygraph Investigation—Initial Experience," *Radiology*, vol. 238, pp. 679-688, 2006.
- [98] H. Plassmann, J. O'Doherty, B. Shiv, and A. Rangel, "Marketing actions can modulate neural representations of experienced pleasantness," *Proceedings of the National Academy of Sciences*, vol. 105, pp. 1050-1054, 2008.
- [99] N. Lee, A. J. Broderick, and L. Chamberlain, "What is 'neuromarketing'? A discussion and agenda for future research," *International Journal of Psychophysiology*, vol. 63, pp. 199-204, 2007.
- [100] G. H. Glover, "Overview of functional magnetic resonance imaging," *Neurosurg Clin N Am*, vol. 22, pp. 133-9, vii, 2011.
- [101] D. Attwell, A. M. Buchan, S. Charpak, M. Lauritzen, B. A. MacVicar, and E. A. Newman, "Glial and neuronal control of brain blood flow," *Nature*, vol. 468, pp. 232-243, 2010.
- [102] D. Attwell and S. B. Laughlin, "An Energy Budget for Signaling in the Grey Matter of the Brain," *J Cereb Blood Flow Metab*, vol. 21, pp. 1133-1145, 2001.
- [103] G. C. Petzold and V. N. Murthy, "Role of astrocytes in neurovascular coupling," *Neuron*, vol. 71, pp. 782-97, 2011.
- [104] R. B. Buxton and L. R. Frank, "A Model for the Coupling Between Cerebral Blood Flow and Oxygen Metabolism During Neural Stimulation," *J Cereb Blood Flow Metab*, vol. 17, pp. 64-72, 1997.
- [105] R. B. Buxton, E. C. Wong, and L. R. Frank, "Dynamics of blood flow and oxygenation changes during brain activation: The balloon model," *Magnetic Resonance in Medicine*, vol. 39, pp. 855-864, 1998.
- [106] T. L. Davis, K. K. Kwong, R. M. Weisskoff, and B. R. Rosen, "Calibrated functional MRI: Mapping the dynamics of oxidative metabolism," *Proceedings of the National Academy of Sciences of the United States of America*, vol. 95, pp. 1834-1839, 1998.
- [107] S. Ogawa, T. M. Lee, A. S. Nayak, and P. Glynn, "Oxygenation-sensitive contrast in magnetic resonance image of rodent brain at high magnetic fields," *Magn Reson Med*, vol. 14, pp. 68-78, 1990.
- [108] S. Ogawa and T. M. Lee, "Magnetic resonance imaging of blood vessels at high fields: in vivo and in vitro measurements and image simulation," *Magn. Reson. Med.*, vol. 16, pp. 9-18, 1990.
- [109] A. Elster, "Magnetism: Susceptibility," 2014.
- [110] L. Pauling and C. D. Coryell, "The Magnetic Properties and Structure of the Hemochromogens and Related Substances," *Proceedings of the National Academy of Sciences*, vol. 22, pp. 159-163, 1936.
- [111] B. J. Casey, M. Davidson, and B. Rosen, "Functional magnetic resonance imaging: basic principles of and application to developmental science," *Developmental Science*, vol. 5, pp. 301-309, 2002.
- [112] A. M. Howseman and R. W. Bowtell, "Functional magnetic resonance imaging: imaging techniques and contrast mechanisms," *Philos Trans R Soc Lond B Biol Sci*, vol. 354, pp. 1179-94, 1999.
- [113] J. W. Belliveau, D. N. Kennedy, Jr., R. C. McKinstry, B. R. Buchbinder, R. M. Weisskoff, M. S. Cohen, *et al.*, "Functional mapping of the human visual cortex by magnetic resonance imaging," *Science*, vol. 254, pp. 716-9, 1991.
- [114] J. A. Detre, J. S. Leigh, D. S. Williams, and A. P. Koretsky, "Perfusion imaging," *Magn Reson Med*, vol. 23, pp. 37-45, 1992.
- [115] X. Golay, J. Hendrikse, and T. C. C. Lim, "Perfusion imaging using arterial spin labeling," *Topics in magnetic resonance imaging : TMRI*, vol. 15, pp. 10-27, 2004.

- [116] T. T. Liu and G. G. Brown, "Measurement of cerebral perfusion with arterial spin labeling: Part 1. Methods," *J Int Neuropsychol Soc*, vol. 13, pp. 517-25, 2007.
- [117] S. Petcharunpaisan, J. Ramalho, and M. Castillo, "Arterial spin labeling in neuroimaging," *World Journal of Radiology*, vol. 2, pp. 384-398, 2010.
- [118] H. Lu and P. C. M. van Zijl, "A review of the development of Vascular-Space-Occupancy (VASO) fMRI," *NeuroImage*, vol. 62, pp. 736-742, 2012.
- [119] H. Lu, J. Hua, and P. C. M. van Zijl, "Non-invasive functional imaging of Cerebral Blood Volume with Vascular-Space-Occupancy (VASO) MRI," *NMR in biomedicine*, vol. 26, pp. 932-948, 2013.
- [120] P. W. Stroman, A. S. Lee, K. K. Pitchers, and R. D. Andrew, "Magnetic resonance imaging of neuronal and glial swelling as an indicator of function in cerebral tissue slices," *Magnetic Resonance in Medicine*, vol. 59, pp. 700-706, 2008.
- [121] R. D. Andrew and B. A. Macvicar, "Imaging cell volume changes and neuronal excitation in the hippocampal slice," *Neuroscience*, vol. 62, pp. 371-383, 1994.
- [122] C. R. Figley, J. K. Leitch, and P. W. Stroman, "In contrast to BOLD: signal enhancement by extravascular water protons as an alternative mechanism of endogenous fMRI signal change," *Magnetic Resonance Imaging*, vol. 28, pp. 1234-1243, 2010.
- [123] C. R. Figley and P. W. Stroman, "The role(s) of astrocytes and astrocyte activity in neurometabolism, neurovascular coupling, and the production of functional neuroimaging signals," *European Journal of Neuroscience*, vol. 33, pp. 577-588, 2011.
- [124] M. E. Raichle, "Behind the scenes of functional brain imaging: A historical and physiological perspective," *Proceedings of the National Academy of Sciences*, vol. 95, pp. 765-772, 1998.
- [125] L. Welberg, "Neuroimaging: Interpreting the signal," *Nat Rev Neurosci*, vol. 10, pp. 166-166, 2009.
- [126] J. Schummers, H. Yu, and M. Sur, "Tuned Responses of Astrocytes and Their Influence on Hemodynamic Signals in the Visual Cortex," *Science*, vol. 320, pp. 1638-1643, 2008.
- [127] N. Zasler, D. Katz, and R. Zafonte, "Brain Injury Medicine: Principles and Practice," Second Edition ed: demosMEDICAL, 2013.
- [128] Y. B. Sirotin and A. Das, "Anticipatory haemodynamic signals in sensory cortex not predicted by local neuronal activity," *Nature*, vol. 457, pp. 475-479, 2009.
- [129] P. W. Stroman, *Essentials of Functional MRI*: CRC Press, 2011.
- [130] R. B. Buxton, "Introduction to Functional Magnetic Resonance Imaging: Principles and Techniques," ed: Macmillan Publishers Limited. All rights reserved, 2002.
- [131] P. Jezzard, "Correction of geometric distortion in fMRI data," *NeuroImage*, vol. 62, pp. 648-651, 2012.
- [132] V. P. Clark, "A history of randomized task designs in fMRI," *NeuroImage*, vol. 62, pp. 1190-1194, 2012.
- [133] T. T. Liu, "The development of event-related fMRI designs," *NeuroImage*, vol. 62, pp. 1157-1162, 2012.
- [134] S. A. Huettel, "Event-related fMRI in cognition," *NeuroImage*, vol. 62, pp. 1152-1156, 2012.
- [135] S. Haller, S. G. Wetzel, E. W. Radue, and D. Bilecen, "Mapping continuous neuronal activation without an ON-OFF paradigm: initial results of BOLD ceiling fMRI," *European Journal of Neuroscience*, vol. 24, pp. 2672-2678, 2006.
- [136] K. M. Visscher, F. M. Miezin, J. E. Kelly, R. L. Buckner, D. I. Donaldson, M. P. McAvoy, *et al.*, "Mixed blocked/event-related designs separate transient and sustained activity in fMRI," *NeuroImage*, vol. 19, pp. 1694-1708, 2003.

- [137] M. J. Lowe, "The emergence of doing "nothing" as a viable paradigm design," *NeuroImage*, vol. 62, pp. 1146-1151, 2012.
- [138] T. Kenet, D. Bibitchkov, M. Tsodyks, A. Grinvald, and A. Arieli, "Spontaneously emerging cortical representations of visual attributes," *Nature*, vol. 425, pp. 954-956, 2003.
- [139] M. P. van den Heuvel and H. E. Hulshoff Pol, "Exploring the brain network: a review on resting-state fMRI functional connectivity," *Eur Neuropsychopharmacol*, vol. 20, pp. 519-34, 2010.
- [140] M. Kublbock, M. Woletz, A. Hoflich, R. Sladky, G. S. Kranz, A. Hoffmann, *et al.*, "Stability of low-frequency fluctuation amplitudes in prolonged resting-state fMRI," *Neuroimage*, vol. 103, pp. 249-57, 2014.
- [141] V. M. Runge, W. R. Nitz, and S. H. Schmeets, *The Physics of Clinical MR Taught Through Images*, Second Edition ed.: Thieme, 2009.
- [142] E. J. Bink, *mri : Physics*, 2010.
- [143] D. W. McRobbie, E. A. Moore, M. J. Graves, and M. R. Prince, *MRI From Picture to Proton*, Second Edition ed.: Cambridge University Press, 2006.
- [144] P. Christakis Constantinides, *Magnetic Resonance Imaging - The Basics*: CRC Press, 2014.
- [145] C. Westbrook, *MRI at a Glance*, 2nd Edition ed.: Wiley-Blackwell, 2009.
- [146] D. Weishaupt;, V. D. Köchli;, and B. Marincek, *How Does MRI Work ?*, Second Edition ed.: Springer, 2008.
- [147] G. Liney, *MRI from A to Z*, Second Edition ed.: Springer, 2010.
- [148] M. A. Bernstein, K. F. King, and X. J. Zhou, *Handbook of MRI Pulse Sequences*: Elsevier, 2004.
- [149] C. Triantafyllou, R. D. Hoge, G. Krueger, C. J. Wiggins, A. Potthast, G. C. Wiggins, *et al.*, "Comparison of physiological noise at 1.5 T, 3 T and 7 T and optimization of fMRI acquisition parameters," *NeuroImage*, vol. 26, pp. 243-250, 2005.
- [150] A. Geissler, A. Gartus, T. Foki, A. R. Tahamtan, R. Beisteiner, and M. Barth, "Contrast-to-noise ratio (CNR) as a quality parameter in fMRI," *Journal of Magnetic Resonance Imaging*, vol. 25, pp. 1263-1270, 2007.
- [151] R. M. Birn, M. A. Smith, T. B. Jones, and P. A. Bandettini, "The respiration response function: The temporal dynamics of fMRI signal fluctuations related to changes in respiration," *NeuroImage*, vol. 40, pp. 644-654, 2008.
- [152] C. Chang, J. P. Cunningham, and G. H. Glover, "Influence of heart rate on the BOLD signal: The cardiac response function," *NeuroImage*, vol. 44, pp. 857-869, 2009.
- [153] K. J. Friston, J. Ashburner, C. D. Frith, J. B. Poline, J. D. Heather, and R. S. J. Frackowiak, "Spatial registration and normalization of images," *Human Brain Mapping*, vol. 3, pp. 165-189, 1995.
- [154] V. Roopchansingh, R. W. Cox, A. Jesmanowicz, B. D. Ward, and J. S. Hyde, "Single-shot magnetic field mapping embedded in echo-planar time-course imaging," *Magnetic Resonance in Medicine*, vol. 50, pp. 839-843, 2003.
- [155] J.-Y. Chung, M.-H. In, S.-H. Oh, M. Zaitsev, O. Speck, and Z.-H. Cho, "An improved PSF mapping method for EPI distortion correction in human brain at ultra high field (7T)," *Magnetic Resonance Materials in Physics, Biology and Medicine*, vol. 24, pp. 179-190, 2011.
- [156] M. Zaitsev, J. Hennig, and O. Speck, "Point spread function mapping with parallel imaging techniques and high acceleration factors: Fast, robust, and flexible method for echo-planar imaging distortion correction," *Magnetic Resonance in Medicine*, vol. 52, pp. 1156-1166, 2004.

- [157] D. Holland, J. M. Kuperman, and A. M. Dale, "Efficient correction of inhomogeneous static magnetic field-induced distortion in Echo Planar Imaging," *NeuroImage*, vol. 50, pp. 175-183, 2010.
- [158] N. Weiskopf, C. Hutton, O. Josephs, R. Turner, and R. Deichmann, "Optimized EPI for fMRI studies of the orbitofrontal cortex: compensation of susceptibility-induced gradients in the readout direction," *Magnetic Resonance Materials in Physics, Biology and Medicine*, vol. 20, pp. 39-49, 2007.
- [159] V. J. Schmithorst, B. J. Dardzinski, and S. K. Holland, "SIMULTANEOUS CORRECTION OF GHOST AND GEOMETRIC DISTORTION ARTIFACTS IN EPI USING A MULTI-ECHO REFERENCE SCAN," *IEEE transactions on medical imaging*, vol. 20, pp. 535-539, 2001.
- [160] N.-k. Chen and A. M. Wyrwicz, "Removal of EPI Nyquist ghost artifacts with two-dimensional phase correction," *Magnetic Resonance in Medicine*, vol. 51, pp. 1247-1253, 2004.
- [161] M. A. Griswold, P. M. Jakob, R. M. Heidemann, M. Nittka, V. Jellus, J. Wang, *et al.*, "Generalized autocalibrating partially parallel acquisitions (GRAPPA)," *Magnetic Resonance in Medicine*, vol. 47, pp. 1202-1210, 2002.
- [162] W. S. Hoge and J. R. Polimeni, "Dual-polarity GRAPPA for simultaneous reconstruction and ghost correction of echo planar imaging data," *Magnetic Resonance in Medicine*, pp. n/a-n/a, 2015.
- [163] H. Li, K. Fox-Neff, B. Vaughan, D. French, J. P. Szaflarski, and Y. Li, "Parallel EPI artifact correction (PEAC) for N/2 ghost suppression in neuroimaging applications," *Magnetic Resonance Imaging*, vol. 31, pp. 1022-1028, 2013.
- [164] J. T. BUSHBERG, J. A. SEIBERT, E. M. L. JR, and J. M. BOONE, *The Essential Physics of Medical Imaging*: LIPPINCOTT WILLIAMS & WILKINS, 2012.
- [165] T. A. Gallagher, A. J. Nemeth, and L. Hacin-Bey, "An Introduction to the Fourier Transform: Relationship to MRI," *American Journal of Roentgenology*, vol. 190, pp. 1396-1405, 2008.
- [166] L. L. Wald, "The future of acquisition speed, coverage, sensitivity, and resolution," *NeuroImage*, vol. 62, pp. 1221-1229, 2012.
- [167] S. Thesen, O. Heid, E. Mueller, and L. R. Schad, "Prospective acquisition correction for head motion with image-based tracking for real-time fMRI," *Magnetic Resonance in Medicine*, vol. 44, pp. 457-465, 2000.
- [168] O. Speck, J. Hennig, and M. Zaitsev, "Prospective Real-Time Slice-by-Slice Motion Correction for fMRI in Freely Moving Subjects," *Magnetic Resonance Materials in Physics, Biology and Medicine*, vol. 19, pp. 55-61, 2006.
- [169] N. White, C. Roddey, A. Shankaranarayanan, E. Han, D. Rettmann, J. Santos, *et al.*, "PROMO – Real-time Prospective Motion Correction in MRI using Image-based Tracking," *Magnetic resonance in medicine : official journal of the Society of Magnetic Resonance in Medicine / Society of Magnetic Resonance in Medicine*, vol. 63, pp. 91-105, 2010.
- [170] J. Schulz, T. Siegert, P. L. Bazin, J. Maclaren, M. Herbst, M. Zaitsev, *et al.*, "Prospective slice-by-slice motion correction reduces false positive activations in fMRI with task-correlated motion," *NeuroImage*, vol. 84, pp. 124-132, 2014.
- [171] D. Margulies, J. Böttger, X. Long, Y. Lv, C. Kelly, A. Schäfer, *et al.*, "Resting developments: a review of fMRI post-processing methodologies for spontaneous brain activity," *Magnetic Resonance Materials in Physics, Biology and Medicine*, vol. 23, pp. 289-307, 2010.
- [172] J. Muschelli, M. B. Nebel, B. S. Caffo, A. D. Barber, J. J. Pekar, and S. H. Mostofsky, "Reduction of motion-related artifacts in resting state fMRI using aCompCor," *Neuroimage*, vol. 96, pp. 22-35, 2014.

- [173] P. Jezzard, P. M. Matthews, and S. M. Smith, *Functional MRI: An Introduction to Methods*: Oxford University Press, 2001.
- [174] L. Friedman and G. H. Glover, "Report on a multicenter fMRI quality assurance protocol," *Journal of Magnetic Resonance Imaging*, vol. 23, pp. 827-839, 2006.
- [175] Neuroimaging Informatics Technology Initiative. *Nifti-1 Data Format*. Available: <http://nifti.nimh.nih.gov/nifti-1>
- [176] J. D. Power, K. A. Barnes, A. Z. Snyder, B. L. Schlaggar, and S. E. Petersen, "Spurious but systematic correlations in functional connectivity MRI networks arise from subject motion," *NeuroImage*, vol. 59, pp. 2142-2154, 2012.
- [177] J. S. Siegel, J. D. Power, J. W. Dubis, A. C. Vogel, J. A. Church, B. L. Schlaggar, *et al.*, "Statistical Improvements in Functional Magnetic Resonance Imaging Analyses Produced by Censoring High-Motion Data Points," *Human brain mapping*, vol. 35, pp. 1981-1996, 2014.
- [178] T. B. Jones, P. A. Bandettini, and R. M. Birn, "Integration of motion correction and physiological noise regression in fMRI," *NeuroImage*, vol. 42, pp. 582-590, 2008.
- [179] B. d. Frederick, L. D. Nickerson, and Y. Tong, "Physiological denoising of BOLD fMRI data using Regressor Interpolation at Progressive Time Delays (RIPTiDe) processing of concurrent fMRI and near-infrared spectroscopy (NIRS)," *NeuroImage*, vol. 60, pp. 1913-1923, 2012.
- [180] J. Diedrichsen and R. Shadmehr, "Detecting and adjusting for artifacts in fMRI time series data," *NeuroImage*, vol. 27, pp. 624-634, 2005.
- [181] R. M. Birn, R. W. Cox, and P. A. Bandettini, "Experimental designs and processing strategies for fMRI studies involving overt verbal responses," *NeuroImage*, vol. 23, pp. 1046-1058, 2004.
- [182] L. Lemieux, A. Salek-Haddadi, T. E. Lund, H. Laufs, and D. Carmichael, "Modelling large motion events in fMRI studies of patients with epilepsy," *Magnetic Resonance Imaging*, vol. 25, pp. 894-901, 2007.
- [183] M. Goto, O. Abe, T. Miyati, H. Yamasue, T. Gomi, and T. Takeda, "Head Motion and Correction Methods in Resting-state Functional MRI," *Magnetic Resonance in Medical Sciences*, vol. advpub, 2015.
- [184] P. T. Fox, "Spatial normalization origins: objectives, applications, and alternatives.," in *Human Brain Mapping 3*, ed, 1995, pp. 161-164.
- [185] A. C. Evans, A. L. Janke, D. L. Collins, and S. Baillet, "Brain templates and atlases," *NeuroImage*, vol. 62, pp. 911-922, 2012.
- [186] A. C. Evans, D. L. Collins, S. R. Millst, E. D. Brown, R. L. Kelly, and T. M. Peters, "3D statistical neuroanatomical models from 305 MRI volumes," 1993, pp. 1813-1817.
- [187] T. White, D. O'Leary, V. Magnotta, S. Arndt, M. Flaum, and N. C. Andreasen, "Anatomic and Functional Variability: The Effects of Filter Size in Group fMRI Data Analysis," *NeuroImage*, vol. 13, pp. 577-588, 2001.
- [188] J.-B. Poline and M. Brett, "The general linear model and fMRI: Does love last forever?," *NeuroImage*, vol. 62, pp. 871-880, 2012.
- [189] S. D. Forman, J. D. Cohen, M. Fitzgerald, W. F. Eddy, M. A. Mintun, and D. C. Noll, "Improved Assessment of Significant Activation in Functional Magnetic Resonance Imaging (fMRI): Use of a Cluster-Size Threshold," *Magnetic Resonance in Medicine*, vol. 33, pp. 636-647, 1995.
- [190] C.-W. Woo, A. Krishnan, and T. D. Wager, "Cluster-extent based thresholding in fMRI analyses: Pitfalls and recommendations," *NeuroImage*, vol. 91, pp. 412-419, 01/08 2014.

- [191] A. Eklund, T. Nichols, and H. Knutsson, "Can parametric statistical methods be trusted for fMRI based group studies?," 2015.
- [192] T. E. Nichols and A. P. Holmes, "Nonparametric permutation tests for functional neuroimaging: A primer with examples," *Human Brain Mapping*, vol. 15, pp. 1-25, 2002.
- [193] K. J. Friston, "Functional and Effective Connectivity: A Review," *Brain Connectivity*, vol. 1, pp. 13-36, 2011.
- [194] NIH. *Human Connectome Project*. Available: <http://humanconnectome.org/>
- [195] NITRC. *1000 Functional Connectomes*. Available: http://fcon_1000.projects.nitrc.org/
- [196] E. Union. *Human Brain Project*. Available: <https://www.humanbrainproject.eu/>
- [197] E. Bullmore and O. Sporns, "Complex brain networks: graph theoretical analysis of structural and functional systems," *Nat Rev Neurosci*, vol. 10, pp. 186-198, 2009.
- [198] M. Guye, G. Bettus, F. Bartolomei, and P. J. Cozzone, "Graph theoretical analysis of structural and functional connectivity MRI in normal and pathological brain networks," *Magnetic Resonance Materials in Physics, Biology and Medicine*, vol. 23, pp. 409-421, 2010.
- [199] S. M. Smith, "The future of fMRI connectivity," *NeuroImage*, vol. 62, pp. 1257-1266, 2012.
- [200] P. A. Valdes-Sosa, A. Roebroeck, J. Daunizeau, and K. Friston, "Effective connectivity: Influence, causality and biophysical modeling," *NeuroImage*, vol. 58, pp. 339-361, 2011.
- [201] J. Zhuang, S. Peltier, S. He, S. LaConte, and X. Hu, "Mapping the Connectivity with Structural Equation Modeling in an fMRI Study of Shape From Motion Task," *NeuroImage*, vol. 42, pp. 799-806, 2008.
- [202] R. S. Patel, F. D. Bowman, and J. K. Rilling, "A Bayesian approach to determining connectivity of the human brain," *Human Brain Mapping*, vol. 27, pp. 267-276, 2006.
- [203] L. R. Price, A. R. Laird, P. T. Fox, and R. J. Ingham, "Modeling Dynamic Functional Neuroimaging Data Using Structural Equation Modeling," *Structural equation modeling : a multidisciplinary journal*, vol. 16, pp. 147-162, 2009.
- [204] J. A. Mumford and J. D. Ramsey, "Bayesian networks for fMRI: A primer," *NeuroImage*, vol. 86, pp. 573-582, 2014.
- [205] M. Song and T. Jiang, "A review of functional magnetic resonance imaging for Brainnetome," *Neuroscience Bulletin*, vol. 28, pp. 389-398, 2012.
- [206] K. J. Friston, J. Kahan, B. Biswal, and A. Razi, "A DCM for resting state fMRI," *NeuroImage*, vol. 94, pp. 396-407, 2014.
- [207] K. J. Friston, L. Harrison, and W. Penny, "Dynamic causal modelling," *NeuroImage*, vol. 19, pp. 1273-1302, 2003.
- [208] J. L. Vincent, I. Kahn, A. Z. Snyder, M. E. Raichle, and R. L. Buckner, "Evidence for a Frontoparietal Control System Revealed by Intrinsic Functional Connectivity," *Journal of Neurophysiology*, vol. 100, pp. 3328-3342, 2008.
- [209] M. E. Raichle, A. M. MacLeod, A. Z. Snyder, W. J. Powers, D. A. Gusnard, and G. L. Shulman, "A default mode of brain function," *Proceedings of the National Academy of Sciences of the United States of America*, vol. 98, pp. 676-682, 2001.
- [210] C. F. Beckmann, M. DeLuca, J. T. Devlin, and S. M. Smith, "Investigations into resting-state connectivity using independent component analysis," *Philosophical Transactions of the Royal Society B: Biological Sciences*, vol. 360, pp. 1001-1013, 2005.
- [211] J. S. Damoiseaux, S. A. R. B. Rombouts, F. Barkhof, P. Scheltens, C. J. Stam, S. M. Smith, et al., "Consistent resting-state networks across healthy subjects," *Proceedings of the National Academy of Sciences of the United States of America*, vol. 103, pp. 13848-13853, 2006.

- [212] K. Friston, J. Ashburner, and T. E. Nichols, *Statistical Parametric Mapping: The Analysis of Functional Brain Images*: Academic Press, 2006.
- [213] G. K. Aguirre, "FIASCO, VoxBo, and MEDx: Behind the code," *NeuroImage*, vol. 62, pp. 765-767, 2012.
- [214] M. Wall. (2012). *fMRI Software (FSL, SPM, BrainVoyager) for beginners – how to choose?* Available: <https://computingforpsychologists.wordpress.com/2011/06/12/fmri-software-fsl-spm-brainvoyager-for-beginners-how-to-choose/>
- [215] J. Ashburner, "SPM: A history," *NeuroImage*, vol. 62, pp. 791-800, 2012.
- [216] M. Jenkinson, C. F. Beckmann, T. E. J. Behrens, M. W. Woolrich, and S. M. Smith, "FSL," *NeuroImage*, vol. 62, pp. 782-790, 2012.
- [217] R. W. Cox, "AFNI: What a long strange trip it's been," *NeuroImage*, vol. 62, pp. 743-747, 2012.
- [218] Z. S. Saad and R. C. Reynolds, "SUMA," *NeuroImage*, vol. 62, pp. 768-773, 2012.
- [219] R. Goebel, "BrainVoyager – Past, present, future," *NeuroImage*, vol. 62, pp. 748-756, 2012.
- [220] B. Fischl, "FreeSurfer," *NeuroImage*, vol. 62, pp. 774-781, 2012.
- [221] D. C. Van Essen, "Cortical cartography and Caret software," *NeuroImage*, vol. 62, pp. 757-764, 2012.
- [222] A. Eklund, P. Dufort, M. Villani, and S. LaConte, "BROCCOLI: Software for Fast fMRI Analysis on Many-Core CPUs and GPUs," *Frontiers in Neuroinformatics*, vol. 8, 2014.
- [223] M. Rubinov and O. Sporns, "Complex network measures of brain connectivity: Uses and interpretations," *NeuroImage*, vol. 52, pp. 1059-1069, 2010.
- [224] S. Whitfield-Gabrieli and A. Nieto-Castanon, "Conn: A Functional Connectivity Toolbox for Correlated and Anticorrelated Brain Networks," *Brain Connectivity*, vol. 2, pp. 125-141, 2012.
- [225] R. A. LaPlante, L. Douw, W. Tang, and S. M. Stufflebeam, "The Connectome Visualization Utility: Software for Visualization of Human Brain Networks," *PLoS ONE*, vol. 9, p. e113838, 2014.
- [226] P. C. G. Marques, J. M. Soares, V. Alves, and N. Sousa, "BrainCAT - a tool for automated and combined functional Magnetic Resonance Imaging and Diffusion Tensor Imaging brain connectivity analysis," *Frontiers in Human Neuroscience*, vol. 7, 2013-November-21 2013.
- [227] V. L. Morgan, B. M. Dawant, Y. Li, and D. R. Pickens, "Comparison of fMRI statistical software packages and strategies for analysis of images containing random and stimulus-correlated motion," *Computerized Medical Imaging and Graphics*, vol. 31, pp. 436-446, 2007.
- [228] T. R. Oakes, T. Johnstone, K. S. Ores Walsh, L. L. Greischar, A. L. Alexander, A. S. Fox, *et al.*, "Comparison of fMRI motion correction software tools," *NeuroImage*, vol. 28, pp. 529-543, 2005.
- [229] S. Gold, B. Christian, S. Arndt, G. Zeien, T. Cizadlo, D. L. Johnson, *et al.*, "Functional MRI statistical software packages: A comparative analysis," *Human Brain Mapping*, vol. 6, pp. 73-84, 1998.
- [230] NIH. (2015). *Neuroimaging Informatics Tools and Resources Clearinghouse (NITRC)*. Available: <http://www.nitrc.org/>
- [231] R. A. Poldrack, P. C. Fletcher, R. N. Henson, K. J. Worsley, M. Brett, and T. E. Nichols, "Guidelines for reporting an fMRI study," *NeuroImage*, vol. 40, pp. 409-414, 2008.
- [232] K. Uludağ and A. Roebroeck, "General overview on the merits of multimodal neuroimaging data fusion," *NeuroImage*, vol. 102, Part 1, pp. 3-10, 2014.

- [233] B. He and Z. Liu, "Multimodal Functional Neuroimaging: Integrating Functional MRI and EEG/MEG," *IEEE reviews in biomedical engineering*, vol. 1, pp. 23-40, 2008.
- [234] T. J. Kimberley and S. M. Lewis, "Understanding Neuroimaging," *Physical Therapy*, vol. 87, pp. 670-683, 2007.
- [235] F. Biessmann, S. Plis, F. C. Meinecke, T. Eichele, and K. Muller, "Analysis of Multimodal Neuroimaging Data," *Biomedical Engineering, IEEE Reviews in*, vol. 4, pp. 26-58, 2011.
- [236] J. Jorge, F. Grouiller, Ö. Ipek, R. Stoermer, C. M. Michel, P. Figueiredo, *et al.*, "Simultaneous EEG–fMRI at ultra-high field: Artifact prevention and safety assessment," *NeuroImage*, vol. 105, pp. 132-144, 2015.
- [237] N. K. Logothetis, "What we can do and what we cannot do with fMRI," *Nature*, vol. 453, pp. 869-878, 2008.
- [238] M. Brett, I. S. Johnsrude, and A. M. Owen, "The problem of functional localization in the human brain," *Nat Rev Neurosci*, vol. 3, pp. 243-249, 2002.
- [239] R. Henson, "What can functional neuroimaging tell the experimental psychologist?," *The Quarterly Journal of Experimental Psychology A*, vol. 58, pp. 193-233, 2005.
- [240] J. P. Simmons, L. D. Nelson, and U. Simonsohn, "False-Positive Psychology: Undisclosed Flexibility in Data Collection and Analysis Allows Presenting Anything as Significant," *Psychological Science*, vol. 22, pp. 1359-1366, 2011.
- [241] J. Carp, "The secret lives of experiments: Methods reporting in the fMRI literature," *NeuroImage*, vol. 63, pp. 289-300, 2012.
- [242] B. Inglis, "A checklist for fMRI acquisition methods reporting in the literature," *The Winnower*, 2015.
- [243] E. Vul and H. Pashler, "Voodoo and circularity errors," *NeuroImage*, vol. 62, pp. 945-948, 2012.
- [244] G. B. Pike, "Quantitative functional MRI: Concepts, issues and future challenges," *NeuroImage*, vol. 62, pp. 1234-1240, 2012.
- [245] E. Bullmore, "The future of functional MRI in clinical medicine," *NeuroImage*, vol. 62, pp. 1267-1271, 2012.
- [246] R. A. Poldrack, "The future of fMRI in cognitive neuroscience," *NeuroImage*, vol. 62, pp. 1216-1220, 2012.
- [247] A. P. Koretsky, "Is there a path beyond BOLD? Molecular imaging of brain function," *NeuroImage*, vol. 62, pp. 1208-1215, 2012.
- [248] A. Meyer-Lindenberg, "The future of fMRI and genetics research," *NeuroImage*, vol. 62, pp. 1286-1292, 2012.
- [249] J. H. Duyn, "The future of ultra-high field MRI and fMRI for study of the human brain," *NeuroImage*, vol. 62, pp. 1241-1248, 2012.
- [250] E. Formisano and N. Kriegeskorte, "Seeing patterns through the hemodynamic veil — The future of pattern-information fMRI," *NeuroImage*, vol. 62, pp. 1249-1256, 2012.
- [251] N. Filippini, B. J. MacIntosh, M. G. Hough, G. M. Goodwin, G. B. Frisoni, S. M. Smith, *et al.*, "Distinct patterns of brain activity in young carriers of the APOE- ϵ 4 allele," *Proceedings of the National Academy of Sciences of the United States of America*, vol. 106, pp. 7209-7214, 2009.
- [252] U. Hasson and C. J. Honey, "Future trends in Neuroimaging: Neural processes as expressed within real-life contexts," *NeuroImage*, vol. 62, pp. 1272-1278, 2012.
- [253] A. M. Owen, K. M. McMillan, A. R. Laird, and E. Bullmore, "N-back working memory paradigm: A meta-analysis of normative functional neuroimaging studies," *Human Brain Mapping*, vol. 25, pp. 46-59, 2005.

- [254] J. Ashburner and K. J. Friston, "Unified segmentation," *NeuroImage*, vol. 26, pp. 839-851, 7/1/ 2005.
- [255] E. T. Rolls, M. Joliot, and N. Tzourio-Mazoyer, "Implementation of a new parcellation of the orbitofrontal cortex in the automated anatomical labeling atlas," *NeuroImage*, vol. 122, pp. 1-5, 2015.
- [256] N. Tzourio-Mazoyer, B. Landeau, D. Papathanassiou, F. Crivello, O. Etard, N. Delcroix, *et al.*, "Automated Anatomical Labeling of Activations in SPM Using a Macroscopic Anatomical Parcellation of the MNI MRI Single-Subject Brain," *NeuroImage*, vol. 15, pp. 273-289, 2002.
- [257] J. D. Ragland, B. I. Turetsky, R. C. Gur, F. Gunning-Dixon, T. Turner, L. Schroeder, *et al.*, "Working memory for complex figures: an fMRI comparison of letter and fractal n-back tasks," *Neuropsychology*, vol. 16, pp. 370-379, 2002.
- [258] I. Drobnyak, "fMRI Simulator: Development and Applications," Doctor of Philosophy, Department of Clinical Neurology, University of Oxford, 2007.
- [259] K. Krupa and M. Bekiesińska-Figatowska, "Artifacts in Magnetic Resonance Imaging," *Polish Journal of Radiology*, vol. 80, pp. 93-106, 2015.
- [260] A. Fornito, A. Zalesky, and M. Breakspear, "Graph analysis of the human connectome: Promise, progress, and pitfalls," *NeuroImage*, vol. 80, pp. 426-444, 2013.
- [261] B. Impact. Available: <http://www.brainimpact.eu/files/brain-fMRI-3d-MAN-33yo.png>
- [262] L. Henriksson. (2011). *Visualization and quantification of fMRI results*. Available: http://www.neurobiotech.ru/sites/default/files/Henriksson_StPetersburg_fMRI_lecture2_visuquan_handouts.pdf
- [263] J. Taylor and R. Henson. (2011). *Multi-modal integration of MEG, EEG & fMRI*. Available: http://www.sbirc.ed.ac.uk/cyril/SPM-course/Talks/2013/5-Multimodal_JTaylor.pdf
- [264] M. S. Project. Available: <http://mindsongproject.co.uk/the-research-project-the-future-of-mindsong/>